

Numerical modeling of pipe leakage in variably saturated soil

Von der Fakultät für
Bauingenieurwesen und Geodäsie der
Gottfried Wilhelm Leibniz Universität Hannover
zur Erlangung des Grades
- Dr.-Ing. -
genehmigte

Dissertation

von
M.Sc. Aaron Peche
geboren am 17.10.1986
in Hildesheim, Deutschland

Hannover, 2018

Committee:

Prof. Dr. Thomas Graf (referent)

Prof. Dr. Olaf Kolditz (co-referent)

Prof. Dr. Regina Maria de Oliveira Barros Nogueira (head of committee)

Prof. Dr. René Therrien (committee member)

Prof. Dr. Uwe Haberlandt (committee member)

Promotion date: 25.02.2019

For my parents.

Natur ist glücklich. Doch in uns begegnen
sich zuviel Kräfte, die sich wirr bestreiten:
wer hat ein Frühjahr innen zu bereiten?
Wer weiß zu scheinen? Wer vermag zu regnen?

Wem geht ein Wind durchs Herz, unwidersprechlich?
Wer faßt in sich der Vogelflüge Raum?
Wer ist zugleich so biegsam und gebrechlich
wie jeder Zweig an einem jeden Baum?

Wer stürzt wie Wasser ber seine Neigung
ins unbekante Glück so rein, so reg?
Und wer nimmt still und ohne Stolz die Steigung
und hält sich oben wie ein Wiesenweg?

Rainer Maria Rilke (1875-1926)

Declaration

I hereby declare that:

- I know the regulations for doctoral candidates at the Faculty of Civil Engineering and Geodetic Science
- I have completed the present thesis independently; and any used materials by others are listed in the references
- I have not paid any monetary benefits regarding the content of the present dissertation
- The present dissertation has not been used as a M.Sc. or similar thesis before, and that the thesis or parts of it have not been published before unless otherwise indicated
- I have not applied for an exam as doctoral candidate at another institution

Hannover, December 2018

Aaron Peche

Abstract

Pipe leakage related to defect urban sewer and stormwater pipe networks may lead to subsurface contamination, reduction of groundwater recharge or a significant decrease of the groundwater table. The quantification of pipe leakage is challenging, mostly due to the uncertain forming of a colmation layer in the defect vicinity and inaccessibility of both, pipe defects and the surrounding soil. Numerical models can be used to quantify leakage. At present times, only few physically-based pipe leakage models exist, all of which either neglect or simplify variably-saturated flow.

In the present dissertation, a novel and unique three-dimensional physically-based pipe leakage model for variably saturated soil is presented. The model consists of the newly implemented coupling between the pipe flow simulator HYSTEM-EXTRAN and the unsaturated-saturated flow simulator OpenGeoSys. The coupling is based on updating of boundary conditions and source terms. The interprocess data transfer is realized using a shared-memory. The pipe leakage model is successfully validated and verified using a newly generated benchmark library for pipe leakage models. Benchmarks are based on two physical experiments described in literature and two newly derived analytical solutions.

A novel method for upscaling pipe leakage is presented. The method enables to significantly reduce the local refinement of spatial discretization in the pipe vicinity, which leads to a substantial reduction of computational costs. The method is based on leakage functions. Two leakage functions representing both, sewer and stormwater pipe leakage are presented. Accuracy and time efficiency of the upscaling method is demonstrated by comparing results from a fully discretized model and an upscaled model.

In the present dissertation, the pipe leakage model is applied to several case studies to investigate the pipe leakage process. Model setups represent (i) a single defect, (ii) a leaky sewer pipe of 30 m length, and (iii) a 53 km long defect stormwater pipe network in an urban catchment.

Results of the single defect and leaky sewer pipe model (models i,ii) show that leaky pipes can hydraulically disconnect from groundwater. It is found that, for a given pipe water level, pipe water exfiltration converges as the groundwater table is lowered. Further, it is found that pipe water exfiltration increases as the intensity and duration of pipe flow events increase. The temporal distribution of pipe flow has a negligible effect on pipe water exfiltration.

Results of the model representing a defect stormwater pipe network in an urban catchment (model iii) show the impact of pipe leakage on urban groundwater. It is shown that groundwater infiltration into a largely defect pipe network may be in the order of annual groundwater recharge. Further, it is shown that groundwater infiltration may reduce the groundwater table by several meters and that the groundwater table may be lowered to the elevation of the pipe network.

Keywords: Pipe leakage modeling, coupled model, pipe flow, unsaturated-saturated soil flow, OpenGeoSys, HYSTEM-EXTRAN

Kurzfassung

Leckage aus undichten Rohrleitungssystemen in das umliegende poröse Medium kann zur Kontamination des Untergrundes, zur Abnahme von Grundwasserneubildung und zur Absenkung des Grundwasserspiegels führen. Die Quantifizierung von Leckageflüssen stellt eine große Herausforderung dar. Dies liegt unter anderem an der Bildung einer schwer zu charakterisierenden Kolmationsschicht und an der Unzugänglichkeit von Rohrdefekten. Numerische Modelle können zur Quantifizierung von Leckageflüssen genutzt werden. Es existieren nur wenige physikalisch-basierte Leckagemodelle. Genewärtige Modelle vernachlässigen oder vereinfachen die zur genauen Berechnung von Leckage existenzielle Sickerströmung.

Die vorliegende Dissertation beschreibt ein neuartiges physikalisch-basiertes Modell zur Berechnung von dreidimensionaler Leckage im variabel gesättigten Untergrund. Dieses Leckagemodell basiert auf der neu implementierten Kopplung zwischen dem Rohrströmungssimulator HYSTEM-EXTRAN und dem Sicker- und Grundwasserströmungssimulator OpenGeoSys. Die Kopplung basiert auf dem Überschreiben von Randbedingungen und Quelltermen. Der Datenaustausch erfolgt über eine shared-memory Schnittstelle. Das Leckagemodell wurde unter Nutzung einer Sammlung von Bezugsmodellen erfolgreich validiert und verifiziert. Die Bezugsmodelle basieren auf zwei in der Literatur beschriebenen physikalischen Experimenten und zwei, im Zuge dieser Dissertation neu entwickelten analytischen Lösungen.

Weiterhin ist in der vorliegenden Dissertation eine neuartige Methode zur Hochskalierung von Leckage beschrieben. Diese Methode ermöglicht eine Verminderung der räumlichen Auflösung des porösen Mediums im Bereich des Rohrdefektes und bewirkt damit eine Ersparnis an Rechenzeit. Die Methode basiert auf sogenannten Leckagefunktionen. In dieser Arbeit werden zwei unterschiedliche Leckagefunktionen präsentiert. Mit diesen Leckagefunktionen wird zum einen Leckage von Abwasser und zum anderen Leckage von Regenwasser abgebildet. In einer Vergleichsstudie zwischen einem voll diskretisierten- und einem hochskalierten Modell werden Genauigkeit und Zeitersparnis der Hochskalierungsmethode aufgezeigt.

Weiterhin wird die Anwendung des Leckagemodells in mehreren Fallstudien beschrieben. Leckagemodelle repräsentieren dabei (i) einen Einzeldefekt, (ii) eine defekte Rohrleitung von 30 m Länge und (iii) ein defektes Rohrnetzwerk von 53 km Länge in einem urbanen Einzugsgebiet.

Ergebnisse des Einzeldefekt- und 30 m Rohrleitungsmodells (Modelle i,ii) führen zu der Erkenntnis, dass es für bestimmte Leckagekonditionen keine hydraulische Anbindung von defekter Rohrleitungen an das Grundwasser gibt. Dies gilt für Grundwasser weit unterhalb der Rohrleitung. In solch einem Fall verändert sich bei gleichbleibendem Rohrwasserstand der Leckagefluss mit absinkendem Grundwasser nicht. Weiterhin wird aufgezeigt, dass sich die Dauer und die Intensität des Rohrabflusses stark auf Leckage in Form von Exfiltration

aus defekten Rohrleitungen auswirkt während die zeitliche Verteilung von Rohrabfluss keinen Einfluss auf Exfiltration hat.

Ergebnisse des defekten Rohrnetzwerkmodells (Modell iii) zeigen die starken Auswirkungen defekter Rohrleitungen auf urbanes Grundwasser auf. Es wird gezeigt, dass Leckage in Form von Grundwasserinfiltration der jährlichen Grundwasserneubildung entsprechen kann. Weiterhin wird gezeigt, dass Grundwasserinfiltration eine Absenkung des Grundwasserspiegels um mehrere Meter bis auf die Höhe des Rohrnetzwerkes zur Folge haben kann.

Keywords: Modellierung von Rohrleckagen, gekoppeltes Modell, Rohrströmung, Sickerströmung, Grundwasserströmung, OpenGeoSys, HYSTEM-EXTRAN

Acknowledgements

First and foremost, I want to express my deepest gratitude to Professor Thomas Graf, who always encouraged me to try new ideas, many of which somehow materialized into the present dissertation. Thank you for fruitful discussions and for being such an excellent mentor. My time under your supervision makes me feel well prepared for the professional life as a scientist. I want to express my gratitude to Professor Insa Neuweiler for always having an open door for constructive discussion and for giving me the chance to be part of her workgroup. Further, I want to thank Dr. Lothar Fuchs for his collaboration, constructive feedback and encouragement regarding our manuscripts for publication.

I truly appreciate the work of the committee members and want to express my gratitude for taking the time to read the present dissertation and act as referee during the defense.

This thesis stems from the German Federal Ministry of Education and Research (BMBF) funded project EVUS ‘Echtzeitvorhersage für urbane Sturzfluten und damit verbundene Wasserkontamination’ (Real-Time Prediction of Pluvial Floods and Induced Water Contamination in Urban Areas). I want to thank the BMBF for financing and the EVUS-research group for the close communication and remarkable collaboration. The EVUS meetings and joint discussions were enlightening and I am personally very thankful for having been part of such a productive interdisciplinary project. Namely, I would like to thank Peter Spönemann for guidance regarding the code coupling. Further, I would like to thank Bora Shehu and Julian Wahl for precipitation and stormwater pipe network data.

Further, I want to thank Dr. Heidi Barlebo and Dr. Jacob Kidmose for taking me into their workgroup at the Geological Survey of Denmark and Greenland in Copenhagen, Denmark, and for being excellent hosts. This exchange was mind broadening, productive, and really fun. I hope we can continue to collaborate in the future. I also want to thank Ida, Lene, Mehrdis and Rena for welcoming me in Denmark and for making this stay very pleasant.

I want to thank all former and present colleagues and friends from the Institute of Fluid Mechanics and Environmental Physics in Civil Engineering, namely Antje, Britta, Eugenia, Jie, Katharina, Aziz, Carlos, Jan, Alina, Clemens, Dianlei, Gergely, Simon, Lisa, Anneke, Natascha, Tuong Vi, and Robert for distraction, discussion and proofreading. Further, I want to thank Arne and Yibo for technical support.

Further, I want to thank the OGS community, namely Professor Marc Walther and Dr. Thomas Kalbacher for introducing me to the OGS source code and for technical support.

This work would not have been possible without my family and girlfriend. I want to acknowledge my parents Luana and Siegfried, my brothers Alexander and Samuel, my sister-in-law Sang-Mi, my ever so cute nieces Na-Young and So-Young, my aunt and uncle Tina and Norbert, and my beloved María as my largest source of emotional support.

Contents

List of Figures	xvii
List of Tables	xix
1 Introduction	1
1.1 Problem definition	1
1.2 Modeling pipe leakage - approaches and challenges	4
1.3 Modeling pipe leakage - applications	7
1.4 Contributions of the present dissertation	11
2 Numerical model for pipe leakage	15
2.1 Objective	15
2.2 OpenGeoSys (OGS)	15
2.3 HYSTEM-EXTRAN (HE)	16
2.4 The new OGS-HE platform	17
2.5 Verification and validation of OGS-HE	21
2.6 Conclusions	26
3 Upscaling pipe leakage using leakage functions	35
3.1 Objective	35
3.2 Leakage function	35
3.3 Conceptual model for leakage function derivation	36
3.4 Derivation of the leakage function	39
3.5 Results	39
3.5.1 Leakage function for sewer leakage	39
3.5.2 Leakage function for stormwater leakage	41
3.6 Validation of the source code modification for upscaled pipe leakage	42
3.7 Conclusions	43
4 Synthetic case study of sewer leakage on a single leaky pipe	45
4.1 Objective	45
4.2 Conceptual model of a leaky pipe	45
4.3 Results	48
4.3.1 Impact of pipe flow volume on sewer leakage	48
4.3.2 Impact of pipe flow duration on sewer leakage	48
4.3.3 Impact of pipe flow peak position on sewer leakage	49
4.4 Conclusions	52
5 Case study of stormwater pipe leakage in an urban subcatchment	55
5.1 Objective	55
5.2 Modified numerical model OGS-HE	55
5.3 Study area	57

5.4	Conceptual model of an urban subcatchment	59
5.5	Groundwater model calibration and sensitivity analysis	59
5.6	Scenario definition	62
5.7	Results	66
5.7.1	Reduction of annual GW recharge by leakage under dry-weather flow conditions	66
5.7.2	Reduction of GW levels by leakage under dry-weather flow conditions	67
5.7.3	Generation of a leakage severity map under dry-weather flow conditions	69
5.7.4	Impact of rain return period and temporal rainfall distribution on stormwater pipe leakage	70
5.8	Conclusions	71
6	Summary and outlook	79
7	Appendix	83
	List of symbols	99
	References	101
	List of dissertations in the institute	111

List of Figures

1.1	Pipe leakage in an urban system.	2
1.2	CCTV-image of a transversal crack-type pipe defect with groundwater infiltration. Reprinted from Davies et al. [2001].	3
1.3	Forming of a colmation layer.	6
2.1	Conceptual model of OGS-HE.	18
2.2	Flowchart of OGS-HE.	20
2.3	Results of benchmark 1.	28
2.4	Results of benchmark 2.	29
2.5	Results of benchmark 3.	30
2.6	Conceptual model of benchmark 4.	31
2.7	Spatial discretization and exemplary numerical model result of benchmark 4.	32
2.8	Results of benchmark 4.	33
3.1	Physical meaning of the LF output and input variables q_{leak} , H_{PW} and p	36
3.2	Schematic visualization of derivation and assignment of a leakage function.	37
3.3	Single pipe defect model domain and boundary conditions.	38
3.4	Leakage function for sewer leakage.	40
3.5	Leakage function for stormwater leakage.	41
3.6	Validation of the source code implementation of the leakage function.	43
4.1	Conceptual model of the 30 m leaky pipe.	47
4.2	Pipe flow Neumann boundary conditions of the 30 m leaky pipe model.	47
4.3	Results depicting the impact of pipe flow volume on sewer leakage.	49
4.4	Exemplary simulation result of the 30 m leaky pipe model.	50
4.5	Results depicting the impact of pipe flow duration on sewer leakage.	51
4.6	Results depicting the impact of pipe flow peak position in time on sewer leakage.	51
4.7	Dynamic evolution of hydraulic gradient and relative permeability in the pipe defect vicinity during pipe leakage.	52
5.1	Calculation of stormwater pipe leakage with OGS-HE.	56
5.2	Stormwater leakage function used for the calculation of pipe water exfiltration.	57
5.3	Test area and conceptual model of the urban subcatchment.	58
5.4	Model domain, permeability zones and numerical grid of the catchment scale model.	60
5.5	Flow chart of the coupled OGS-MATLAB calibration procedure.	61
5.6	Results of the GW model calibration.	62
5.7	Results from the GW model sensitivity analysis.	63
5.8	Conceptual model for the scenarios of the catchment scale simulations.	64
5.9	Rain events used as Neumann boundary conditions in the pipe flow model for the catchment scale simulations.	65

5.10	Reduction of Q_{recharge} by $Q_{\text{leak,net,dry-weather}}$	67
5.11	Effect of $Q_{\text{leak,net,dry-weather}}$ on Q_{recharge} for different standard defect sizes.	68
5.12	Effect of standard defect size on GW level change.	69
5.13	Spatial distribution of GW level reduction for a standard defect of $A_{\text{defect}} = 1 \cdot 10^{-4} \text{ m}^2$ per m pipe.	73
5.14	Spatial distribution of GW level reduction for standard defects of $A_{\text{defect}} = 1 \cdot 10^{-5} \text{ m}^2$ (above) and $A_{\text{defect}} = 1 \cdot 10^{-6} \text{ m}^2$ (below) per m pipe.	74
5.15	Leakage severity map for a standard defect $A_{\text{defect}} = 4 \cdot 10^{-7} \text{ m}^2$ per m pipe.	75
5.16	Cumulative GW infiltration and cumulative stormwater exfiltration for rain events with different temporal distribution.	76
5.17	Exemplary model result of the catchment scale model.	77
7.1	Images of colmation layers.	91
7.2	van Genuchten [1980] retention curve and relative permeability function representing the trench backfill and aquifer strata given in Table 3.1.	92
7.3	Pipe flow events used for the single defect model.	92
7.4	Pipe water levels above the defect calculated for the single defect model.	93
7.5	Pipe flow event used for the comparison of the fully discretized model with the LF-model.	93
7.6	Results of the grid convergence study for the fully discretized single pipe defect simulations.	94
7.7	Results of the grid convergence study for the leakage function-model single pipe defect simulations.	94
7.8	Results of the grid convergence study for the 30 m leaky pipe model.	95
7.9	Initial spatial distribution of soil water pressure at pipe invert for the urban subcatchment model.	96
7.10	Dynamic evolution of dry-weather flow leakage in the catchment scale model.	97

List of Tables

1.1	Conceptualization of flow processes in pipe leakage models from previous studies.	12
2.1	Benchmark 1: Material hydraulic parameters and fluid properties.	22
2.2	Benchmark 2: Retention curve and relative conductivity function data.	24
3.1	Material hydraulic parameters and fluid properties for the single pipe defect domain.	38
5.1	Permeabilities of the calibrated model and initial permeabilities used for the calibration.	61
7.1	Single pipe defect bottom boundary pressures used for the single defect model.	89
7.2	Total number of elements and colmation layer elements within all meshes used for the grid convergence study with the single pipe defect model.	89
7.3	Total number of elements for the grid convergence study with the single pipe defect leakage function-model.	90
7.4	Total number of elements within all meshes used for the grid convergence study with the 30 m leaky pipe model.	90

1 Introduction

Parts of this chapter have been published in Peche et al. [2017] and Peche et al. [2019].

1.1 Problem definition

Urban subsurface pipe networks have been constructed in Europe since the mid-nineteenth century in order to drain sewage and excessive land surface-bound water, and by doing so to protect public health, safety and quality of life [Ellis and Bertrand-Krajewski, 2010]. Existing urban subsurface pipe infrastructure is increasing in age and renewal levels may be in the time scale of many decades up to a hundred years [Fenner, 2000; Wirahadikusumah et al., 2001; Wells and Melchers, 2015]. Increasing pipe age leads to an increased likelihood of occurring pipe defects [Micevski et al., 2002; Wolf et al., 2006]. Different types of pipe defects exist. Fuchs-Hanusch et al. [2016] generalized pipe defects to circular holes, open joints, transversal or longitudinal cracks (all caused by faulty construction, physical stress and deformation) [Dohmann, 2013], and corrosion clusters (caused by biochemical processes driven by e.g. the discharge of chemicals into sewers) [Dohmann, 2013; Clemens et al., 2015]. Pipe defects may be discovered using in-pipe video inspection (closed circuit televising - CCTV) [Read and Vickridge, 1996; Butler and Davies, 2003], geophysical methods (e.g. ground penetrating radar, electrical resistivity measurements) [Ogai and Bhattacharya, 2018], and acoustic methods measuring acoustic reflections on inner pipe walls [Romanova et al., 2013]. Statistically, pipe defects in a pipe network can be described using the standard defect size per m pipe concept [Karpf, 2012]. The presence of pipe defects leads to exchange fluxes between pipes and the saturated-unsaturated subsurface, called pipe leakage. Pipe leakage may lead to significant changes in urban hydrology [Lerner, 1986], may lead to large costs and may represent a threat to humankind and the environment, especially in areas where groundwater is a potable resource [DeSilva et al., 2005].

Pipe leakage denotes the hydraulic interaction between pipe systems and the surrounding saturated-unsaturated zone. The term ‘leakage’ includes both, groundwater (GW) infiltration (flow of GW into pipes), and pipe water exfiltration (flow from pipes into the surrounding unsaturated-saturated subsurface) as shown in Figure 1.1. In the present dissertation, leakage from and to partially pressurized defect pipe networks consisting of

sewers or stormwater pipes are regarded. Pressurized pipes such as water mains for drinking water supply will not be discussed. Groundwater infiltration occurs when the GW level is above the pipe water level. Pipe water exfiltration occurs when the GW level is below the pipe water level. The quantification of pipe leakage is challenging, which is due to the inaccessibility of pipe defects. Indirect methods, such as analytical investigations of surface and groundwater (measurement of licit/illicit drugs and pharmaceuticals and personal care products) [Wolf et al., 2006; Rosi-Marshall et al., 2015] or in-pipe tracer tests [Knudsen et al., 1996] may be used in order to quantify pipe leakage. Consequences associated with pipe leakage are discussed below.

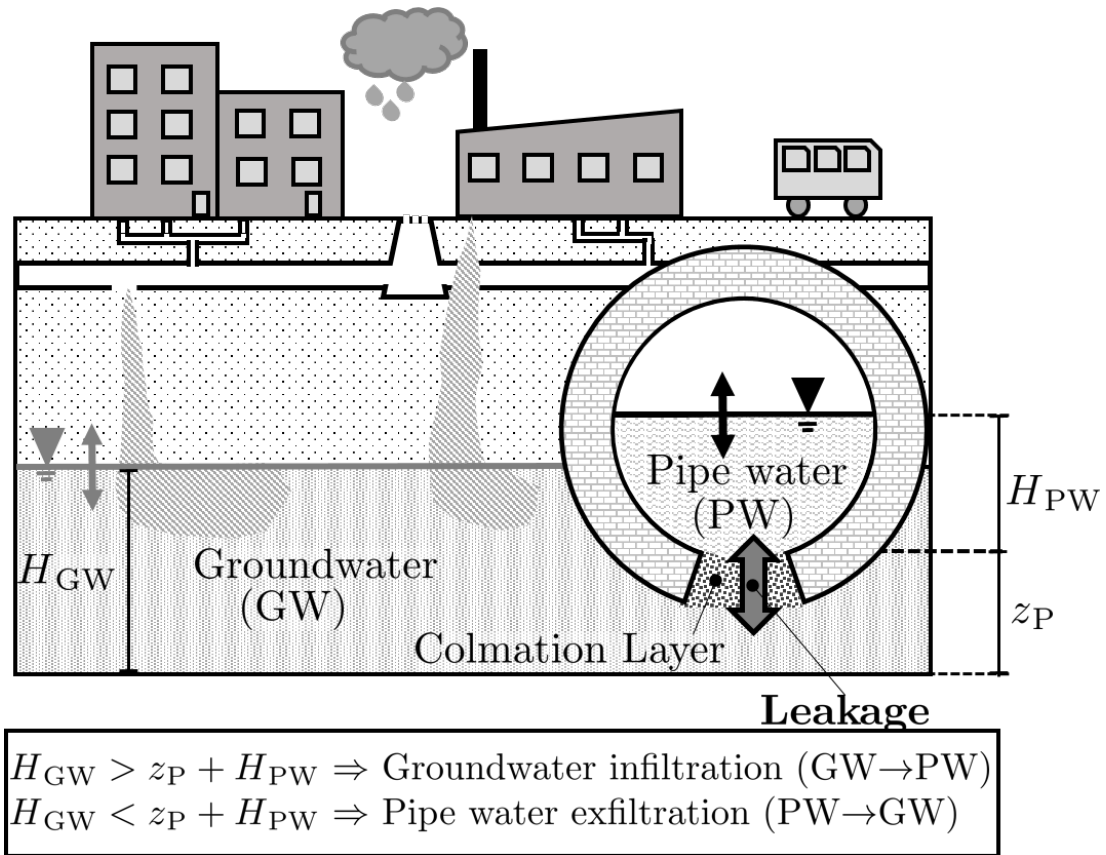


Figure 1.1: Pipe leakage in an urban system.

A CCTV-image showing a GW infiltration through a transversal crack into a sewer pipe is given in Figure 1.2. Infiltration of contaminated GW into sewer pipes can lead to increased pollution loads in the pipe system and at the pipe system outlet [Pitt, 1993; Xu et al., 2014]. Further, GW infiltration can lead to a decreased sewer capacity, increased likelihood of sewer overflow (and surface contamination), and reduced waste water treatment efficiency [Ellis, 2001; Weiss et al., 2002; Karpf and Krebs, 2013]. Analogously, GW infiltration into stormwater pipes results in a reduced stormwater pipe capacity, which may lead to increased manhole surcharge and surface flooding, especially in case of heavy rain

events. GW infiltration may decrease the groundwater table of an urban system [Wittenberg and Aksoy, 2010]. This may evoke land subsidence [Martinez et al., 2011]. However, GW infiltration-driven decreasing GW levels may be beneficial and prevent damage to underground structures [Gustafsson, 2000; Karpf and Krebs, 2013]. GW infiltration may lead to soil mobilization and drainage of soil into the pipe network [Schrock, 1994; Davies et al., 2001], which may evoke sinkholes [Guo et al., 2013; Tang et al., 2017] and cause damage to urban infrastructure. Further, GW infiltration in combination with a decrease in GW levels leads to a lack of baseflow in rivers and streams [Reichel and Getta, 2008] which may affect the environment.



Figure 1.2: CCTV-image of a transversal crack-type pipe defect with groundwater infiltration. Reprinted from Davies et al. [2001].

Pipe water exfiltration may lead to soil and GW contamination [Hornef, 1983; Bishop et al., 1998; Rutsch et al., 2008]. Sewage and stormwater may be highly enriched with contaminants [Rogers, 1996; Birch et al., 2004], such as disease-causing pathogens [Davis and McCuen, 2005], heavy metals [Elliott et al., 1986] stemming from e.g. road debris, herbicides like glyphosate [Eriksson et al., 2007] stemming from agricultural land use, and polychlorinated biphenyls (PCBs) stemming from industrial land use (e.g. lubricants and hydraulic oils) [Rossi et al., 2004; Tondera et al., 2018]. Exfiltrating pipe water may cause erosion or the dissolution of soluble bedrock and evoke sinkholes [Harvey and McBean,

2014], which can lead to substantial damage of urban infrastructure. A devastating sinkhole event happened in Guatemala (among other sinkhole events known as the ‘Guatemala sinkhole problem’), where leaky pipes caused the erosion of limestone up to a point where a large sinkhole swallowed a multistory building [Hermosilla, 2012; Coppola, 2015].

Understanding pipe leakage is essential to take measures against above listed problems or to encourage advantages associated with leakage (e.g. GW drainage induced by GW infiltration). The use of physically-based numerical models is crucial in order to gain a detailed process understanding of the pipe leakage process. Aim of the present dissertation is the development of a validated, physically-based, coupled pipe flow and unsaturated-saturated flow model for the simulation of pipe leakage in variably saturated soil. By using this model, further aim of this dissertation is to gain process understanding about pipe leakage under saturated-unsaturated conditions and to investigate the impact of pipe leakage on urban GW.

1.2 Modeling pipe leakage - approaches and challenges

Modeling pipe leakage requires the modeling of pipe flow, variably saturated subsurface flow, and the pipe leakage process in form of exchange fluxes through pipe defects. Pipe flow can be calculated dynamically using the Saint-Venant equations [de Saint-Venant, 1871] [e.g. Karpf and Krebs, 2005; Thorndahl et al., 2016a] or it can be represented by some constant water level (representing e.g. dry-weather flow) above a pipe defect [e.g. Mohrlök et al., 2008; Ly and Chui, 2012], depending on the purpose of the model. Variably saturated subsurface flow can be calculated dynamically using Richards’ equation [Richards, 1931] [e.g. Mohrlök et al., 2008; Karpf et al., 2009; Thorndahl et al., 2016a], which is computationally costly, especially on large spatial scale. As a simplification, the hydraulic connection of defect pipes and soil may be represented by the distance of pipe defect and groundwater [e.g. Eiswirth and Hötzl, 1997; Rutsch et al., 2008; Boukhemacha et al., 2015].

Several approaches for modeling the pipe leakage process exist. A widely used method for the calculation of leakage is the leakage factor method based on Darcy’s law, as first proposed by Rauch and Stegner [1994], and further used by e.g. Vollertsen and Hvitved-Jacobsen [2003] and Karpf and Krebs [2005]. In that approach, a factor represents hydraulic properties of the soil in the defect vicinity. Despite the benefit of small model complexity and short computation times, the leakage factor approach does not take the dynamic evolution of water pressure and relative intrinsic permeability of the soil in the defect vicinity into account. Considering these dynamic changes is known to be very important for the calculation of leakage [Karpf et al., 2009] because they capture the non-

linear relationship between pipe water exfiltration flux and hydraulic gradient.

An approach which can capture this nonlinear relationship is an exponential function first proposed for river-aquifer exchange fluxes by Rushton and Tomlinson [1979], and transferred to the concept of pipe leakage by Rutsch et al. [2008]. Drawback of that approach is the required calibration of three non-physical leakage parameters. A detailed description of that approach is given in Becker et al. [2009].

A further approach describes leakage flux as a function of head difference between groundwater and pipe water, and an exchange coefficient depending on the hydraulic radius of the pipe and a user defined coefficient [Thorndahl et al., 2016a]. That coefficient contains information about the intrinsic permeability and geometry of the soil in the defect vicinity and has to be calibrated. That approach is used in the pipe flow model MOUSE [DHI, 2017].

Empirical approaches or approaches based on Darcy's theory are often restricted or fail to successfully predict leakage [Rutsch et al., 2008], which is due to the necessity of parameter calibration and the inability to capture the nonlinear behaviour of leakage under unsaturated conditions. Physically-based models for pipe flow and variably saturated subsurface flow are required to estimate pipe leakage with sufficient precision [Mohrlok et al., 2008].

Modeling the pipe leakage process is challenging. The following two main challenges exist. The first challenge stems from the fact that leakage flow is governed by a highly variable and inaccessible filtration layer forming in the vicinity of the pipe defect, called colmation layer. The colmation layer forms due to particle input from exfiltrating water (sewage, stormwater), biomass growth and chemical precipitation [Schwarz, 2004; Ellis et al., 2009; Karpf, 2012] as illustrated in Figure 1.3. Images of colmation layers including raster electron microscopy images of colmated soil pores and coated soil grains are given in Figure 7.1 in the Appendix.

Pipe leakage (or wastewater/stormwater exfiltration)-driven colmation layer forming is investigated in several physical experiments [Okubo and Matsumoto, 1983; Rauch and Stegner, 1994; Vollertsen and Hvitved-Jacobsen, 2003; Blackwood et al., 2005; Karpf, 2012; Dohmann, 2013]. Results from these experiments in form of exfiltration rate, colmation layer hydraulic properties and colmation layer geometry differ by several orders of magnitude. This large deviation highlights the dependency of colmation layer properties on on-site conditions such as initial soil type, physico-chemical wastewater signature, vertical distance from defect to groundwater, and pipe water level. A key finding of these studies is that, for stationary conditions, exfiltration reaches a constant value after some time when colmation layer characteristics are no longer changing. In leakage modeling, this leads to the assumption that colmation layer geometry, intrinsic permeability and

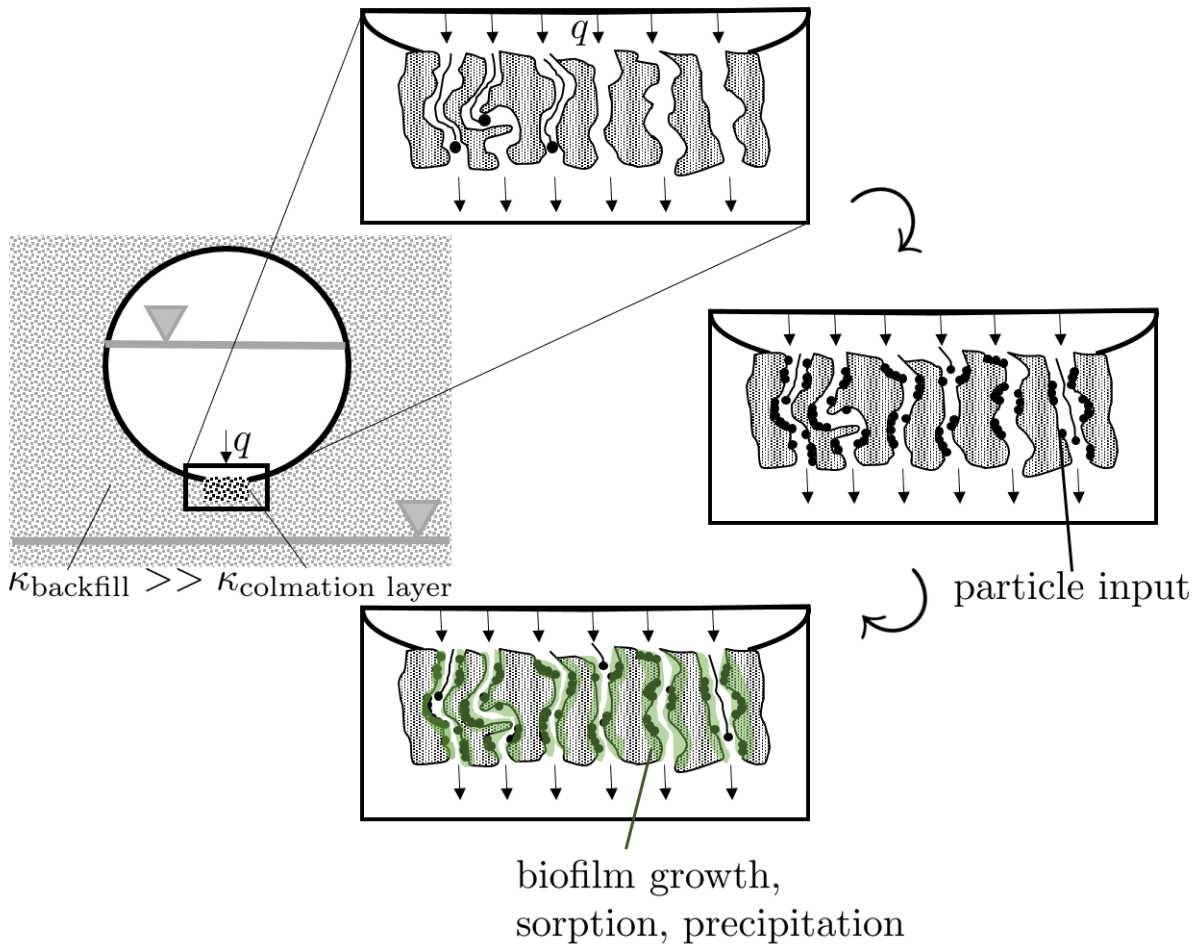


Figure 1.3: Forming of a colmation layer.

porosity are constant.

Colmation layers of sewer and stormwater pipe systems differ significantly. The reason for this is the difference of sewage and urban stormwater composition leading to different hydraulic properties of colmation layers. While the amount of total suspended solids in sewage and stormwater may be similar, the amount of organic matter in sewage exceeds that in stormwater [Booth, 2006]. As shown in Siegrist [1987], larger organic matter loads in the infiltrate lead to a more severe soil clogging (through settlement of organic matter and biofilm growth), and to larger reduction in porosity and intrinsic permeability. Therefore, permeability and porosity of sewer colmation layers are generally small compared to stormwater colmation layers, and values have to be chosen judiciously. In the present dissertation, values for sewer colmation layer intrinsic permeability and colmation layer geometry are taken from physical experiments described in Karpf [2012], because these results represent colmation layers for sewer leakage in a German system. Values for stormwater colmation layer intrinsic permeability and colmation layer geometry are approximated from Le Coustumer et al. [2012] and Karpf [2012]. van Genuchten [1980]

parameters are taken from Carsel and Parrish [1988].

The second challenge in modeling pipe leakage occurs when pipe water exfiltrates under unsaturated conditions at which the relationship of leakage and hydraulic gradient is non-linear. At this stage, beside the hydraulic gradient, relative intrinsic permeabilities in the colmation layer govern leakage. In order to accurately consider the relative intrinsic permeability, Richards' equation with a retention curve parametrization [e.g. Brooks and Corey, 1966; van Genuchten, 1980] must be solved. In leakage modeling, this is often neglected in order to reduce model complexity and save computational costs.

In the present dissertation, a coupled pipe flow-saturated unsaturated flow model will be presented. This novel model calculates leakage under saturated and unsaturated conditions in a physically-based manner, considers the presence of a colmation layer, and takes the nonlinearity of the leakage process under unsaturated conditions into account. A parameter calibration is not required if colmation layer hydraulic properties and geometry are known. As a consequence, this dissertation provides novel insights about the nonlinear process of pipe leakage under unsaturated conditions.

1.3 Modeling pipe leakage - applications

The present section gives an overview of existing studies on modeling pipe leakage highlighting conceptual models and key findings. Several studies on modeling pipe leakage exist, many of which with different key findings and purpose. Depending on the purpose, the conceptual models used in these studies vary.

Karpf and Krebs [2011] introduced an improved model for the approximation of sewage exfiltration based on Darcy's law, which is extended by empirical relationships stemming from numerical simulations. Results from a sensitivity analysis showed that pipe water level and duration of the clogging process that causes the development of the colmation layer have a high impact on pipe leakage, and that structural input data (soil and backfill conductivity, trench measures, damage width) has a low impact on pipe leakage.

Shaad and Burlando [2018] used a coupled surface water-GW model consisting of the physically-based flow simulators 2dMb [Shaad, 2015] and MODFLOW VSF [Thoms et al., 2006] in order to simulate urban shallow groundwater dynamics including leakage in Jakarta, Indonesia. In that model, leakage is assigned as a constant source term and calculated based on population density and water consumption per capita. An outcome of that study is that leakage is a significant contributor to the urban water cycle. That model was not coupled to a pipe flow model.

Boukhemacha et al. [2015] set up a steady-state hydrological model including pipe leakage for a part of Bucharest, Romania. They mathematically described pipe water exfiltration and groundwater infiltration with a calibrated and modified form of Darcy's law, and a calibrated leakage factor approach, respectively. In both cases, the potential gradient was calculated as head difference between groundwater and pipe water table. This study shows the large impact that leakage may have on an urban flow system. It was concluded that sewer and water supply pipe network contribute with 53% and 18% to groundwater recharge, respectively. Furthermore, 76% of total groundwater discharge in this urban catchment is drained into the sewer system.

Reichel and Getta [2008] used a leakage model in order to investigate sewer rehabilitation-driven rise of GW levels in a case study representing an urban area in the Emscher catchment, Germany. That model is a numerical GW model which is set up using the GW simulator SPRING [delta h Ingenieurgesellschaft GmbH, 2017], and in which leakage is included using source terms assigned to nodes representing the pipe network. The calculation of leakage is based on the leakage factor approach. It was found that sudden pipe rehabilitation may lead to a local rise in groundwater levels of more than two meters. It was further found that the GW level rise leads to contact of GW and house basements in the test area resulting in significant structural damage. In that model, pipe flow and variably saturated flow were neglected and leakage factors were calibrated.

Tubau et al. [2017] used a water balance approach including pipe leakage combined with a physically-based GW model in order to quantify urban GW recharge in Barcelona, Spain. In that approach, leakage is accounted for by a constant factor describing the fraction of pipe water leaking through pipe defects and contributing to GW recharge. That factor was estimated based on a study by Chisala and Lerner [2008] and the fraction of GW recharge stemming from leakage varies between 1% and 30%, depending on different scenarios. In that model, the physically-based modeling of pipe flow and flow in the variably-saturated zone is not regarded. Tubau et al. [2017] highlight the importance of flow models in order to accurately quantify leakage.

Gogu et al. [2017] modelled pipe leakage in Bucharest, Romania, with a steady-state urban subsurface model including groundwater flow, pipe flow and interaction with surface water and underground structures such as tunnels. They found that 20% of the pipe network is prone to groundwater infiltration. It was also shown that $0.92 \text{ m}^3/\text{s}$ of pipe water surplus originates from groundwater infiltration. Leakage was calculated with the leakage-factor approach.

Xu et al. [2014] used a simplified model proposed by Karpf and Krebs [2011] to quantify non-stormwater inflow into the stormwater drainage system of Shanghai, China. They

concluded that 10% of total pipe flow in their test area is from non-stormwater sources. The calculation of leakage is based on a water balance. Leakage is calculated only for dry-weather flow conditions, and transient exfiltration from stormwater pipes is not regarded.

Vizintin et al. [2009] coupled the sewer infiltration and exfiltration model NEIMO [DeSilva et al., 2007] to an urban water management model and to a variably saturated subsurface flow model, and applied it to an urban catchment. In that coupled approach, leakage rates were approximated with a modified form of Darcy's law. Exfiltration was estimated from pipe geometry and pipe water level without considering the matrix potential in the soil. Leakage rates were then used as boundary condition for the subsurface flow model. A case study showed that 63 % of groundwater recharge in the city of Ljubljana stems from water mains and sewer leakage.

Mohrlok et al. [2008] approximated three-dimensional pipe exfiltration and solute transport from a single pipe leak into a variably saturated subsurface with a physically-based model based on Richards' equation and using the random walk method. They calculated breakthrough curves of solutes for sand and silty loam, and found that breakthrough of pipe leakage to the groundwater table located below the leak was reached within a few hours for both soils. They further observed long-term residence times of solute due to lateral spreading. That model was not coupled to a pipe flow model.

Ly and Chui [2012] used a physically based two-dimensional model for the investigation of the hydraulic interactions between a single leaky sewage pipe, groundwater and surface-bound stormwater drains in Singapore. That numerical model solved Richards' equation coupled with an advection-dispersion equation in order to simulate flow and transport. That study deals with the impact of pipe leakage on subsurface contamination. It was concluded that complete subsurface contaminant remediation after pipe rehabilitation takes several years. A further result of that study was that water quality of sewer leakage-caused infiltration into stormwater drains is low in dry years.

Bhaskar et al. [2015] used a coupled surface-subsurface flow model in order to quantify the long-term impact of leakage on subsurface storage in Baltimore, US. They used the coupled surface flow-groundwater flow simulator ParFlow [Maxwell et al., 2009] to calculate variably saturated subsurface flow. Pipe leakage is not calculated but estimated based on measured data from local pipe flow monitoring. Bhaskar et al. [2015] concluded that net leakage (groundwater infiltration minus pipe water exfiltration) decreased subsurface storage by 11% in one year. That model was not coupled to a pipe flow model.

Iwalewa et al. [2016] used a numerical model to investigate GW level rise driven by pipe water exfiltration in a case study in Dammam city, Saudi Arabia. That model takes saturated-unsaturated flow into account and consists of a coupled MODFLOW [Harbaugh

et al., 2000]-HYDRUS [Simunek et al., 2005] procedure. Full saturated GW flow is calculated in two spatial dimensions and variably saturated flow in one spatial dimension. That model takes only pipe water exfiltration into account (because GW is below pipes in that area) by assigning source terms representing the defect pipe network. Leakage is based on estimations and comprises a constant value equal to 20% of pipe flow. It was found that leakage is a major contributor to rising GW levels, which may be in order of several meters within one year. GW was found to rise above land surface causing surface flooding in certain urban areas and times of year. That model was not coupled to a pipe flow model.

Sommer et al. [2009] used a coupled surface-subsurface model including physically-based pipe flow, surface flow and groundwater flow in order to calculate surface inundation in Dresden, Germany. Leakage fluxes were calculated with Darcy's law. By comparing inundated areas calculated by both, a coupled surface-subsurface flow model and an uncoupled surface flow model, it was found that a coupling to a subsurface flow model can be neglected in this specific case study. Sommer et al. [2009] also showed that infiltration of flood water into sewers is the main reason for sewer overloading. That model did not consider variably saturated groundwater flow.

Thorndahl et al. [2016a] used a coupled model incorporating variably saturated flow, groundwater flow and solute transport, and sewer flow for modeling sewer infiltration in an urban catchment in Denmark. They showed that seasonal groundwater level fluctuations affect pipe leakage. They further showed that a leaky pipe system located below the groundwater table may lower groundwater levels by several dozens of centimeters. In that study, the calibration of mathematical coefficients was necessary for an estimation of only infiltration (exfiltration was not considered).

In a coupled pipe flow-subsurface flow approach by Kidmose et al. [2015], leakage is calculated using the difference between groundwater level and pipe water level, and an exchange coefficient. The calculation of variably saturated flow is carried out using MIKE-SHE [DHI, 017b], where variably saturated flow is reduced to one spatial dimension. Kidmose et al. [2015] found that infiltration can exceed exfiltration by a few orders of magnitude. Maximum infiltration rates for pipe segments with a length of approximately 50 m reached 800 l/day and maximum exfiltration rates reached 50 l/day. The presence of a colmation layer for pipe exfiltration was not regarded in that study.

In the above listed studies, the conceptualization of pipe flow, variably saturated flow, and GW flow differs. In some approaches, flow processes are calculated in a coupled and physically-based manner, while other approaches neglect certain processes or use simplified empirical and decoupled models. The used flow processes and type of model (simplified or

physically-based) of the most complex models used in above listed studies are summarized in Table 1.1.

At present time, no physically-based modeling approach incorporating one-dimensional pipe flow and three-dimensional saturated-unsaturated flow for the approximation of pipe leakage (groundwater infiltration and sewer exfiltration) exists. In this dissertation, a newly developed unique model for physically based three-dimensional pipe leakage modeling in a variably saturated subsurface will be applied to case studies as large as urban subcatchment scale. Further, the present study presents a novel method to upscale pipe leakage, which enables to simulate pipe leakage through numerous pipe defects with significantly reduced computational cost. Last, the model is used in order to investigate the pipe leakage process, and in order to investigate the impact of pipe leakage on urban GW.

1.4 Contributions of the present dissertation

The present dissertation aims at understanding the pipe leakage process and contributing to solving the problems caused by pipe leakage described in section 1.1. The described work is based on prior studies on pipe leakage described in sections 1.2 and 1.3. The present section serves the purpose to list the main contributions of the present dissertation.

- A contribution of the present dissertation is the generation of a novel physically-based model for the simulation of pipe leakage in variably saturated soil. A physically-based pipe flow model is coupled with a physically-based unsaturated-saturated flow model. The newly implemented coupling scheme is based on a cost-effective bidirectional data transfer using a shared-memory. The coupling is based on updating of boundary conditions and source terms. Leakage flux is calculated based on hydraulic properties of the colmation layer and the gradient of hydraulic potential in the colmation layer. This model is the first of its kind at present time, because it calculates one-dimensional pipe flow, three-dimensional unsaturated-saturated flow, and pipe leakage in a physically-based manner. In comparison, pipe leakage models described in prior studies (as listed in section 1.3) are simplified by e.g. neglecting time-dependent pipe flow, neglecting variably saturated flow or reducing variably saturated flow to one spatial dimension.

The newly developed pipe leakage model is successfully validated and verified using a novel benchmark library for pipe leakage consisting of in total four benchmark cases. Two benchmark cases are based on physical experiments describing one-dimensional pipe water exfiltration with both, constant and variable pipe water level. Remaining two benchmark cases are based on two newly developed analytical models describ-

Table 1.1: Conceptualization of flow processes in pipe leakage models from previous studies.

Simulated processes → ↓ Authors	Pipe flow	Variably saturated flow	GW flow	Pipe leakage
Reichel and Getta [2008]	-	-	✓ ^{2D,S}	Leakage factor
Boukhemacha et al. [2015]	-	-	✓ ^{2D,S}	Leakage factor
Tubau et al. [2017]	-	-	✓ ^{3D,S}	Estimated from field measurements
Gogu et al. [2017]	-	-	✓ ^{3D,S}	Leakage factor
Iwalewa et al. [2016]	-	✓ ^{1D,T}	✓ ^{2D,T}	Estimated
Sommer et al. [2009]	✓ ^{1D,T}	-	✓ ^{3D,T}	Darcy's law
Shaad and Burlando [2018]	-	✓ ^{3D,T}	✓ ^{2D,T}	Estimated
Mohrlök et al. [2008]	-	✓ ^{3D,T}	✓ ^{3D,T}	Direct
Ly and Chui [2012]	-	✓ ^{2D,T}	✓ ^{2D,T}	Leakage factor
Bhaskar et al. [2015]	-	✓ ^{3D,T}	✓ ^{3D,T}	Estimated from field measurements
Vizintin et al. [2009]	✓ ^{1D,S}	✓ ^{0D,S}	✓ ^{3D,S}	Darcy's law
Thorndahl et al. [2016a]	✓ ^{1D,T}	✓ ^{0D,T}	✓ ^{3D,T}	Leakage factor
Kidmose et al. [2015]	✓ ^{1D,T}	✓ ^{1D,T}	✓ ^{3D,T}	Leakage factor
present study	✓ ^{1D,T}	✓ ^{3D,T}	✓ ^{3D,T}	Direct, Leakage function

^{0-3D} Spatial dimension

^S Steady-state, ^T transient

Direct - Calculation of leakage using dynamically calculated hydraulic gradient and saturation-dependent hydraulic properties of the soil in the vicinity of the pipe defect.

ing steady-state pipe water exfiltration into both, a one-dimensional vertical aquifer, and a two-dimensional horizontal aquifer.

- Another contribution of the present dissertation is the development of a novel method for upscaling pipe leakage. This upscaling enables a significant reduction of local refinement of spatial discretization around (otherwise strongly refined) pipe defects. The upscaling is based on transfer functions describing leakage flux through the colmation layer as a nonlinear function of pipe water level and soil water pressure below the colmation layer. Transfer functions are derived using a series of fully discretized single pipe defect simulations. In total two transfer functions describing both, sewer leakage, and stormwater pipe leakage are presented in the present dissertation. Accuracy and time efficiency of the upscaling is demonstrated by comparing results from a fully discretized model and a model using the upscaling. The upscaled model is successfully applied on a model setup representing a leaky sewer pipe with 30 pipe defects and a model setup representing a stormwater pipe network in an urban catchment with 1211 pipe defects.
- Another contribution of the present dissertation is the application of the leakage model on a setup representing a leaky sewer pipe of 30 m length in order to investigate the pipe leakage process. One finding is, that, for a given pipe water level, pipe water exfiltration converges as soil water pressures become more negative. Although such a hydraulic disconnection is well described for surface water-groundwater interaction [e.g. Brunner et al., 2009], it is firstly described for pipe water-groundwater interaction in the present dissertation.

Further, it is found that intensity and duration of pipe flow events have a large impact on pipe leakage, while the temporal distribution of pipe flow is irrelevant.

- The final contribution of the present dissertation is the application of the leakage model on a setup representing leaky stormwater pipes in an urban subcatchment in order to investigate the impact of stormwater pipe leakage on urban GW. In a series of simulations with setups representing pipe systems of different conditions (from small pipe defects to large pipe defects), the impact of leakage on urban GW under dry-weather flow conditions is investigated. It is found that stormwater pipe leakage may be in the order of effective GW recharge and that it may lower local GW levels by several meters. In another study on rainfall-driven stormwater pipe leakage, the leakage response on return period and temporal distribution of rain events is investigated.

2 Numerical model for pipe leakage

This chapter describes the newly developed coupled model for pipe leakage including the novel coupling framework and model validation and verification. Parts of the work in this chapter have been published in Peche et al. [2017] and Peche et al. [2018].

2.1 Objective

A newly developed model for pipe leakage is described. This chapter has two key objectives.

- The first objective is to describe the newly developed numerical model for pipe leakage, including its constituents, governing equations, and coupling strategy.
- The second objective is to present the validation and verification of the newly developed leakage model with a novel benchmark library for pipe leakage models. This library consists of in total 4 benchmark cases including two benchmarks derived from physical experiments, and another two benchmarks based on newly developed analytical solutions.

2.2 OpenGeoSys (OGS)

OGS is an open-source multiphysics modelling software, which can be used to simulate THMC (thermal, hydraulic, mechanical, and chemical) processes for geological and hydrological applications [Kolditz et al., 2012a]. OGS is associated with a wide range of applications, such as thermomechanical heat storage for geothermal reservoir engineering applications [Lehmann et al., 2017], variable density-driven flow for coastal aquifer management [Walther et al., 2012], and clay deformation for nuclear waste disposal applications [Zieffle et al., 2017]. The software has been thoroughly benchmarked by Kolditz et al. [2012b, 2015, 2016, 2018].

In OGS, fully and variably saturated porous medium flow is calculated with the Richards' equation [Richards, 1931]. Richards' equation is formulated in a form that depends only

on water pressure as a primary variable [Kolditz et al., 2012b]:

$$\phi\rho\frac{\partial S}{\partial p}\frac{\partial p}{\partial t} - \nabla \cdot \left[\rho\frac{\kappa\kappa_r}{\mu}(\nabla p - \rho g) \right] = \frac{\rho \cdot Q}{V_{\text{unit}}} \quad (2.1)$$

where ϕ [-] is porosity, ρ [M L⁻³] is fluid density, S [-] is water saturation, p [M L⁻¹ T⁻²] is water pressure, t [T] is time, ∇ [L⁻¹] is nabla operator, κ_r [-] is relative permeability, κ [L²] is intrinsic permeability, which is related to saturated hydraulic conductivity K_s [L T⁻¹] in the form of $K_s = \kappa\rho g/\mu$, where g [L T⁻²] is gravitational acceleration, and μ [M L⁻¹ T⁻¹] is fluid dynamic viscosity. Q [L³ T⁻¹] is a source term and V_{unit} [L³] is unit volume. In OGS, the centered Galerkin finite element method (FEM) is used to discretize Richards' equation. Time integration is carried out using an implicit scheme and the Newton-Raphson scheme [e.g. Wriggers, 2008] or the Picard method [Celia et al., 1990] is used to linearize the nonlinear system of equations. The soil retention curve in form of a capillary pressure-saturation relationship is parameterized using van Genuchten's closed form [van Genuchten, 1980]:

$$-p = \frac{\rho \cdot g}{\alpha} \left[S_e^{\frac{-1}{m}} - 1 \right]^{\frac{1}{n}} \quad m = 1 - (n^{-1}) \quad (2.2)$$

where α [L⁻¹] is the inverse of capillary rise, m and n [-] are pore size distribution parameters. The effective saturation S_e [-] reads

$$S_e = \frac{S - S_r}{S_m - S_r} \quad (2.3)$$

where S_r [-] is residual saturation, and S_m [-] is maximum saturation. That parametrization leads to the following formulation for relative permeability

$$\kappa_r = S_e^{1/2} \left[1 - (1 - S_e^{1/m})^m \right]^2 \quad (2.4)$$

An exemplary retention curve and relative permeability function are given in the Appendix as Figure 7.2. A program code for an exemplary numerical model solving Richards' equation with van Genuchten parametrization, and linearized with a Newton-Raphson scheme, is given in the Appendix as source code 7.1. This exemplary code solves the problem presented by Celia et al. [1990].

2.3 HYSTEM-EXTRAN (HE)

HE is a hydrological-hydrodynamic model, which can be used to compute urban flow processes such as pipe flow. HE consists of two coupled modules. The module HYSTEM

calculates the effective rainfall and the time-dependent flow into a pipe network. Another module, called EXTRAN, calculates the flow in the pipe network [Jahanbazi and Egger, 2014]. HE is associated with applications such as real-time control of sewer pipe networks [Fuchs et al., 1997; Fuchs and Beeneken, 2005], dimensioning of pipe networks, and flood risk management [Sommer et al., 2009].

In HE, pipe flow is modelled as open channel flow. Pressurized pipe flow is transformed into free surface flow using a Preissmann slot [Preissmann, 1961] or an iterative approach. Pipe flow is calculated with HE using the complete 1D Saint-Venant equations [de Saint-Venant, 1871] and solved with a finite volume method. The governing equations which consist of the continuity equation (2.5) and equation of motion (2.6) are

$$\frac{\partial A}{\partial t} + \frac{\partial(v \cdot A)}{\partial x} = \frac{Q}{\Delta x} \quad (2.5)$$

$$\frac{1}{g} \frac{\partial v}{\partial t} + \frac{v}{g} \frac{\partial v}{\partial x} + \frac{\partial H_{PW}}{\partial x} = I_s - I_r \quad (2.6)$$

where A [L^2] is cross-sectional surface area, v [$L T^{-1}$] is flow velocity, x [L] is spatial coordinate, Q [$L^3 T^{-1}$] is a source term, Δx [L] is pipe length, H_{PW} [L] is pipe water level, I_s [-] is bottom slope, and I_r [-] is friction slope that is parameterized using the Darcy-Weißbach equation in combination with the Prandtl-Colebrook friction law [itwh, 2010].

2.4 The new OGS-HE platform

A novel contribution of this dissertation is the implementation of the OGS (version 5) extension for a non-iterative model coupling between the two C based codes OGS (C++) and HE [version 7.7 or newer] (C++, C#). This coupling strategy enables the generation of a physically-based urban subsurface flow model. The aim of this coupling is to reproduce water exchange between the subsurface and the pipe network in a realistic fashion. A schematical visualization of the conceptual model is given in Figure 2.1.

The coupling is based on timestep-wise updating of boundary conditions and source terms. Two non-iterative coupling strategies (based on exchange of model results) are implemented as part of the present study. Both coupling strategies enable to simulate the leakage process in the form of infiltration and exfiltration.

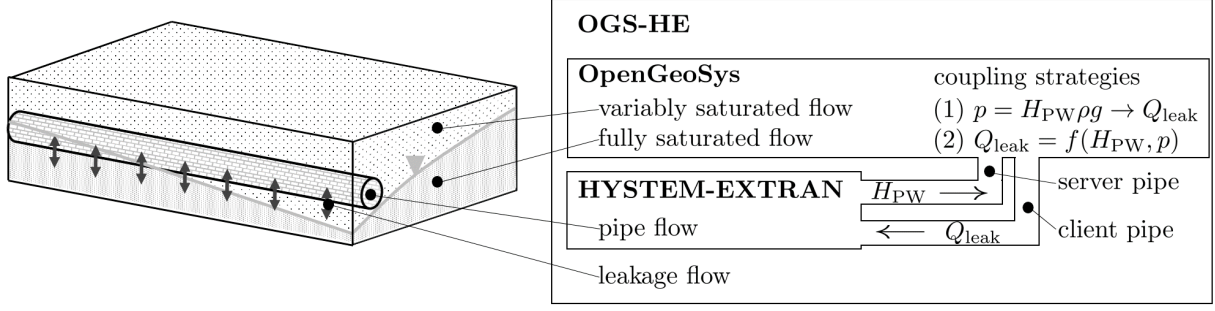


Figure 2.1: Conceptual model of OGS-HE incorporating variably saturated porous media flow, pipe flow and leakage.

The first coupling strategy [(1) in Figure 2.1] includes conversion of the HE-calculated pipe water level H_{PW} into a hydrostatic pressure p , which is then imposed as Dirichlet boundary condition on top of the the colmatation layer in OGS. The pressure p is then determined using $p = \rho \cdot g \cdot H_{PW}$. Subsequent simulation of variably saturated flow using Eq. (2.1) gives the pressure distribution that is used to calculate the source term Q_{leak} . The calculated Q_{leak} is processed back to HE by replacing the source term Q in Eq. (2.5). Q_{leak} in Eq. (2.1) is zero in this case of coupling strategy (1). This coupling strategy (1) has been used for single defect simulations since it requires a detailed spatial discretization around the particular pipe defect and colmatation layer, and therefore leads to high CPU load.

The second coupling strategy [(2) in Figure 2.1] enables to omit the fine spatial discretization of pipe defect and colmatation layer, such that the CPU load is significantly reduced. That strategy is based on the use of leakage functions as described in chapter 3. These functions empirically relate the pipe water level H_{PW} calculated with HE and the water pressure p below the colmatation layer calculated with OGS directly to the leakage flow Q_{leak} through the colmatation layer bottom in a form

$$Q_{leak} = f(H_{PW}, p) \quad (2.7)$$

The calculated Q_{leak} is subsequently implemented as a source or a sink term in both codes, OGS and HE, respectively. This leads to a replacement of the source term Q with Q_{leak} in Eq. (2.1) and Eq. (2.5). The coupling between both codes is realized using the Windows based interprocess communication method called ‘Named Pipes’. That ‘First in First out’ (FiFo) method is considered as a cost-effective and easy-to-implement in-memory push-migration solution [Laszewski and Nauduri, 2012]. In detail, a server program creates one or more Named Pipes and assigns a data sequence in a hierarchical order to each pipe. A client program connects to the one or more Named Pipes and is able to access the data

one-by-one according to the given order. That shared-memory based interprocess communication enables a bidirectional data transfer. This form of interprocess communication is not file-based, hence writing and reading text files is not necessary, which is highly efficient regarding CPU load. Exemplary source code for interprocess data transfer between two C++-based programs is given in the Appendix as source code 7.2.

Regarding the present model coupling, HE acts as a server and OGS as a client for bidirectional communication within a total of two Named Pipes (Figure 2.1). At initialization, HE calls OGS and the Named Pipes are created and connected. During the simulation, HE-calculated water levels are transferred to OGS where they are used to update boundary conditions and source or sink terms. OGS calculates the corresponding leakage flow, which is transferred back to HE and used as a source or sink term in the next timestep. A flowchart of the main processes and decisions is given in Figure 2.2. In the remainder of the present manuscript, the coupled model will be referred to as OGS-HE. The extended version of OGS (version 5) can be downloaded from the custom branch available at <https://github.com/APeche/OGS-HYSTEM-EXTRAN.git>.

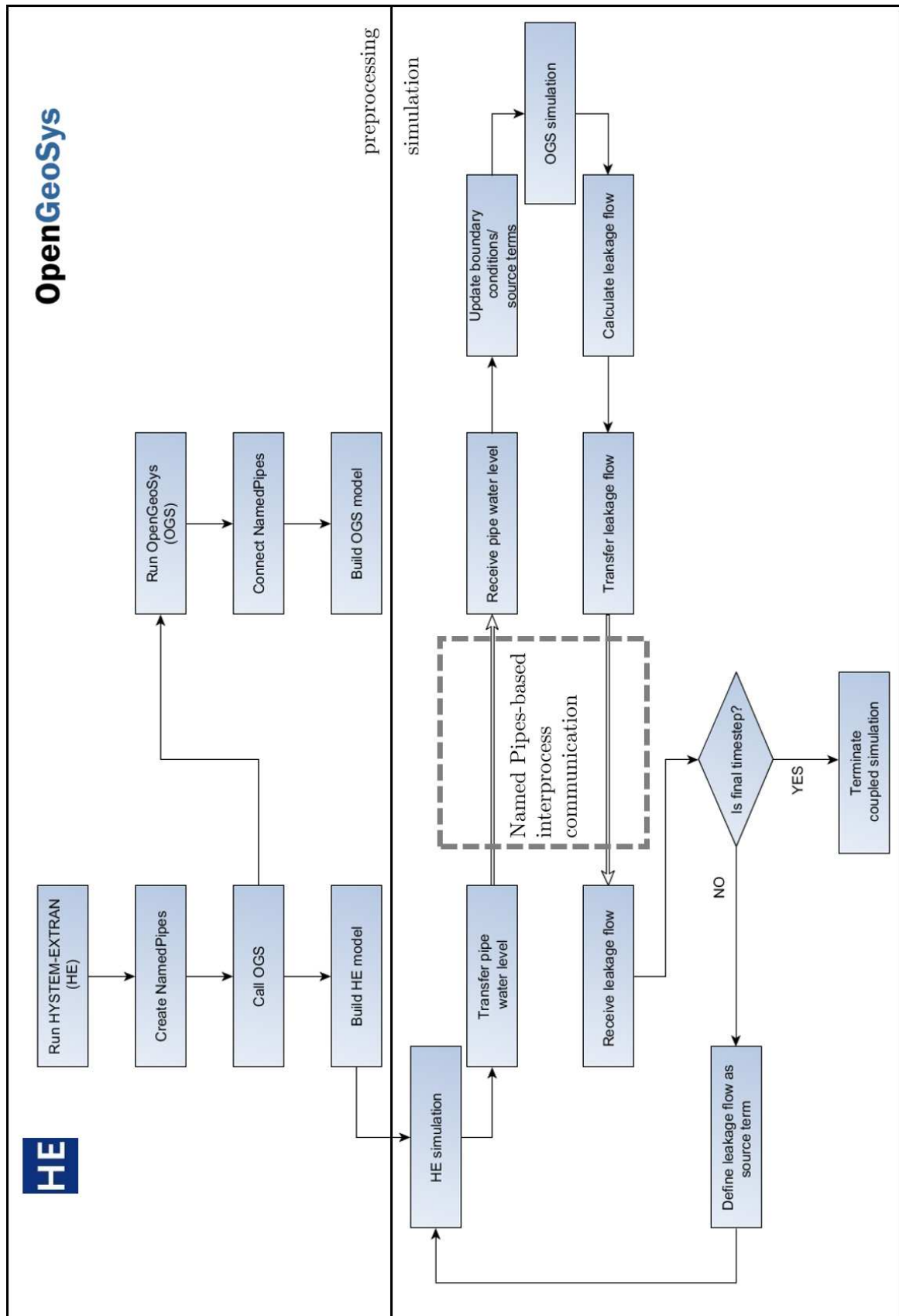


Figure 2.2: Flowchart of OGS-HE.

2.5 Verification and validation of OGS-HE

The following sections serve the purpose to demonstrate that the interprocess data transfer (between OGS and HE) and updating of Dirichlet-type boundary conditions are correctly implemented. Both numerical simulators, OGS and HE, are widely used in practice and well tested for result accuracy. An extensive validation of the Richards flow process implemented in OGS is given in Kolditz et al. [2012b]. Pipe flow in HE is based on the open-source pipe flow platform SWMM [Gironás et al., 2009]. Result accuracy of SWMM is ensured with a quality assurance program [Rossman, 2006]. Verification and validation examples for OGS-HE include two newly developed analytical solutions and two examples based on observations from two physical experiments [Skaggs et al., 1970; Siriwardene et al., 2007]. All benchmark examples were chosen according to their relevance for pipe leakage.

Benchmark 1: Analytical solution of stationary constant water level-driven infiltration into a horizontally layered soil column

Brunner et al. [2009] proposed a one-dimensional analytical model for surface water-groundwater interaction. That analytical model can be modified such that it is a broad approximation of pipe leakage into a horizontally layered soil, where a pipe defect is located above a colmation layer overlaying the aquifer strata. An analytical solution used for the validation of OGS-HE can be derived with a modified setup of that model. The setup of the analytical model is visualized in Figure 2.3(a). Flow is driven by a Dirichlet boundary condition of constant pressure at the domain bottom and a constant pipe water level at the domain top. Assuming a constant cross-sectional area and volume conservation results in the same specific discharge through the fully saturated colmation layer q_1 [L T⁻¹] and the fully saturated part of the aquifer strata q_2 as

$$q_1 = q_2 \quad (2.8)$$

Assuming linear pressure profiles, reformulation using Darcy's law results in

$$-K_c \frac{(H_{PW} + h_c - p_{\text{int}} \cdot (\rho g)^{-1} + 0)}{h_c} = -K_a \frac{(p_{\text{int}} \cdot (\rho g)^{-1} + h_w - 0 + 0)}{h_w} \quad (2.9)$$

where K_c and K_a [L T⁻¹] are hydraulic conductivities of colmation layer and aquifer strata at full saturation, respectively, h_c [L] is colmation layer thickness, p_{int} [M L⁻¹ T⁻²] is pressure at the colmation layer interface, and h_w [L] is the thickness of the saturation front in the aquifer strata. Eq. (2.9) can be reformulated to a form that describes p_{int} as

Table 2.1: Benchmark 1: Material hydraulic parameters and fluid properties.

soil properties						
	α [m^{-1}]	m [-]	κ [m^2]	S_r [-]	S_s [-]	ϕ [-]
aquifer strata	3	0.56	$4.1297 \cdot 10^{-12}$	0.14	1	0.41
colmation layer	3	0.47	$1.3052 \cdot 10^{-12}$	0.16	1	0.41
fluid properties						
ρ [$kg\ m^{-3}$]	1000					
μ [$kg\ m^{-1}\ s^{-1}$]	0.001					

a function of H_{PW} and h_w :

$$p_{\text{int}} = \left(\left[\left(\frac{K_c h_w}{h_c K_a} (H_{PW} + h_c) \right) - h_w \right] \left(1 + \frac{K_c h_w}{h_c K_a} \right)^{-1} \right) \cdot \rho g \quad (2.10)$$

The setup of the numerical model is visualized in Figure 2.3(b). The pipe flow model represents a pipe of 30 m length. Pipe flow was controlled by an upstream Dirichlet-type boundary condition, where H_{PW} was either 0.07 m or 0.5 m. Downstream boundary condition of the pipe flow model was set as free outflow boundary condition. It should be noted that the details of the pipe flow setup are irrelevant as long as they lead to a fixed and known water level above the pipe defect. This is the case in the present examples.

Geometry and spatial discretization of the porous subsurface model are given in Figure 2.3(b). The steady-state was calculated using different bottom boundary conditions regulated by p_{bot} (band width $-6000\text{ Pa} < p_{\text{bot}} < -50\text{ Pa}$). The initial condition was pre-calculated until steady-state pressure distribution based on a similar setup with a constant global pressure of -100 Pa . Material properties of aquifer strata and colmation layer represent sandy loam and loamy sand, respectively. Parameters originate from Carsel and Parrish [1988] and Roth [2006] and are given in Table 2.1, where α and m are parameters of the van Genuchten parametrization and S_r and S_s [-] are residual and maximal saturation, respectively. Fluid properties are also given in Table 2.1. Varying H_{PW} and p_{bot} enabled a variation of h_w and thus leads to a different result of p_{int} , which was then compared with the analytical solution. Clearly, results agree well with the analytical solution as shown in Figure 2.3(c).

Benchmark 2: Physical experiment of transient, constant water level-driven infiltration into a homogeneous soil column

Skaggs et al. [1970] presented a physical experiment, which describes one-dimensional infiltration into an initially dry soil column. In that experiment, infiltration was driven by keeping a constant water table on top of the soil column. Skaggs et al. [1970] measured the infiltration rate and depth of the wetting front over a time interval of 90 minutes. That experiment was numerically reproduced using OGS-HE, where infiltration is driven by a time-constant pipe water level. The domain of the pipe flow model is similar to the one described in section 2.5. The upstream boundary was set to the Dirichlet-type boundary condition $H_{PW} = 0.0075$ m. The downstream boundary of the pipe flow model was assigned as free outflow boundary condition.

Initial condition, boundary conditions, temporal and spatial discretization as well as material properties of the porous subsurface model are given in Figure 2.4(a). Values for retention curve and relative conductivity curve are taken from Tian and Liu [2011] and Vogel [1987] and are given in Table 2.2. Fluid properties of $\rho = 999.7$ kg m⁻³ and $\mu = 0.00125$ kg m⁻¹ s⁻¹ are used. A detailed description of a numerical model setup for the reproduction of the physical experiment is given in Vogel [1987]. Again, numerical results agree well with the observed data, and are given in Figure 2.4(b).

Benchmark 3: Physical experiment of transient, variable water level-driven infiltration into a homogeneous soil column

In the physical experiment conducted by Siriwardene et al. [2007], a column was filled with a sand layer and a gravel layer on top. Water levels were varied in the gravel layer. The gravel layer was filled such that a water column of 0.75 m was on top of the sand-gravel-interface. Then, the column was drained such that water levels above the sand-gravel-interface continually decreased to a minimum of 0.05 m. Siriwardene et al. [2007] conducted a total of 14 refill-drainage cycles over a time interval of approximately 24 hours, and continuously measured the outflow at the bottom of the column.

In the one-dimensional OGS-HE numerical model, the sand-gravel-interface represents the pipe defect. This defect is located in a pipe flow model domain similar to the model domain described in section 2.5. Refill-drainage cycles have been reproduced using a time-variable Dirichlet-type boundary condition located at the upstream boundary of the pipe flow model. H_{PW} was regulated according to Siriwardene et al. [2007], representing water levels between 0.05 m and 0.75 m. The downstream boundary condition of the pipe flow model was set as free outflow boundary condition.

Table 2.2: Benchmark 2: Retention curve and relative conductivity function data.

retention curve		relative conductivity function	
S [-]	p_c [Pa]	S [-]	κ_r
0.080	19614.1	0.080	0.001
0.177	9807.1	0.143	0.008
0.243	7845.7	0.286	0.015
0.331	5884.2	0.429	0.030
0.509	3922.8	0.500	0.050
0.757	1961.4	0.571	0.082
0.874	980.7	0.643	0.250
1	0	0.714	0.550
		0.786	0.886
		0.821	0.963
		0.857	0.992
		0.874	0.997
		1	1

The setup of the porous subsurface model in terms of initial condition, boundary conditions, spatial and temporal discretization as well as material properties is given in Figure 2.5. Fluid properties of $\rho = 998.2 \text{ kg m}^{-3}$ and $\mu = 0.001 \text{ kg m}^{-1} \text{ s}^{-1}$ are used. Simulation results were compared to experimental results from Siriwardene et al. [2007] from experiment runtime of 11 to 24 hours and numerical results from Browne et al. [2008]. Clearly, simulation results of OGS-HE agree well with the measured data at late times. At early times, model results show a deviation compared with experimental results, which might be due to the warm-up phase of the physical experiment, which may have an effect on the solution as described by Browne et al. [2008].

Benchmark 4: Analytical solution of stationary constant water level-driven infiltration into a two-dimensional horizontal aquifer

For this verification example, subscripts ‘c’ and ‘a’ represent the colmation layer and the aquifer, respectively. The conceptual model is given in Figure 2.6. One-dimensional flow through the colmation layer is described with Darcy’s law

$$Q_c = -\Delta x_c \cdot b \cdot K_c \cdot \frac{(H_{PW} - \psi_{\text{int}})}{\Delta y_c} \quad (2.11)$$

where Q is flow [L^3T^{-1}], Δx_c is colmation layer width [L], b is thickness [L], K is hydraulic conductivity [LT^{-1}], H_{PW} is pipe water level [L], ψ_{int} is matric potential at the boundary from colmation layer to aquifer [L], and Δy_c is colmation layer length [L]. Radial flow through the aquifer strata is also described with Darcy’s law for radial flow [Rushton, 2004] as

$$Q_a = -\pi \cdot b \cdot K_a \cdot r \cdot \frac{\partial \psi}{\partial r} \quad (2.12)$$

where r is radius of isolines of matric potential [L]. Integration of Eq. (2.12) with regards to $\partial \psi$ (from any circular matric potential isoline in the full saturated part of the aquifer $\psi(r)$ to the matric potential at the wetting front ψ_{wf}) and $\frac{r}{\partial r}$ (from any radius representing a matric potential isoline in the saturated part of the aquifer r to the radius of the wetting front r_{wf}) yields

$$\psi_{\text{wf}} - \psi(r) = \frac{Q_a}{\pi \cdot b \cdot K_a} \ln \left(\frac{r_{\text{wf}}}{r} \right) \quad (2.13)$$

Assuming volume conservation

$$Q_a = Q_c \quad (2.14)$$

a uniform thickness of the aquifer b , a half-circular form of the wetting front, and a matric potential of zero at the wetting front interface enables to reformulate Eq. (2.13) to

$$\psi(r) = \frac{\left(\Delta x_c \cdot K_c \cdot \frac{(H_{PW} - \psi_{\text{int}})}{\Delta y_c}\right)}{\pi \cdot K_a} \cdot \ln\left(\frac{r_{\text{wf}}}{r}\right) \quad (2.15)$$

Eq. (2.15) is used for the verification of the numerical model OGS-HE. The model domain of the pipe flow model is similar to the model domain described in section 2.5. The pipe water level above the defect was kept constant using a Dirichlet-type boundary condition located at the upstream boundary of the pipe flow model. Numerical studies with different pipe water levels of $H_{PW} = 0.1$ m, $H_{PW} = 0.25$ m, and $H_{PW} = 0.5$ m were carried out.

The setup of the porous subsurface model in form of numerical model domain extent, initial condition, and boundary conditions is illustrated in Figure 2.6. Model realizations with a constant aquifer hydraulic conductivity of $K_a = 7.84 \cdot 10^{-7}$ m/s and varying hydraulic conductivities of the colmation layer $K_c = 1/2 \cdot K_a$, $K_c = 1/3 \cdot K_a$, and $K_c = 1/4 \cdot K_a$ were carried out. Van Genuchten parameters of all materials are $\alpha = 14.5 \text{ m}^{-1}$ and $m = 0.627$. Residual and maximum saturation are set to 0.1 and 1, respectively.

The values of ψ_{int} and r_{wf} are taken from numerical simulation results and $\tilde{\mathbf{r}}$ is a vector from $\Delta x/2$ to r_{wf} . The solution $\tilde{\psi}(\tilde{\mathbf{r}})$ is a vector and can be plotted over $\tilde{\mathbf{r}}$ for result visualization. An exemplary result from the numerical model is shown in Figure 2.7. Results in form of ψ_k over $\tilde{\mathbf{r}}$ are shown in Figure 2.8. Clearly, results agree well.

2.6 Conclusions

A newly developed model for pipe leakage is described in this chapter. The model is developed by coupling between a groundwater flow simulator and a pipe flow simulator. Verification and validation of the model is shown with a novel benchmark library for pipe leakage models. Main conclusions of this chapter are:

- A coupled model for the transient three-dimensional pipe leakage problem in variably saturated soil has been developed. The coupling between the two software packages OGS and HE has been realized using a bi-directional shared-memory based coupling strategy. This non-iterative coupling is realized by updating boundary conditions and source terms between the two software packages, which can be seen in the literature for numerous similar problems [e.g. Camporese et al., 2010; Kalbacher et al., 2012; Liu et al., 2016]. Non-iterative coupling strategies are disadvantageous in terms of interdependency, coordination and information flow [Kalbacher et al., 2012]. Additionally, non-iterative coupling strategies may lead to worse numerical stability

and result accuracy compared to iteratively coupled approaches or monolithic approaches [Huang and Yeh, 2009]. However, the successful validation of the present coupled model demonstrates high result accuracy, and the coupling based errors are assumed to be negligible.

In all examples described in this work, pipe leakage volumes are small ($< 1\%$) compared to pipe flow volumes. In case of larger leakage volumes, the proposed non-iterative coupling may not be accurate enough, such that leakage and pipe water levels might not be convergent. The shared-memory based coupling method used in this study is assumed to be strongly beneficial for reducing computation costs, since no data is written or read from files.

- The successful verification and validation of the leakage model with regards to correctness of modified source codes, interprocess data transfer, and updating of boundary conditions has been shown using a novel benchmark library for pipe leakage models. The presented benchmark cases include two newly developed analytical solutions describing stationary pipe leakage for one and two-dimensional problems. Further two benchmark cases are based on physical experiments carried out by Skaggs et al. [1970], and Siriwardene et al. [2007]. Benchmarks based on physical experiments represent both, constant and time-varying pipe water level-driven transient infiltration into a one-dimensional vertical soil column.

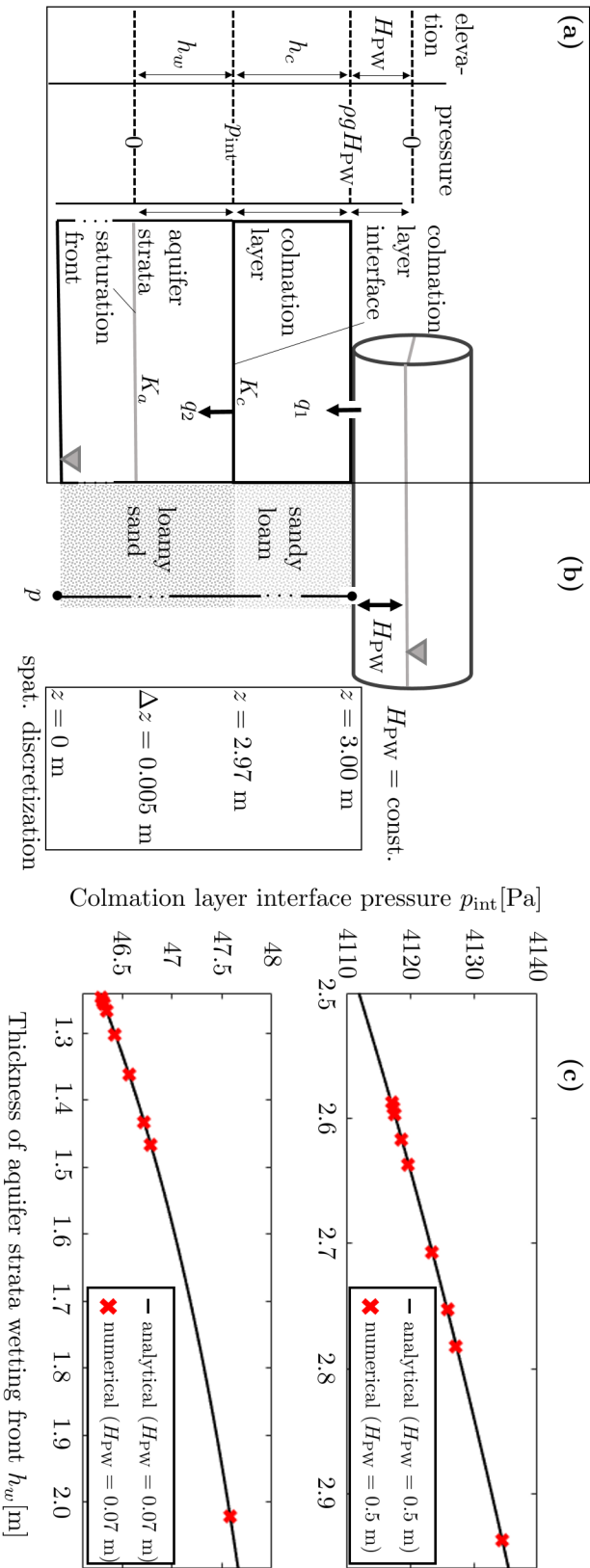


Figure 2.3: Benchmark 1: Comparison of OGS-HE against an analytical solution describing constant pipe water level-driven infiltration into a layered soil column. (a) analytical model modified from Brunner et al. [2009], (b) conceptual model of OGS-HE, (c) verification results.

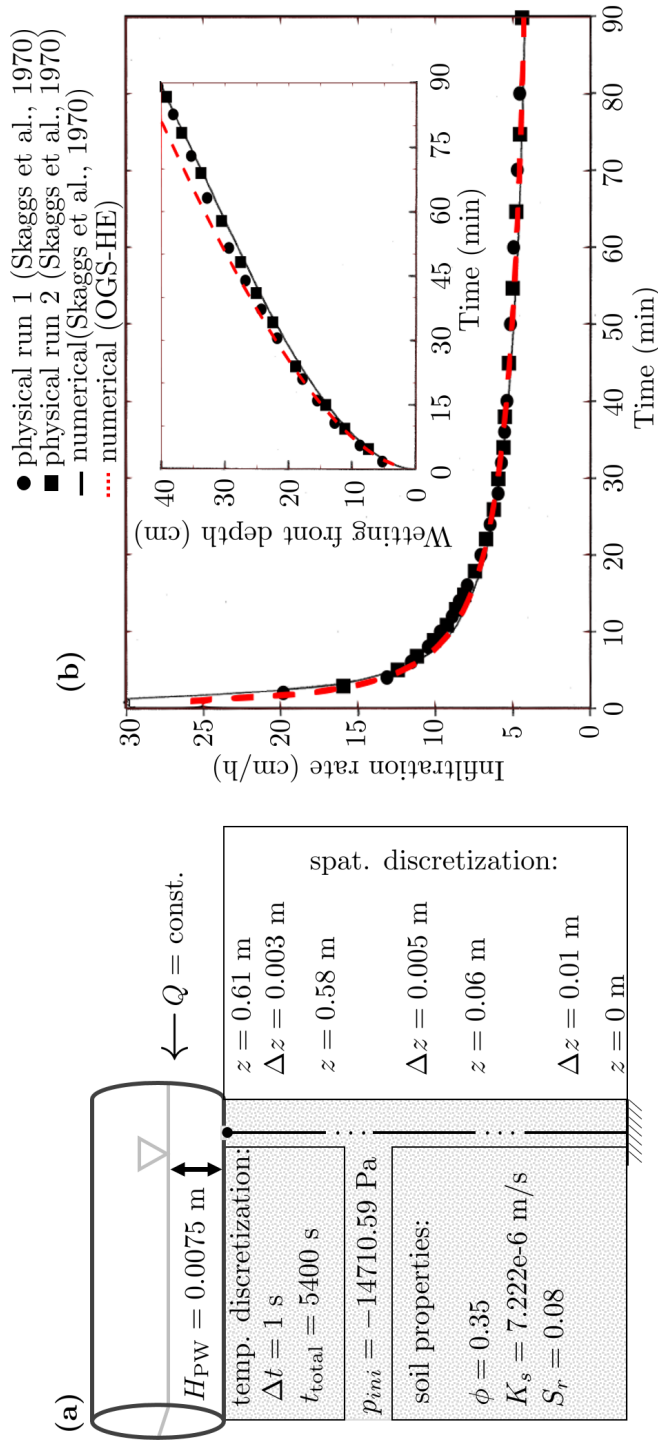


Figure 2.4: Benchmark 2: Comparison of OGS-HE against the physical experiment by Skaggs et al. [1970]: (a) conceptual model of OGS-HE, (b) validation results.

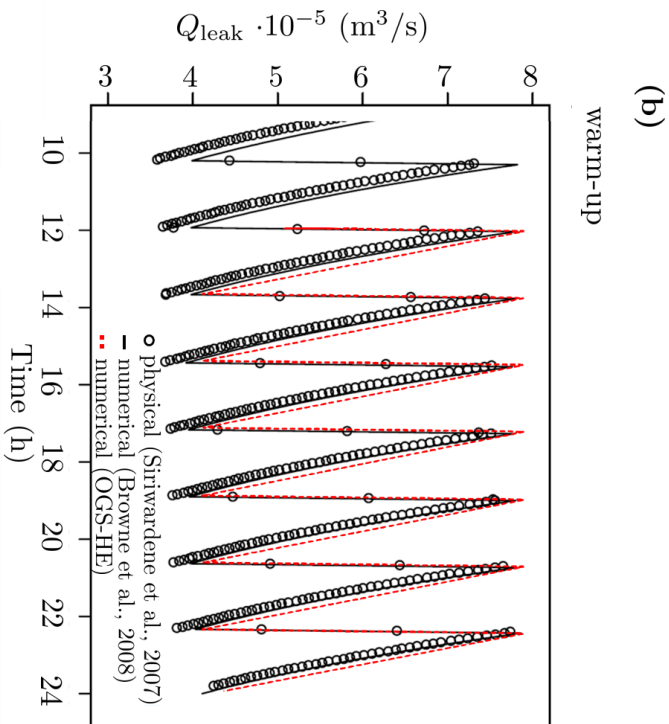
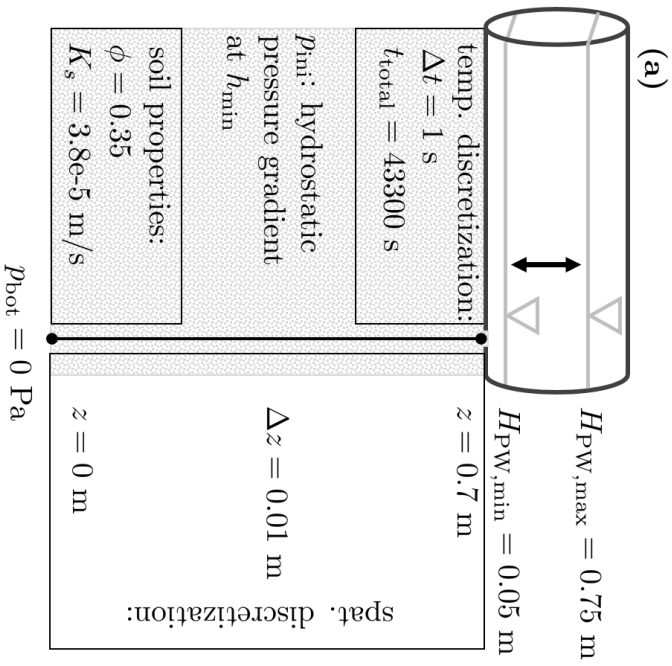


Figure 2.5: Benchmark 3: Comparison of OGS-HE against the physical experiment by Siriwardene et al. [2007]: (a) conceptual model of OGS-HE (b) validation results.

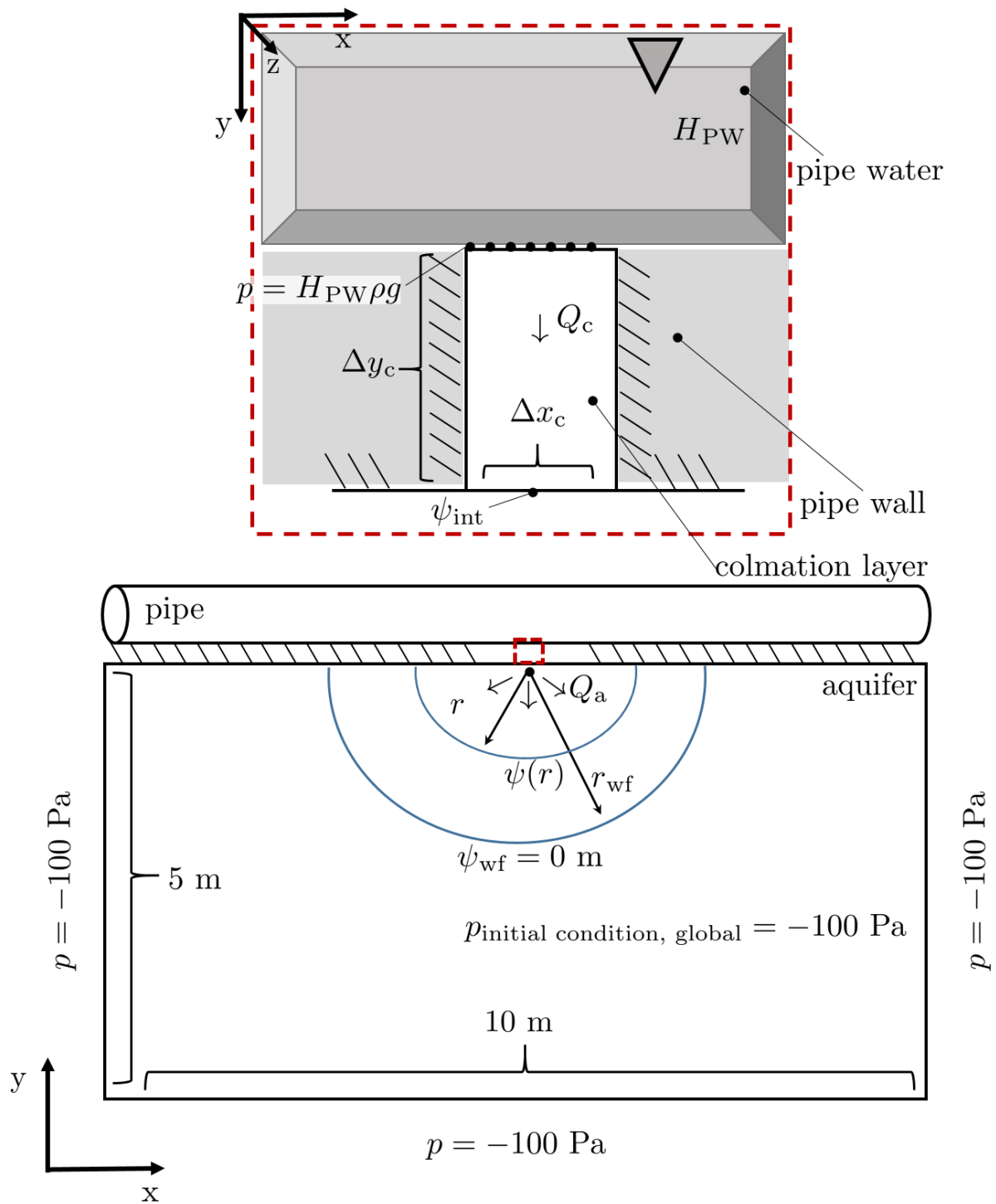


Figure 2.6: Benchmark 4: Conceptual model for the analytical solution and numerical model setup of Benchmark 4.

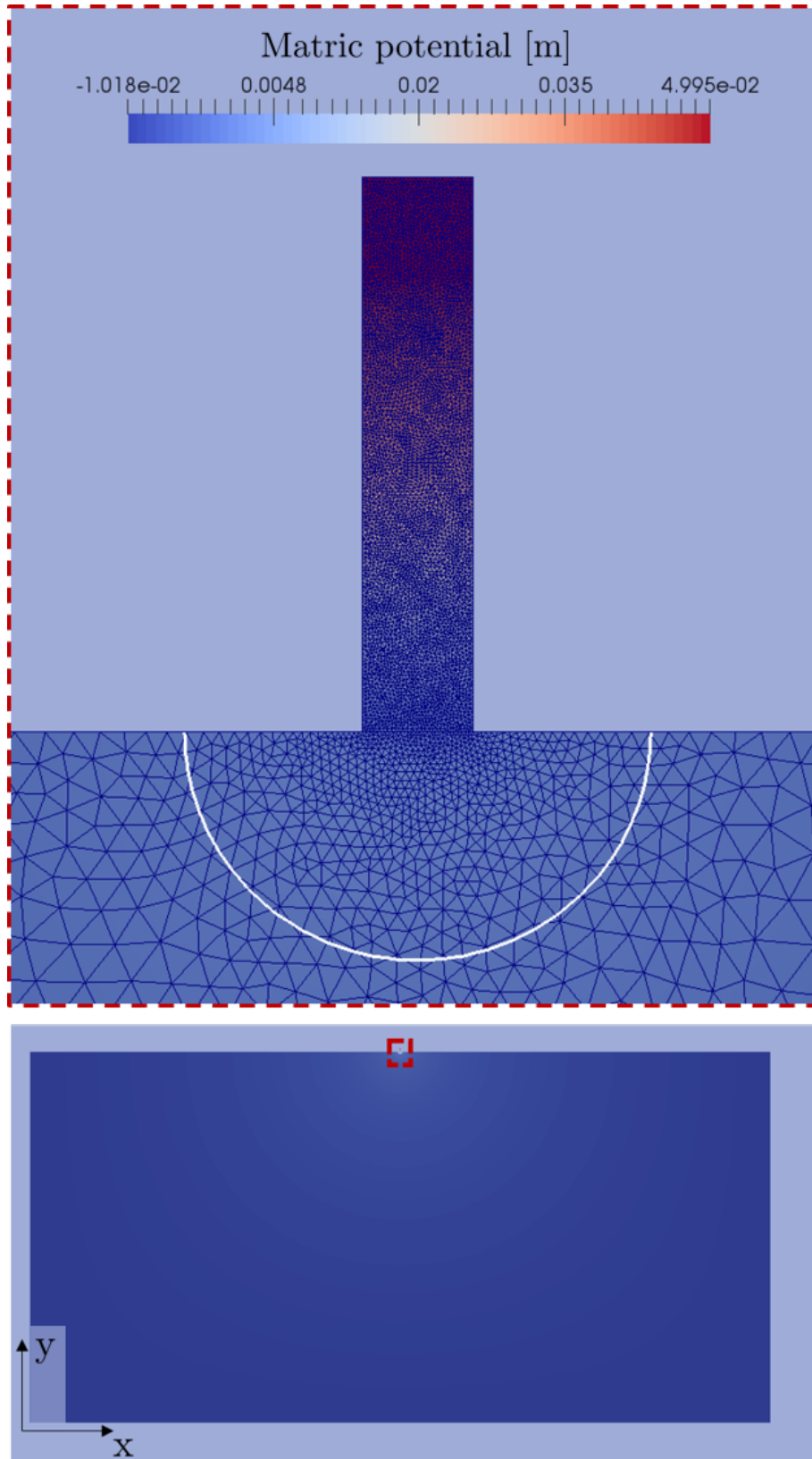


Figure 2.7: Benchmark 4: Spatial discretization and exemplary result of the numerical model for a setup with $H_{PW} = 0.05$ m and $K_a = 7.84 \cdot 10^{-7}$ m/s. The white line represents the wetting front with $\psi_{wf} = 0$ m.

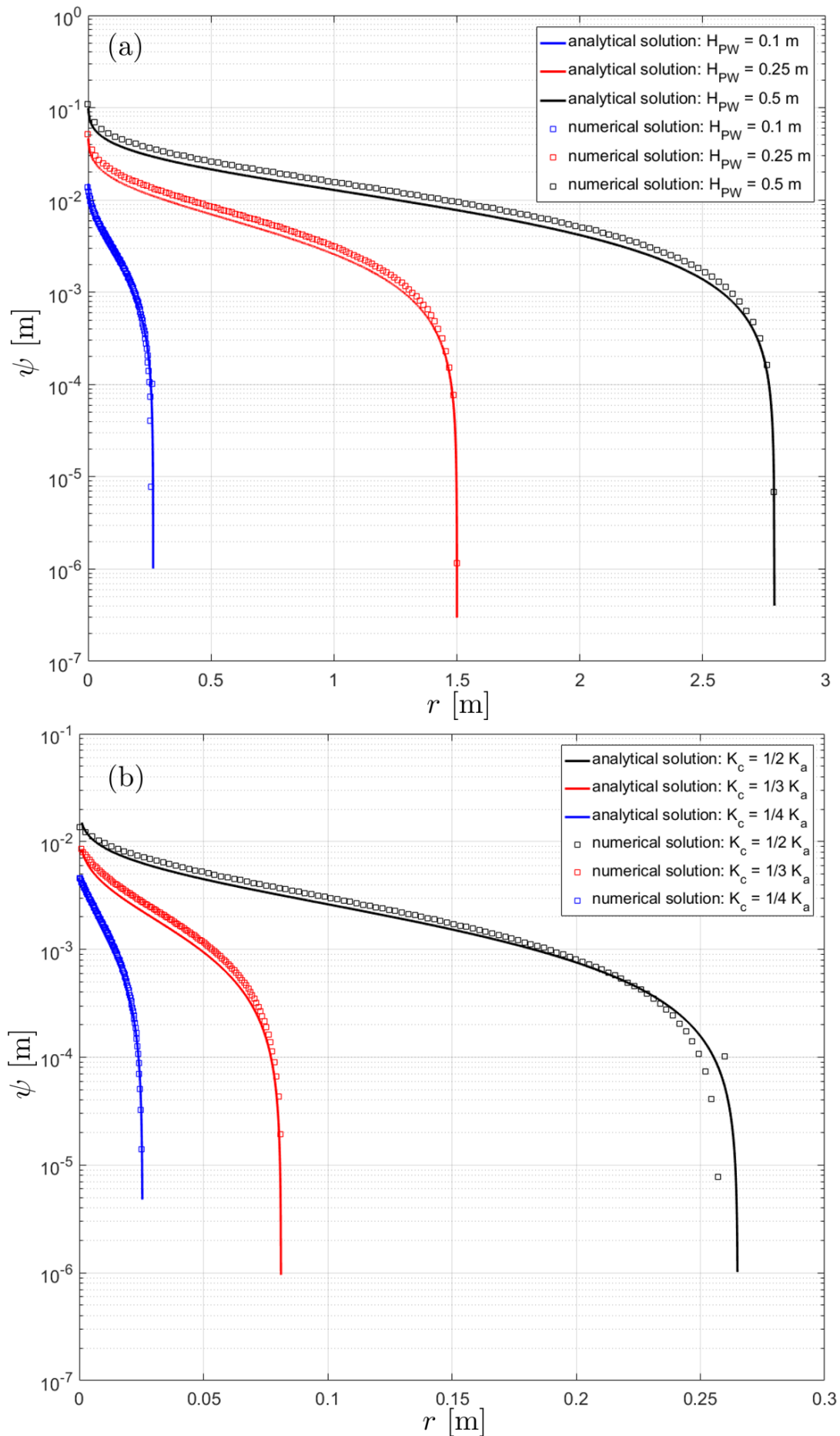


Figure 2.8: Benchmark 4: (a) Numerical and analytical model results for a setup with $K_a = 7.84 \cdot 10^{-7}$ m/s, $K_c = 1/2 \cdot K_a$, and variable H_{PW} . (b) Numerical and analytical model results for a setup with $H_{PW} = 0.1$ m, $K_a = 7.84 \cdot 10^{-7}$ m/s, and variable K_c .

3 Upscaling pipe leakage using leakage functions

This chapter describes a newly developed method for upscaling pipe leakage. Parts of the work in this chapter have been published in Peche et al. [2017] and Peche et al. [2019].

3.1 Objective

A novel method for upscaling pipe leakage is described. This method can be used in order to time-efficiently simulate pipe leakage on a large spatial scale with numerous pipe defects without (otherwise costly) mesh refinement around pipe defects. This chapter has three key objectives.

- First objective is to present the numerical model of a single pipe defect used for the derivation of the upscaling, and to show the simulation results of the single pipe defect model.
- Second objective is to demonstrate the derivation of a functional relationship between pipe water level, soil water pressure and leakage, and its mathematical formulation.
- Third objective is to describe the validation of the modified source code (after implementation of the upscaling) in a model comparison between a fully discretized model and the upscaled model. This model comparison is also used to demonstrate time-efficiency of the upscaling in form of reduced computation time.

3.2 Leakage function

The upscaling is based on leakage functions (LFs), which are derived from a series of transient single pipe defect simulations. The use of a LF enables to omit a spatially refined mesh discretization of colmation layer and pipe vicinity. Several pipe defects can be simulated in one model with a significantly reduced number of mesh elements and computation time. The LF describes flux through the bottom of the colmation layer q_{leak} [L T^{-1}] as a function of mean water pressure at the interface of colmation layer and backfill trench p [$\text{M L}^{-1} \text{T}^{-2}$] and pipe water level H_{PW} [L] as visualized in Figure 3.1. This flux can be

converted to leakage flow for a specific standard defect A_{defect} using $Q_{\text{leak}} = q_{\text{leak}} \cdot A_{\text{defect}}$. The upscaling described in the present dissertation is a continuation of previous work by

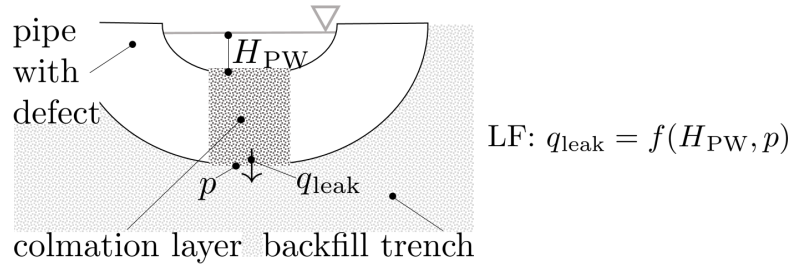


Figure 3.1: Physical meaning of the LF output and input variables q_{leak} , H_{PW} and p .

e.g. DeSilva et al. [2005] and Karpf and Krebs [2011]. Main difference to previous work is that the present upscaling includes the dynamic calculation of water pressure below the colmation layer using a groundwater model. The LF can be applied to a mesh node representing a local pipe defect. Further, the LF can be distributed along a line if only statistical information about pipe defects is available and exact locations of pipe defects are unknown. In that case, the LF assigned to a line represents a statistical standard defect assigned to a certain length of pipe network. Figure 3.2(a) visualizes a locally refined single defect used for the LF derivation. Figure 3.2(b) shows the application of the derived LF to a mesh node, and Figure 3.2(c) visualizes the application of the derived LF along a line. The value for a nodal LF-source term is given in the dimension of $[\text{L}^3 \text{T}^{-1}]$, and the value for a LF-source term assigned along a line is given in the dimension of $[\text{L}^3 \text{T}^{-1} \text{L}^{-1}]$. Clearly, Figures 3.2(b,c) indicate that representing pipe leakage with a LF allows for a much coarser spatial discretization than explicitly simulating leakage [Figure 3.2(a)], thereby significantly reducing CPU load.

A total of two LFs are derived. The first LF represents leakage through a sewer pipe defect and a typical sewer colmation layer. The second LF represents leakage through a storm water pipe defect and typical stormwater pipe colmation layer. The clear distinction between sewer colmation layer and stormwater colmation layer stems from the distinction between sewage and urban stormwater composition leading to different hydraulic properties of colmation layers as described in Section 1.2.

3.3 Conceptual model for leakage function derivation

LFs were derived with a single pipe defect model, for which the mesh is shown in Figure 3.2(a), and the conceptual model is shown in Figure 3.3. The domain of the pipe flow model represents a single pipe of 10 m length. The upstream boundary of the pipe domain was set to a Neumann-type boundary condition of time-variable flow Q_{IN} . The downstream

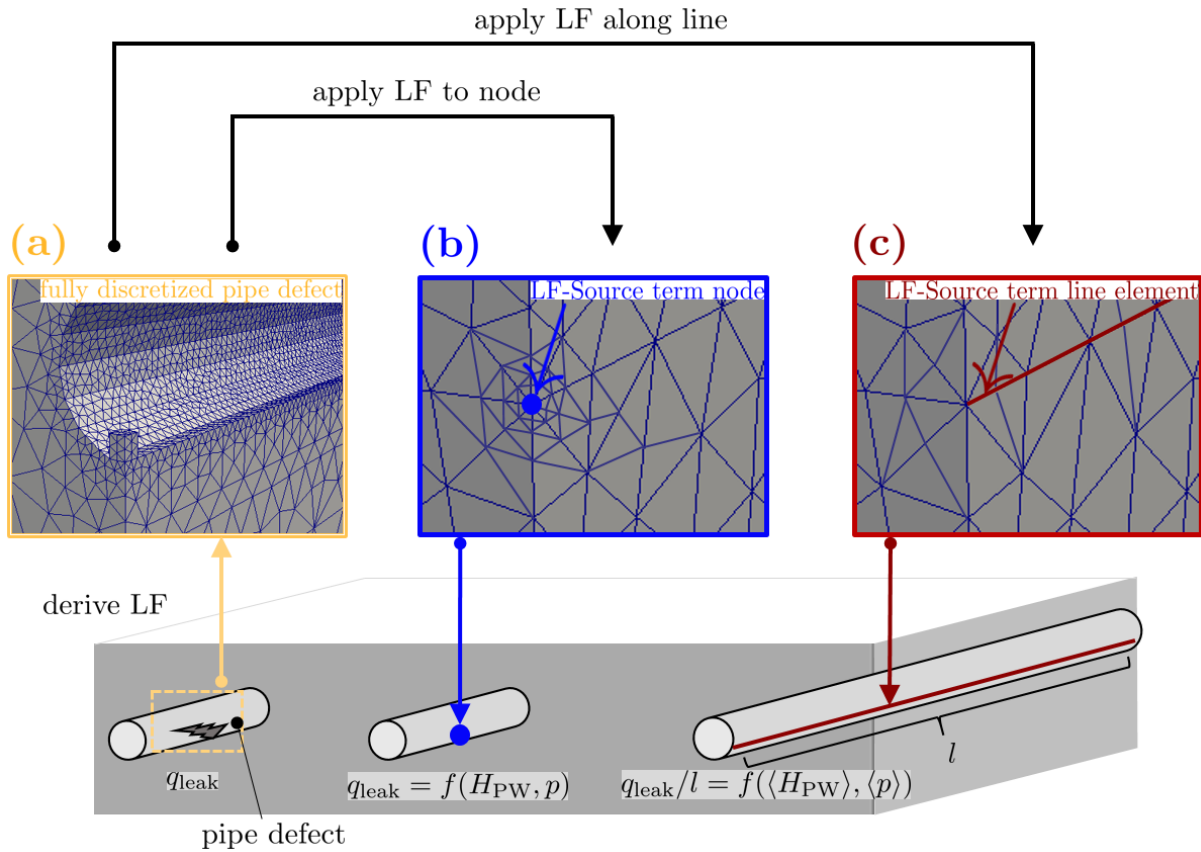


Figure 3.2: Urban subsurface flow domain with a pipe defect located in the dashed box. (a) Fully discretized defect for the LF derivation. (b) Application of the LF as a nodal source term. (c) Application of the LF along a line, where $\langle H_{\text{PW}} \rangle$ and $\langle p \rangle$ are mean values.

boundary was set as free outflow boundary condition. Initial pipe flow was assumed to be dry-weather flow of $0.011 \text{ m}^3/\text{s}$, which results in the dry-weather flow water level of $H_{\text{PW}} = 0.04 \text{ m}$. Due to axis symmetry, the size of the domain representing the isotropic subsurface surrounding the pipe flow model was reduced to a quarter. The value for a Dirichlet-type boundary condition was calculated using the OGS-HE calculated pipe water level located above the defect using $p = \rho g H_{\text{PW}}$ and assigned to the colmation layer surface A_{col} . Size of A_{col} was chosen according to Karpf [2012] who defined this size as quadratic standard defect size for the city of Dresden with a size $4 \cdot A_{\text{col}}$. The domain bottom boundary was set to the Dirichlet-type boundary condition p_{bot} . Pipe wall, domain side as well as top boundaries were set to no-flow (impermeable) Neumann-type boundary conditions. The initial pressure distribution in the subsurface has been pre-calculated representing a steady-state exfiltration at a dry-weather flow water level of $H_{\text{PW}} = 0.04 \text{ m}$. Hydraulic properties of aquifer strata and parameters of pipe backfill trench and colmation layer (for both sewer and storm water pipe colmation layer) in form of retention curve parameters α, m , intrinsic permeability κ and porosity ϕ are given in

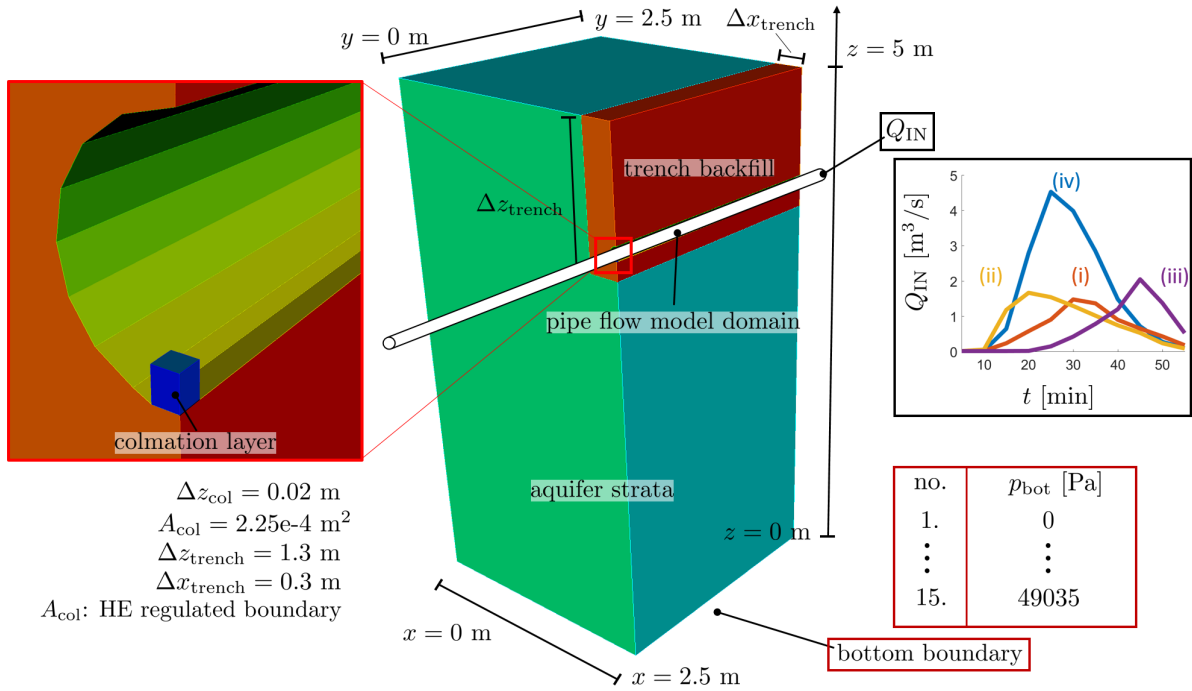


Figure 3.3: Single pipe defect model domain and boundary conditions.

Table 3.1. Hydraulic parameters for the aquifer strata, for a typical backfill sand used in Germany and for both colmation layers are taken from Carsel and Parrish [1988] and Karpf [2012]. κ for the sewage and storm water colmation layer were approximated from Karpf [2012] and Le Coustumer et al. [2012], respectively. Fluid properties at $T = 10^\circ\text{C}$ are also listed in Table 3.1.

Table 3.1: Material hydraulic parameters and fluid properties for the single pipe defect domain.

soil properties	van Genuchten α [m^{-1}]	van Genuchten m [-]	intrinsic permeability κ [m^2]	porosity ϕ [-]
aquifer strata	14.5	0.627	$1.3312 \cdot 10^{-11}$	0.1
trench backfill	14.5	0.627	$7.9902 \cdot 10^{-11}$	0.14
sewage colmation layer	2	0.291	$1.3317 \cdot 10^{-14}$	0.02
storm water colm. layer	2	0.291	$1.3317 \cdot 10^{-12}$	0.02
fluid properties				
ρ [kg m^{-3}]	999.7			
μ [$\text{kg m}^{-1} \text{s}^{-1}$]	$1.306 \cdot 10^{-3}$			

A total of four model sets have been defined, each representing a scenario with a different upstream pipe flow Q_{IN} : (i) a normally distributed event, (ii) an early peak event, (iii) a late peak event, and (iv) a normally distributed event with a large peak as shown in Figure 3.3. Resulting water levels above the pipe defect are given in the Appendix in Figure 7.3. Corresponding pipe water levels above the defect are given in Figure 7.4. Within each

event, 15 simulations have been realized, giving a total of 120 simulations for the two setups with different colmation layer properties. In each of the 15 different simulations, the groundwater level (regulated by p_{bot}) was varied representing groundwater levels below, at or above the pipe defect. A larger number of simulations with groundwater tables in the vicinity of the defect was conducted in order to capture the highly nonlinear dependency of p , H_{PW} and q_{leak} for such groundwater tables. Values for p_{bot} are listed in Table 7.1.

Prior to simulating, a spatial grid convergence study for the single pipe defect model has been carried out in order to determine mesh accuracy. A constant groundwater level at the domain bottom ($p_{\text{bot}} = 0$ Pa) and a constant pipe water level of $H_{\text{PW}} = 0.05$ m were assumed for the grid test. For increasingly fine grids, the steady-state flow across the colmation layer was compared, and a deviation of 1% was chosen as convergence criterion [Graf and Degener, 2011]. Grid convergence was accomplished for a total number of 22215 elements including 142 colmation layer elements. Coarser grids tend to overestimate colmation layer flow. Results of the grid convergence study are given in the Appendix in Figure 7.6 and Table 7.2.

3.4 Derivation of the leakage function

Results of all 120 model runs on the single defect domain with sewage colmation layer and stormwater colmation layer were used to derive a LF for sewage leakage, and a LF for stormwater leakage. For the derivation of each LF, numerical model results (q_{leak} , p , H_{PW}) were fitted with a 4th order polynome using the method of least squares. Lower or higher order polynomials lead to underfitting and overfitting. The general mathematical formulation of the LF polynome is given as follows.

$$q_{\text{leak}} = \frac{1}{2.25 \cdot 10^{-4}} \cdot (a_{00} + a_{10} \cdot p + a_{01} \cdot H_{\text{PW}} + a_{20} \cdot p^2 + a_{11} \cdot p \cdot H_{\text{PW}} + a_{02} \cdot H_{\text{PW}}^2 + a_{30} \cdot p^3 + a_{21} \cdot p^2 \cdot H_{\text{PW}} + a_{12} \cdot p \cdot H_{\text{PW}}^2 + a_{03} \cdot H_{\text{PW}}^3 + a_{40} \cdot p^4 + a_{31} \cdot p^3 \cdot H_{\text{PW}} + a_{22} \cdot p^2 \cdot H_{\text{PW}}^2 + a_{13} \cdot p \cdot H_{\text{PW}}^3) \quad (3.1)$$

3.5 Results

3.5.1 Leakage function for sewer leakage

Coefficients of the polynome [Eq. 3.1] for sewer leakage are given as follows (note that units of the a -coefficients are SI-units and are omitted for legibility).

The parameterized LF is given in Figure 5.2. With a $R^2 = 0.97533$, the continuous

$$\begin{array}{lll}
a_{00} = 4.033 \cdot 10^{-11} & a_{10} = -7.524 \cdot 10^{-14} & a_{01} = 5.254 \cdot 10^{-10} \\
a_{20} = -1.700 \cdot 10^{-17} & a_{11} = 1.187 \cdot 10^{-13} & a_{02} = 8.304 \cdot 10^{-10} \\
a_{30} = 2.095 \cdot 10^{-21} & a_{21} = -8.228 \cdot 10^{-18} & a_{12} = -1.054 \cdot 10^{-13} \\
a_{03} = -2.716 \cdot 10^{-10} & a_{40} = -8.070 \cdot 10^{-26} & a_{31} = 1.279 \cdot 10^{-22} \\
a_{22} = 3.434 \cdot 10^{-18} & a_{13} = 2.390 \cdot 10^{-14} &
\end{array}$$

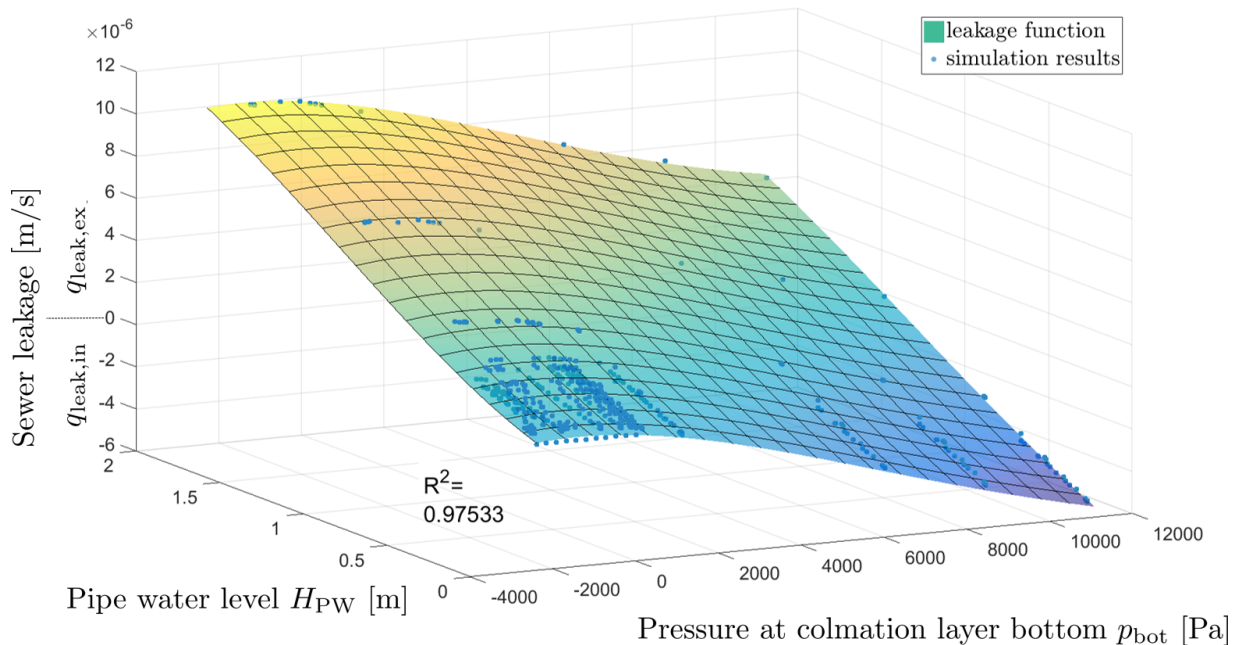


Figure 3.4: LF for sewer leakage. Blue dots represent simulation results and the surface represents the LF.

leakage function is fitted well to the discrete simulation results. Values of leakage are in the same order of magnitude compared with results from both, numerical studies and physically-based experiments of comparable setup [Vollertsen and Hvitved-Jacobsen, 2003; Karpf et al., 2009]. The correction was added that q_{leak} is zero for negative pressure values and $H_{\text{PW}} \leq 0.001$ m to guarantee that no leakage takes place in unsaturated soil for pipe water levels close to zero.

The LF fulfills two purposes: First, q_{leak} is quantified without the need to locally refine the grid. Second, the approximated q_{leak} shown in Figure 5.2 reveals the following aspects of the pipe leakage process. For any given interface pressure p , leakage flow increases linearly with increasing pipe water level. For any given pipe water level H_{PW} , negative flow (infiltration) increases linearly with pressure in case of positive pressure values (full saturation, groundwater table above the defect). This linearity is due to Darcy's law, where constant cross sectional area and saturated hydraulic conductivity result in a proportionality between flow and hydraulic gradient. The nonlinear flow behaviour for negative pressures is due to the nonlinear behaviour of variably saturated flow. Interestingly, for a given H_{PW} , q_{leak} converges as the groundwater table is lowered below

the defect (for very dry soils). This is due to a quasi-steady-state in dry soil, which forms when the groundwater table disconnects from the leaking pipe. Saturation (as expressed by κ_r) directly below the colmation layer converges to a constant value (for the sewer colmation layer: $S_e \approx 0.55$) leading to a dependency of q_{leak} only on H_{PW} . This result is in agreement with results of surface water-groundwater interaction described in [Brunner et al., 2009].

3.5.2 Leakage function for stormwater leakage

Results of all 60 model runs on the single defect domain with stormwater colmation layer were used to derive the LF for storm water leakage according to section 3.5.1. The a -coefficients of the LF for stormwater leakage are given as follows

$$\begin{array}{lll} a_{00} = -2.463 \cdot 10^{-10} & a_{10} = -7.15 \cdot 10^{-12} & a_{01} = 1.174 \cdot 10^{-7} \\ a_{20} = -8.423 \cdot 10^{-16} & a_{11} = 1.531 \cdot 10^{-12} & a_{02} = -2.664 \cdot 10^{-9} \\ a_{30} = 2.874 \cdot 10^{-20} & a_{21} = -2.56 \cdot 10^{-16} & a_{12} = -1.055 \cdot 10^{-12} \\ a_{03} = -1.056 \cdot 10^{-8} & a_{40} = 1.282 \cdot 10^{-24} & a_{31} = 1.008 \cdot 10^{-20} \\ a_{22} = 7.679 \cdot 10^{-17} & a_{13} = 1.414 \cdot 10^{-13} & \end{array}$$

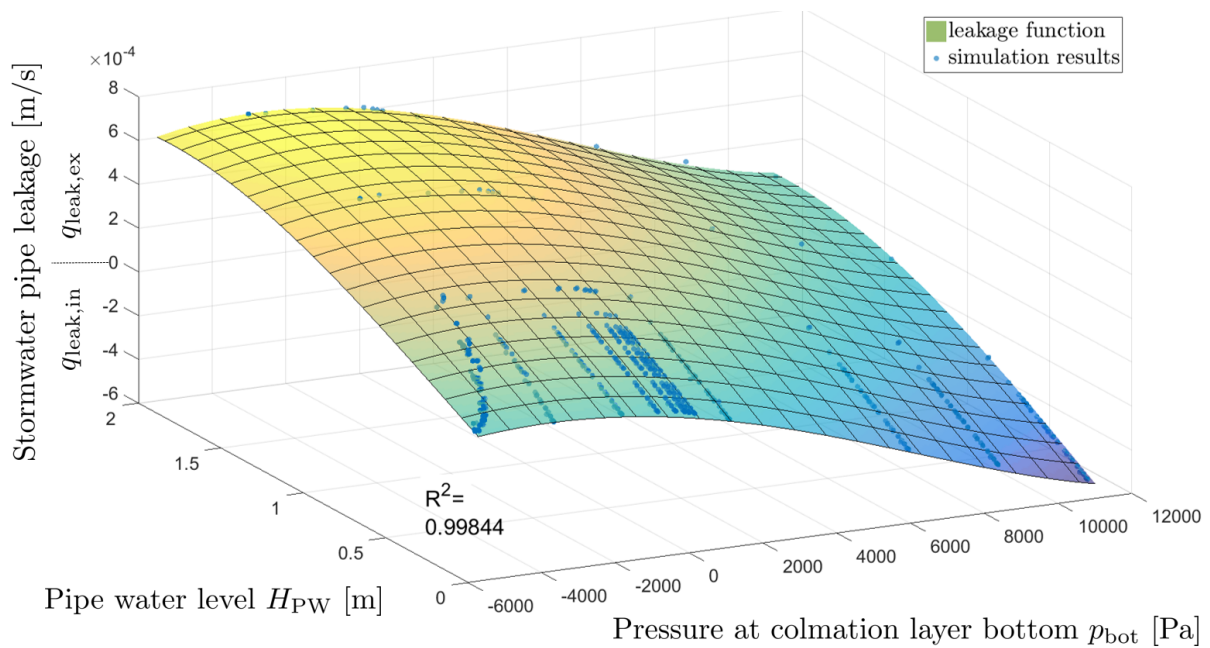


Figure 3.5: LF for stormwater leakage. Blue dots represent simulation results and the surface represents the LF.

The parameterized LF is given in Figure 3.5. Again, with a $R^2 = 0.99844$, continuous leakage function and discrete simulation show high agreement. Similar to the LF for sewer

leakage, the LF for stormwater leakage shows that leakage flux can disconnect hydraulically from the groundwater table.

3.6 Validation of the source code modification for upscaled pipe leakage

This section serves the purpose to demonstrate the correctness of the implementation of the LF approach in the source code of OGS-HE. Both models represent sewer leakage. Results of a single defect simulation with fully discretized colmatation layer (fully discretized model) and a single defect simulation using the LF approach [nodal LF as per Figure 3.2(b)] are compared. This model comparison also serves the purpose to evaluate the efficiency and accuracy of the LF approach. The spatial discretization of the pipe defect in both models is schematically visualized in Figure 3.6(a) and 3.6(b). The model setup of the fully discretized model is slightly modified to the model setup described in section 3.3 by neglecting the locally refined discretization of pipe cavity and colmatation layer. The LF-model uses a source term node regulated by a LF for sewer leakage (Figure 5.2) according to Eq. (3.1). This node is located at the elevation of the interface between colmatation layer and backfill in the fully discretized model. Pipe flow model setup, temporal discretization and initial condition are the same as in the fully discretized model [Figure 3.2(a)].

Spatial discretization of the LF-model was determined with a grid convergence study, in which the steady-state pressure at the LF source term node was calculated and compared with the pressure obtained from the other levels of spatial discretization. The soil hydraulic and fluid properties as well as initial condition of this convergence study were similar to those used in section 3.3. The lower boundary condition was set to a constant pressure of 19614 Pa. A constant infiltration flow of $6 \cdot 10^{-14} \text{ m}^3 \text{ min}^{-1}$ was used as LF-source term. Results of the grid convergence study as well as information about the levels of spatial discretization are given in the Appendix in Figure 7.7 and Table 7.3. The number of mesh elements in the LF-model is reduced by approximately 50% compared to the fully discretized model.

Transient simulations were completed for a fully saturated (bottom boundary pressure $p_{\text{bot}} = 44132 \text{ Pa}$ leading to a GW-table 0.63 m above pipe defect) and a variably saturated (bottom boundary pressure $p_{\text{bot}} = 0 \text{ Pa}$ leading to a GW-table 3.87 m below pipe defect) problem with the fully discretized model and the LF-model. A normally distributed pipe flow event was imposed to Q_{IN} . This event is visualized in the Appendix as Figure 7.5. Results in form of leakage flow over time are given in Figure 3.6(c).

Results show that the LF approach depicts the pipe infiltration process under fully satu-

rated conditions with high accuracy evidenced by a $R^2 \approx 0.99$. Using the LF-model with its significantly coarser mesh yields considerably reduced computation times. Comparing both models, computation time for the LF-model was decreased by approximately 49% and 25% for the variably and fully saturated problem, respectively.

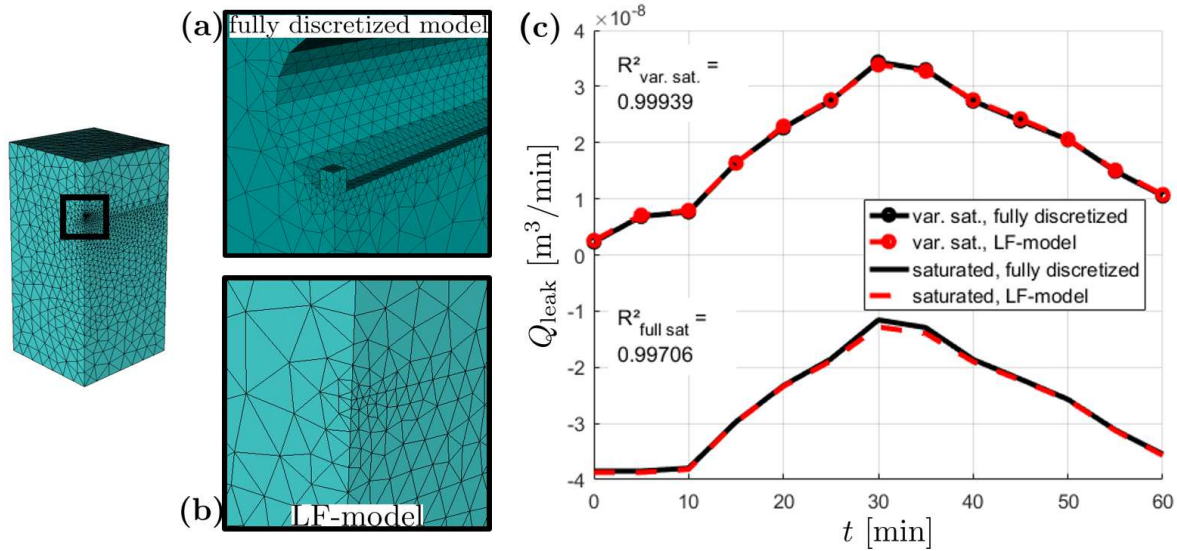


Figure 3.6: Model domains of the (a) fully discretized model, and (b) LF-model. (c) OGS-HE results for sewer leakage.

3.7 Conclusions

In this chapter, two LFs for upscaling pipe leakage were successfully derived with a single pipe defect model. The two LFs represent sewer leakage and stormwater leakage, respectively. The implementation in the source code was successfully tested in a study comparing results of a full model and a upscaled model. The time-efficiency of the upscaling was demonstrated by comparing computation time of the fully discretized model and the upscaled model. Main results of the study in this chapter are:

- Leakage can be upscaled using a LF. The LF is successfully implemented in the source code and applied in a study comparing results from the fully discretized model and the upscaled model. This upscaling leads to a significant reduction in mesh elements and computation time with only little drawback in result accuracy. Time-efficiency could only be tested on a single pipe defect model because of large computation times for a fully-discretized model with numerous pipe defects.

Both LFs demonstrated in the present chapter are based on hydraulic properties and geometric extent from literature [Karpf, 2012; Le Coustumer et al., 2012]. However, the properties of a colmation layer depend on the local conditions (e.g. initial soil conditions and hydraulic properties, land-use-specific physico-chemical signature of pipe water) and should ideally be determined in a catchment-specific manner.

- Comparing both LFs demonstrated in the present chapter shows that leakage fluxes may differ by several orders of magnitude. This deviation is large and correlates with the deviation of saturated intrinsic permeabilities of colmation layers. This fact highlights the dependence of leakage on colmation layer properties and it can be concluded that colmation layer properties should be chosen judiciously and with large confidence for the accurate calculation of leakage.
- A new result of this study is that a sinking GW level leads to the hydraulic disconnection of pipe leakage in form of pipe water exfiltration from GW. For a given pipe water level, pipe water exfiltration converges as soil water pressure becomes more negative. This process is well studied for surface water-groundwater interaction through streambeds [e.g. Sophocleous, 2002; Brunner et al., 2009, 2011] but is firstly described for pipe leakage in the present dissertation. For sewer leakage and stormwater leakage as regarded in this chapter, the hydraulic disconnection from groundwater occurs when pressures below the colmation layer are smaller than -4000 Pa and -6000 Pa, respectively.

4 Synthetic case study of sewer leakage on a single leaky pipe

This chapter describes a case study of sewer leakage on a 30 m leaky pipe. The work in this chapter has been published in Peche et al. [2017].

4.1 Objective

A transient case study of a 30 m leaky pipe was simulated with OGS-HE using upscaled sewer pipe leakage with the LF-approach. Only the effect of pipe water exfiltration was regarded in this case study. In the present chapter, the response of leakage flow to pipe flow volume, pipe flow duration and peak position of pipe flow is systematically analyzed. The objective of the present chapter is to draw conclusions about:

- The impact of the total volume of pipe flow on sewer leakage. This scenario deals with the leakage response for events with different pipe flow volumes. All events are distributed over the same time interval.
- The impact of pipe flow duration on sewer leakage. This scenario deals with the leakage response for pipe flow events with different duration. All events have the same flow volume.
- The impact of different pipe flow peak positions on sewer leakage. This scenario deals with the leakage response to pipe flow events with a symmetric, a right skewed (early peak) and a left skewed (late peak) temporal distribution. All events have the same flow volume and the same duration. They are based on inflow data from a sewage plant that is representative for a major German city and represent the pipe water flow during the half-time break of the 2014 soccer world championship final. This scenario will be referred to as ‘half-time break scenario’.

4.2 Conceptual model of a leaky pipe

The variably saturated subsurface domain is 4600 m³ large and includes a leaky pipe of 30 m length, shown in Figure 4.1. At the upstream boundary of the pipe domain,

the Neumann boundary condition Q_{IN} was assigned. Q_{IN} was imposed as different time functions for each of the three systematic scenarios investigating the response of leakage flow to different pipe flow events (Figure 4.2). The downstream boundary of the pipe domain was set as free outflow boundary condition. Initial condition was dry-weather flow with $H_{\text{PW}} = 0.04$ m for the first two systematic scenarios [as per Figure 4.2(a),(b)] and $H_{\text{PW}} = 0.4$ m for the half-time break scenario [as per Figure 4.2(c)]. Lateral and top boundaries of the model domain representing the surrounding subsurface of the pipe were set as no-flow Neumann-type boundary conditions. The bottom boundary was set as the Dirichlet-type boundary condition $p_{\text{bot}} = 29614$ Pa, representing a groundwater table of 0.3 m below the pipe defect.

For the half-time break scenario, additional simulations with $p_{\text{bot}} = 33344$ Pa representing a groundwater table of 0.075 m below the defect were carried out. The leaky pipe was defined as a LF source term line element [LF along a line as per Figure 3.2(c)]. 30 standard defects after Karpf [2012]) were distributed along the pipe domain such that each defect is distributed over each 1 m pipe. The mean pipe water level $\langle H_{\text{PW}} \rangle$ and the mean pressure $\langle p \rangle$ along the pipe length were used to calculate leakage using the LF. Initial condition was the steady-state water pressure distribution at dry weather flow of $H_{\text{PW}} \approx 0.04$ m (first two scenarios [as per Figure 4.2(a),(b)]), which corresponds to the total leakage $Q_{\text{leak}} = 3 \cdot 10^{-8}$ m³/min) and of $H_{\text{PW}} \approx 0.4$ m (half-time break scenario, which corresponds to the total leakage $Q_{\text{leak}} = 8.36 \cdot 10^{-6}$ m³/min).

Material properties for aquifer strata and trench backfill, as well as fluid properties are given in Table 3.1. A visualization of conceptual model and corresponding grid is given in Figure 4.1. Simulation time in all model runs varied between 9 and 72 minutes, each with constant temporal discretization of $\Delta t = 1$ s.

Analogous to section 3.3, a grid convergence study based on the criterion by Graf and Degener [2011] was carried out in order to determine spatial discretization of the subsurface surrounding the pipe. In the convergence study, p_{bot} was set to 19614 Pa. A Neumann-type boundary condition of constant leakage flow of $Q_{\text{leak}} = 1.8 \cdot 10^{-9}$ m³/min was assigned to the pipe domain line elements. All other boundaries were set as no-flow Neumann-type. Initial condition was defined as hydrostatic pressure distribution with $p_{\text{bot}} = 20000$ Pa. When the simulation reached steady-state, the mean nodal pressure of all nodes along the LF line elements was taken and compared between levels of increasing spatial discretization. High accuracy was achieved for a locally refined mesh with 249000 elements, visualized in Figure 4.1 (a). Results of the grid convergence study are given in the Appendix in Table 7.4 and Figure 7.8.

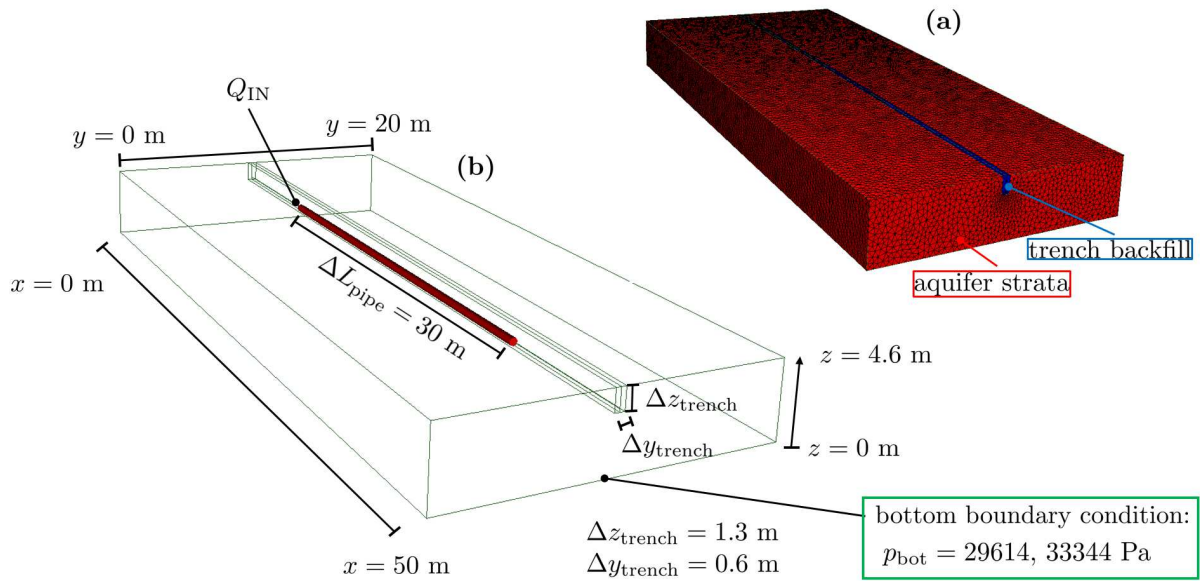


Figure 4.1: Conceptual model of the 30 m leaky pipe case study: (a) mesh, and (b) boundary conditions and geometric extent of the subsurface (transparent) and pipe flow domain (red).

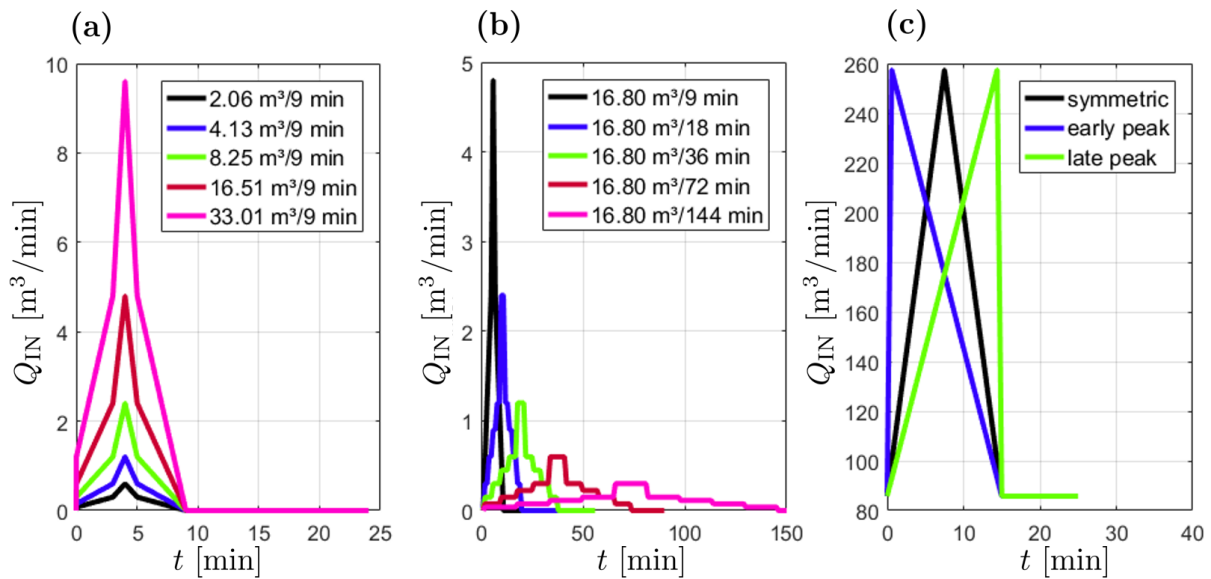


Figure 4.2: Pipe flow Neumann boundary conditions of the 30 m leaky pipe model. Neumann boundary conditions were used for investigating (a) the impact of pipe flow volume, (b) the impact of pipe flow duration and (c) the impact of pipe flow peak positions on leakage.

4.3 Results

4.3.1 Impact of pipe flow volume on sewer leakage

This setup aimed at investigating the effect of pipe flow volume on leakage [Figure 4.2 (a)]. In this first scenario, different water volumes ranging from 2.06 m^3 to 33.01 m^3 were distributed over the same time interval of 9 minutes and assigned as Q_{IN} . Figure 4.3 shows the effect of different pipe flow volumes on leakage. Clearly, the simulated Q_{leak} qualitatively follow the same temporal pattern as the imposed flow Q_{IN} . Total leakage volume increases with increasing pipe flow volume. Regarding large flow volumes, this can be explained with large pipe water levels and subsequent large potential differences between pipe and soil matrix, and with larger saturation in the pipe vicinity leading to increased relative intrinsic permeabilities. Interestingly, leakage volume increases with pipe flow volume in a nonlinear fashion. This is due to the dependency of relative conductivity on saturation and due to the dependency of water level on pipe cross sectional form (e.g. circular, oval). A simulation result in form of subsurface pressure distribution and flow field cross sections is given in Figure 4.4.

It should be noted that large potential gradients in the colmation layer such as used in this study may lead to a breaking-up behaviour (by washing out particles and thus increasing the hydraulic conductivity) resulting in short-term large leakage. This behaviour is called leakage pulse [Ellis et al., 2009]. However, the model described in the present study is not able to describe such a breaking-up behaviour of the colmation layer because movement of solid particles is not represented in the model.

4.3.2 Impact of pipe flow duration on sewer leakage

This setup aimed at investigating the effect of pipe flow duration on leakage [Figure 4.2 (b)]. In this second scenario, the same water volume of 16.8 m^3 was distributed over different time intervals and assigned as Q_{IN} . Figure 4.5 shows the effect of pipe flow duration on leakage. Again, the simulated Q_{leak} qualitatively follow the temporal pattern of the flow imposed by the Neumann boundary condition Q_{IN} . The duration of a pipe flow event has a significant effect on total leakage volume. Larger pipe flow event durations result in larger leakage despite of same pipe flow volumes. This result shows that the response of subsurface flow to pipe flow is slow. Fast changing pipe flow levels are confronted with a slowly changing subsurface. In conclusion, pipe flow events of long duration are more severe with regards to leakage and to potential subsurface contamination.

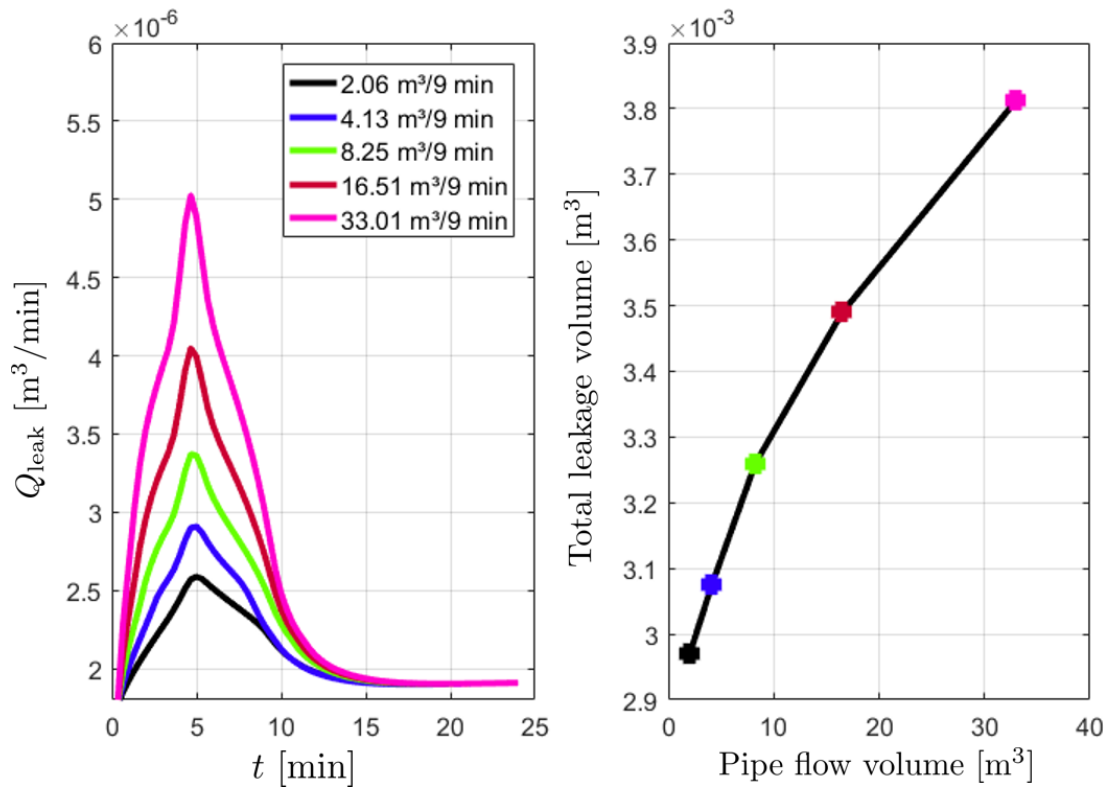


Figure 4.3: Results depicting the impact of pipe flow volume on sewer leakage. Left: exfiltration leakage Q_{leak} over time. Right: cumulative leakage over total pipe flow volume.

4.3.3 Impact of pipe flow peak position on sewer leakage

The setup of the half-time break scenario aimed at investigating the effect of pipe flow peak position on leakage [Figure 4.2 (c)]. In this third scenario, the same input volume of 3432 m^3 was distributed (i) symmetrically, (ii) with an early peak, and (iii) with a late peak over the same time interval of 25 minutes and assigned as Q_{IN} . This scenario was repeated with two different distances between pipe defect and groundwater table (dGW), where $\text{dGW} = 0.075 \text{ m}$ and $\text{dGW} = 0.3 \text{ m}$, giving a total of 6 events. Figure 4.6 shows the effect of the position of peak flow on leakage for both dGW. Again, the temporal pattern of Q_{leak} and Q_{IN} correlate. For both dGW, the total leakage volume resulting from the three different pipe flow events remains nearly identical. This leads to the conclusion that, for a given dGW, the peak position of the pipe flow event has only little effect on total leakage. However, Figure 4.6 also indicates that total leakage volume increases with decreasing dGW.

To better understand results shown in Figure 4.6, the hydraulic gradient within the colmation layer ($[H_{\text{PW}} - (p/\rho g)]/h_c$) and the relative permeability below the colmation layer (κ_r), both affecting leakage, are plotted over time for all 6 events, shown in Figure 4.7.

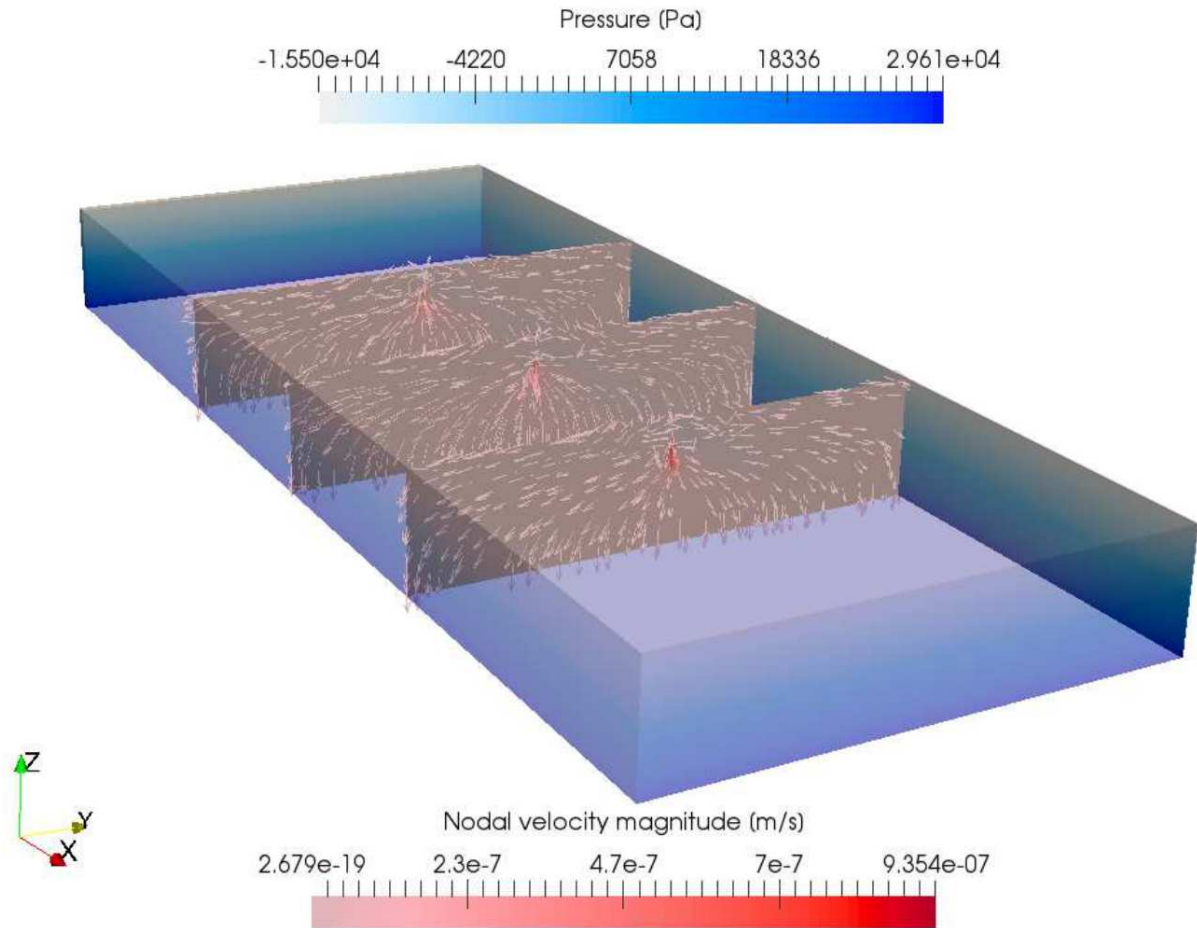


Figure 4.4: Exemplary simulation result of the 30 m leaky pipe model visualizing subsurface pressure distribution (blueish colors) and flow field cross sections (reddish colors).

For $dGW=0.3$ m, the vicinity of the defect is drier than for $dGW=0.075$ m, resulting in reduced saturation and, hence, reduced negative pressure below the colmation layer. As a result, the hydraulic gradient within the colmation layer is overall larger (by the factor ≈ 1.25) for $dGW=0.3$ m than for $dGW=0.075$ m [Figure 4.7 (a)]. However, reduced saturations in the vicinity of the defect also lead to significantly reduced relative permeability [by 4 orders of magnitude; Figure 4.7 (b)] for $dGW=0.3$ m. In combination, both effects lead to reduced total leakage volume for $dGW=0.3$ m demonstrated by Figure 4.6. It can be concluded that, for varying dGW , total leakage volume strongly depends on soil saturation (expressed by κ_r), and that the impact of a changing hydraulic gradient on total leakage volume is much less pronounced.

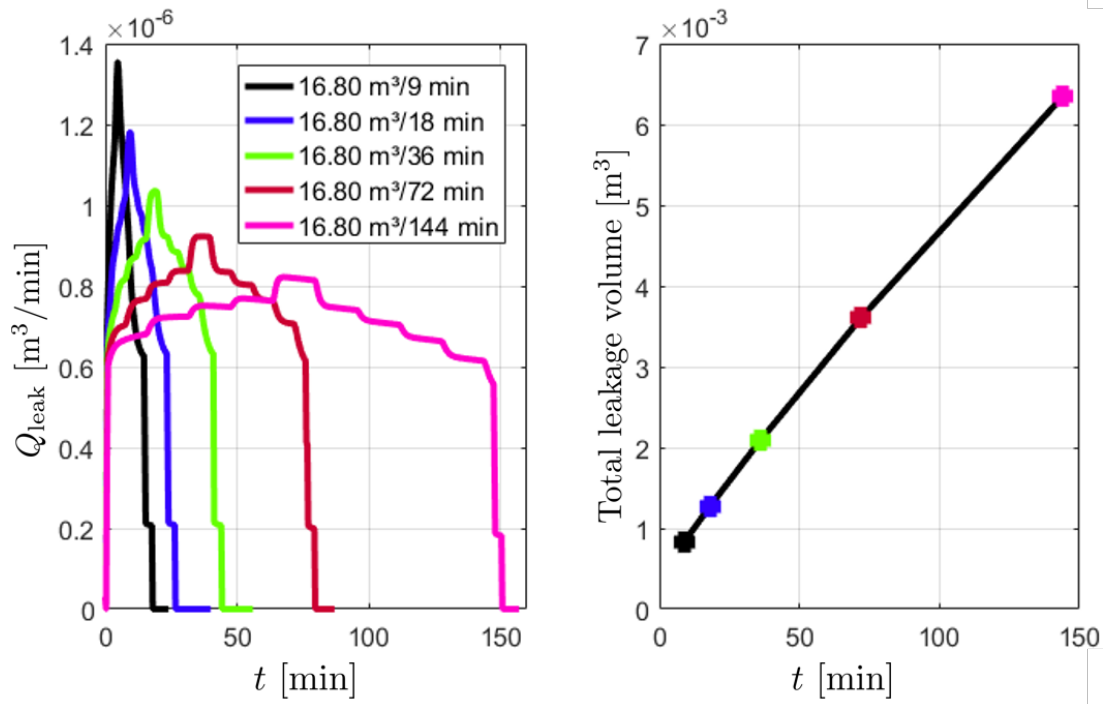


Figure 4.5: Results depicting the impact of pipe flow duration on sewer leakage. Left: exfiltration leakage Q_{leak} over time. Right: cumulative leakage over pipe flow duration.

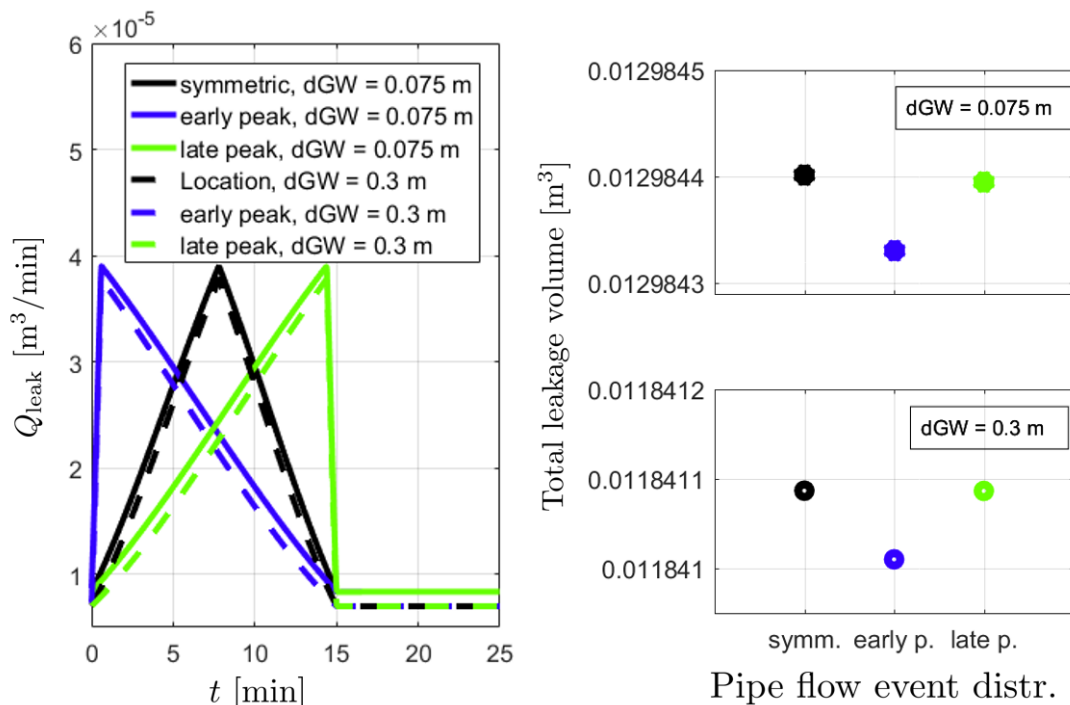


Figure 4.6: Results depicting the impact of pipe flow peak position in time on sewer leakage. Left: exfiltration leakage Q_{leak} for symmetric, early peak and late peak pipe flow. Right: cumulative leakage volume over pipe event.

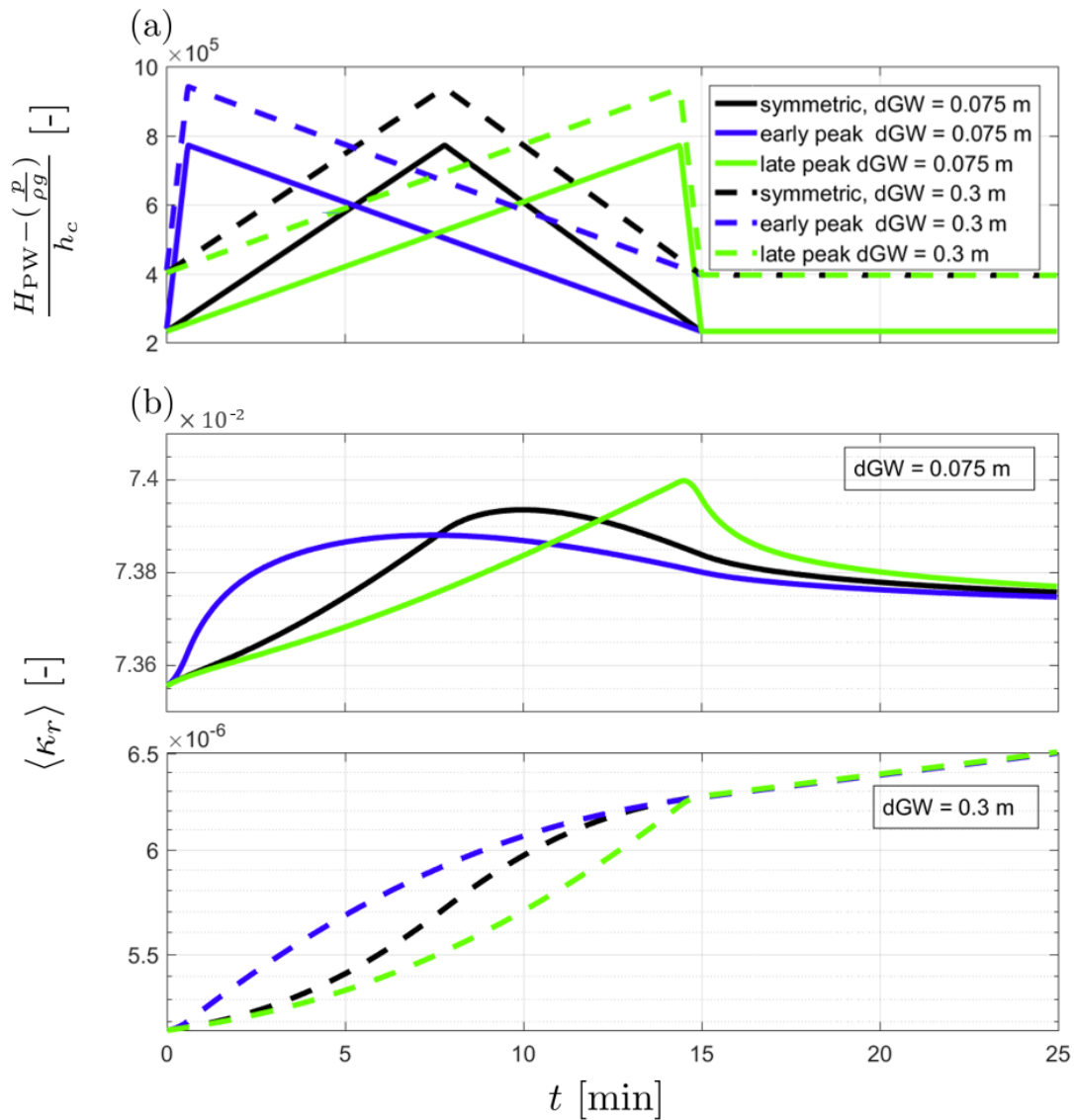


Figure 4.7: (a) Hydraulic gradient within the colmation layer over time. (b) Relative permeability in the backfill κ_r over time.

4.4 Conclusions

The study in this chapter demonstrates the application of OGS-HE in a synthetic case study on a subsurface domain including a 30 m leaky sewer pipe. The effect of differently distributed pipe flow events on leakage is investigated. In summary, key contributions and findings are:

- A systematic numerical study investigating the effect of pipe flow event distribution on leakage was conducted. Results of this study show that pipe flow events of high intensity and/or long duration result in largest leakage. It was also found that the temporal distribution of pipe flow (for identical flow volume and flow duration) is

irrelevant.

- The study in this chapter demonstrates that the impact of pipe flow duration on leakage is large. This can be concluded with the dissimilarity in time scale between pipe flow and variably saturated zone flow. Analogous to time dissimilarities of surface water-groundwater flow systems described in Swain and Wexler [1996] and Singh and Frevert [2003], a pipe flow event may occur in a time frame of minutes and hours, while corresponding groundwater flow varies in hours, days or months. It is intuitive that, on the one hand, a very large pipe flow event of short duration may evoke little leakage (despite of the large pipe flow) because the response time of groundwater flow is by orders of magnitude smaller compared with pipe flow. On the other hand, a small pipe flow event with large duration may evoke large leakage.
- A larger distance from groundwater table to the pipe defect d_{GW} leads to a non-linear relationship to pipe water exfiltration. This is the case until d_{GW} evokes a hydraulic disconnection between pipe and groundwater (as described in chapter 3). The nonlinear change in pipe water exfiltration with d_{GW} is due to the evolution of a constant soil saturation (expressed by κ_r) directly below the colmation layer. In comparison, the effect of the pipe water level on pipe water exfiltration is much less pronounced than the effect of saturation directly below the colmation layer. Simplified leakage models as proposed by Rauch and Stegner [1994] or De-Silva et al. [2005] can not capture these nonlinear effects and physically-based models solving Richards' equation [Mohrlok et al., 2008] are needed to accurately capture the nonlinear behaviour of pipe water exfiltration into a variably saturated soil.

5 Case study of stormwater pipe leakage in an urban subcatchment

This chapter describes a case study of stormwater leakage in a typical northern German urban subcatchment. The work in this chapter has been published in Peche et al. [2019].

5.1 Objective

A case study of stormwater leakage in an urban subcatchment was simulated using the LF-approach. In a series of scenarios, the effect of pipe leakage on urban GW for stormwater pipe networks of different ages and conditions (young [largely intact] to old [largely defect]) was investigated. Further, the impact of different rain events on stormwater leakage was investigated. The objective of this chapter is to draw conclusions about:

- The reduction of annual GW recharge by leakage under dry-weather flow conditions for different standard defect sizes.
- The quantification of the impact of leakage on GW level reduction under dry-weather flow conditions for different standard defect sizes.
- The generation of a leakage severity map highlighting pipes with largest leakage in the pipe network. This map can be used in the decision making for pipe rehabilitation.
- The evaluation of the impact of rain return period and temporal rainfall distribution on SPL.

5.2 Modified numerical model OGS-HE

For the numerical simulations in this chapter, the software package OGS-HE was extended. In the present study, leakage for an entire pipe section is assigned as a source term to a single node in the GW model. That node is located at the midpoint of the pipe section. Leakage in the form of GW infiltration and stormwater exfiltration is calculated differently in OGS-HE (Figure 5.1).

For GW infiltration, the soil in the pipe vicinity is fully saturated, such that GW infiltration is a linear process. This process is calculated as specific flux $q_{\text{leak, in}}$ [L T^{-1}] using Darcy's law

$$q_{\text{leak, in}} = \kappa_{\text{backfill}} \frac{\rho g}{\mu} \cdot \frac{(H_{\text{PW}} + \Delta z) - \left(\frac{p_{\text{bot}}}{\rho g}\right)}{\Delta z} \quad (5.1)$$

where κ_{backfill} [L^2] is backfill intrinsic permeability. Note that $q_{\text{leak, in}}$ is always negative [because $p_{\text{bot}}/(\rho g) > (H_{\text{PW}} + \Delta z)$], and it is used as a sink term in the GW model. For the pipe flow model, $-q_{\text{leak, in}}$ is assigned as a source term. Multiplication with the standard defect size per m pipe ($A_{\text{defect}}/1 \text{ m}$ [L]) and with the pipe length Δx gives the GW infiltration flow rate $Q_{\text{leak, in}} = q_{\text{leak, in}} \cdot (A_{\text{defect}}/1 \text{ m}) \cdot \Delta x$.

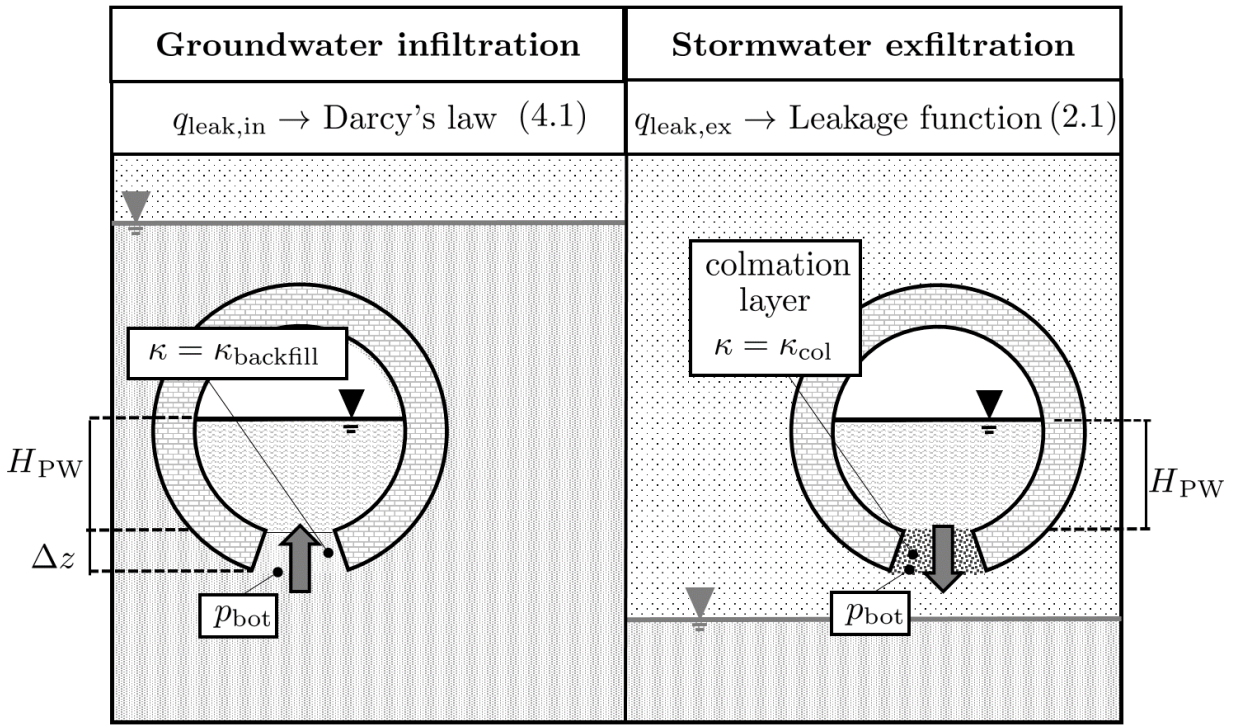


Figure 5.1: Calculation of stormwater pipe leakage with OGS-HE.

Stormwater exfiltration is calculated with the LF described in section 3.5.2. Since groundwater infiltration is calculated according to Eq. 5.1, the LF used in this study represents leakage only for negative pressures as visualized in Figure 5.2. Note that $q_{\text{leak, ex}}$ is positive because it is assigned as a source term to the GW model. For the pipe flow model, $-q_{\text{leak, ex}}$ is assigned as a sink term. Stormwater exfiltration flow rate for an entire pipe segment is calculated using $Q_{\text{leak, ex}} = q_{\text{leak, ex}} \cdot (A_{\text{defect}}/1 \text{ m}) \cdot \Delta x$. For $p_{\text{bot}} < -6000 \text{ Pa}$ (very dry conditions where the GW table is very low) and a given H_{PW} , $q_{\text{leak, ex}}$ is constant because very small pressures ($p_{\text{bot}} < -6000 \text{ Pa}$) lead to a hydraulic disconnection between leakage and GW level. For the calculation of $q_{\text{leak, ex}}$ with $p_{\text{bot}} < -6000 \text{ Pa}$, this leads to

an updating of $p_{\text{bot}} = -6000$ Pa in Eq. (3.1) in the numerical model code such that p_{bot} in Eq. 3.1 is always $p_{\text{bot}} \geq -6000$ Pa.

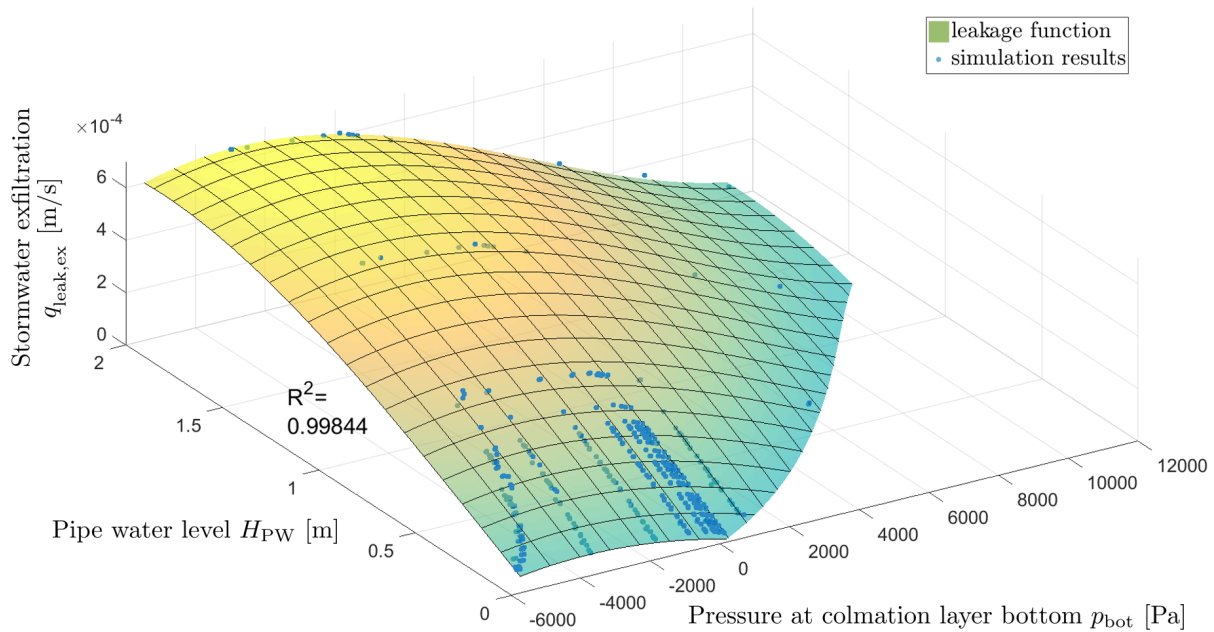


Figure 5.2: Stormwater leakage function used for the calculation of pipe water exfiltration.

5.3 Study area

The test area is an anonymous catchment in a northern German city. The catchment was chosen such that it contains a stormwater pipe network which is located above and below groundwater in order to capture both, GW infiltration and stormwater exfiltration, respectively. It is assumed that the catchment represents a typical northern German urban area with its relatively small surface slope, its complex stormwater pipe network, and its aquifer consisting of mainly gravelly and sandy sediments with till and clay lenses [Ehlers and Gibbard, 1996; Bauer et al., 2014]. The vast majority (> 99%) of stormwater pipes is of circular profile and pipe diameters are larger than 0.3 m. This represents German construction guidelines [Gujer, 2007].

The catchment has a surface area of 5 km² and a stormwater pipe system of 1211 connected individual pipes with a total length of 53 km. The pipe lengths vary from 1 to 130 m. Both land surface and pipes are sloped towards the east with an average slope of 0.6%. The pipe system discharges into a river that delineates the catchment in the east. River, stormwater pipe network, elevation, and GW isolines are visualized in Figure 5.3.

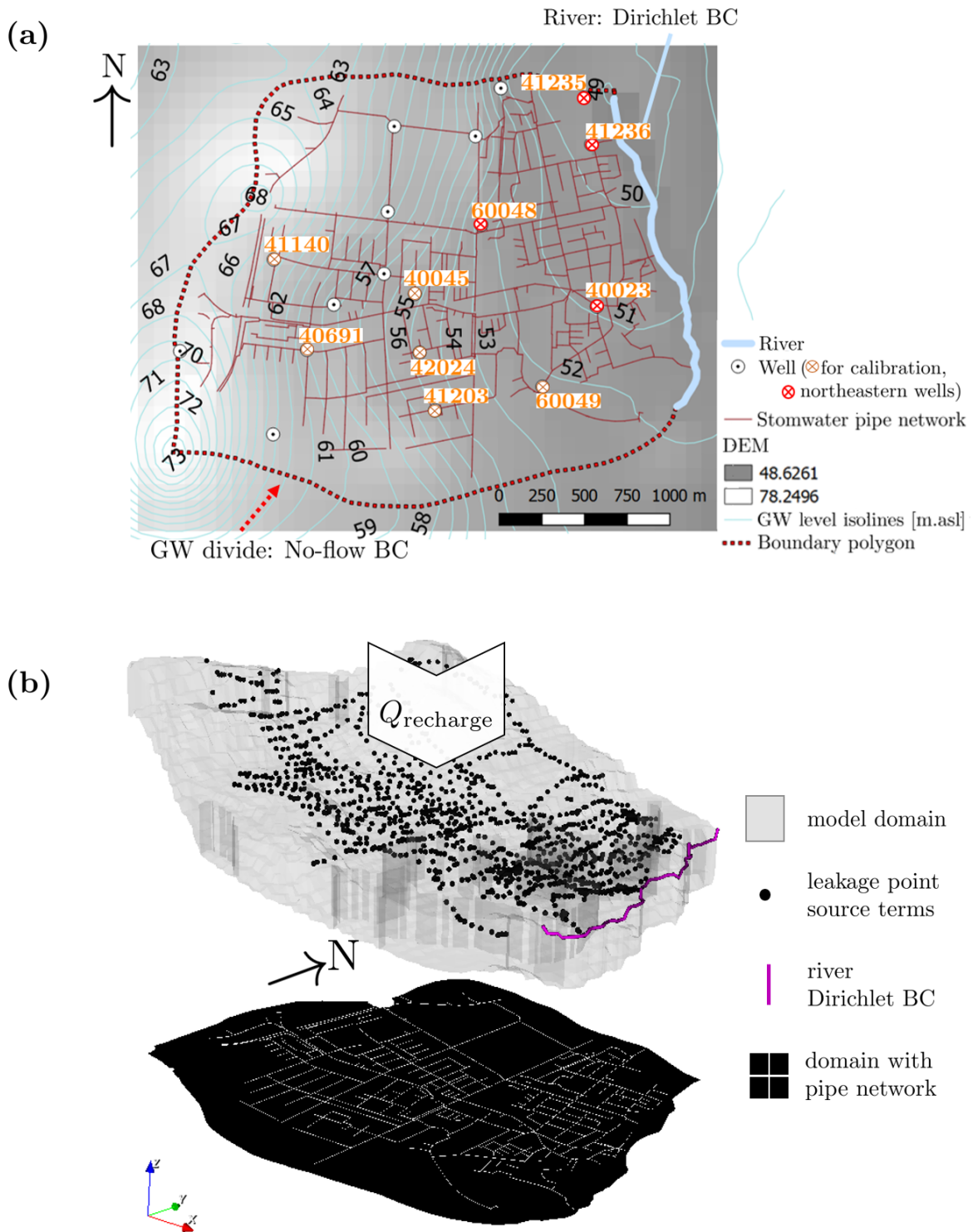


Figure 5.3: Test area and conceptual model of the urban subsubcatchment: (a) Map of the subcatchment with assigned boundary conditions. (b) Conceptual model of the subcatchment. Note that the z -coordinate of the 3D domain is exaggerated by a factor of 60 and that the domain with pipe network is given for orientation.

5.4 Conceptual model of an urban subcatchment

In order to set up a conceptual model of the test area, a model domain was delineated and boundary conditions were defined using a GIS analysis. The GW divides at the northern, western and southern boundary of the test area are assigned no-flow Neumann-type boundary conditions. By analyzing GW isolines, the river along the eastern boundary was found to be in effluent connection to the GW such that the river is assigned a Dirichlet-type boundary condition. Mean annual GW recharge of $q_{\text{recharge}} = 3 \cdot 10^{-9}$ m/s was estimated from NIBIS map server [NIBIS, 2017] and assigned on the top boundary of the model. The domain delineation and boundary conditions are also visualized in Figure 5.3. The thickness of the GW model was set to 9 m. The GW model is sufficiently thick to include the stormwater pipe system, and flow direction is assumed to be parallel to the GW model base (no vertical exchange fluxes through the bottom boundary of the model).

A numerical grid consisting of tetrahedrons and prisms was generated. This grid was locally refined in x - y direction around well locations and the middle points of each pipe. In z -direction, the grid was locally refined within the variably saturated zone and at the z -elevation of the stormwater pipe system as displayed in Figure 5.4 (b). Smallest local refinement was set at the depth of the pipe defects with a z -extent of prism elements of approximately 0.02 m. This extend represents the colmation layer thickness and is recommended for the LF-based upscaling. In total, the grid consists of 345487 tetrahedrons and prisms with a minimum, mean and maximum edge length of 0.0004 m, 40 m, and 232 m, respectively. That element size is similar to the one used in other coupled flow models on the catchment scale [e.g. Jones et al., 2008; Yang et al., 2015]. The pipe backfill was neglected in the model domain to increase model efficiency. Alternatively, the effects of pipe backfill were taken into account by the LF and Eq. (5.1) for the simulation of stormwater pipe leakage. For the simulation of leakage, a statistical standard defect per meter pipe [Karpf, 2012] was used.

5.5 Groundwater model calibration and sensitivity analysis

Due to lack of field observations on pipe flow or pipe discharge, results from the pipe flow model could not be validated. However, a GW model calibration could be carried out. For the stationary calibration of the intrinsic permeability distribution in the hydrogeological model, continuous GW level measurements from 10 observation wells were available (Figure 5.3). Data for the remaining 8 wells was scarce and neglected. The data was used to calculate mean annual GW levels, and to generate a GW level isoline map using interpolation. Assuming a constant q_{recharge} , and using Darcy's law, the distances between

individual neighboring GW level isolines were classified and used to delineate intrinsic permeability zones. The GW model domain was divided into 5 different permeability zones displayed in Figure 5.4 (a). By analyzing a hydrogeological soil characterization described in NIBIS [2017] and by analyzing distances between GW isolines, it was concluded that permeabilities in the eastern part of the model domain (permeability zones κ_1 , κ_2) are large compared to permeability zones in the western part. This analysis enabled to qualitatively estimate initial values of permeability used for the calibration (initial permeability set κ_{ini}). Values for κ_{ini} are given in Table 5.1. In this study, intrinsic permeability is assumed to be constant in z -direction.

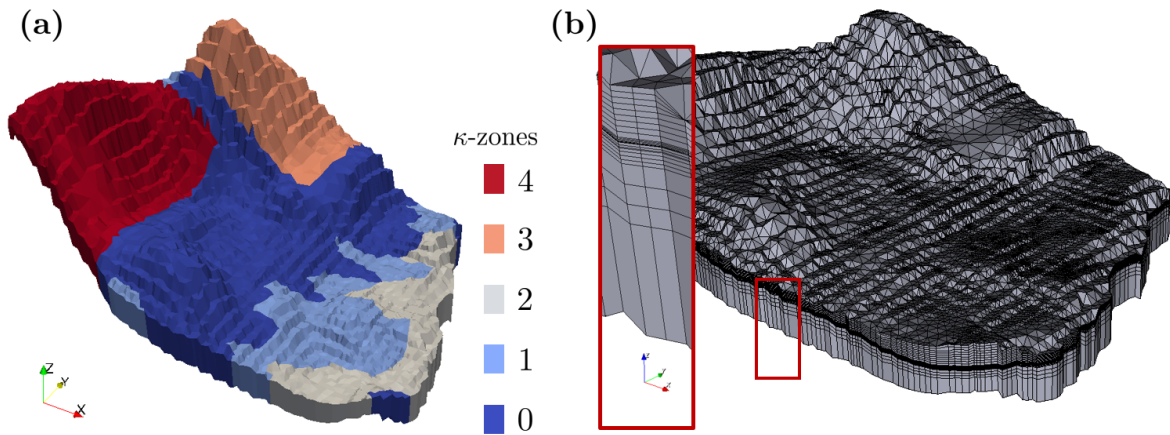


Figure 5.4: (a) GW model domain with intrinsic permeability zones. (b) Locally refined mesh. Note that the z -coordinate of (a) and (b) is vertically exaggerated by a factor of 30.

For the automated calibration, a file-based procedure including MATLAB [The Mathworks Inc., 2016] and OpenGeoSys was generated. The flow chart of the procedure is given in Figure 5.5. The Nelder-Mead-Simplex algorithm [Nelder and Mead, 1965] was used for parameter optimization. This downhill algorithm enables to optimize values of a parameter set (here: values of intrinsic permeability) in order to minimize errors for the corresponding objective function. This direct optimization method has proven to be efficient and productive and is widely used for such type of problems [Musy et al., 2014].

Results of the calibration are given in Figure 5.6. Clearly, with a mean deviation of 0.64 m, calculated GW levels agree well with observed GW levels. Calibration results and measured values show better agreement for wells in the western and southern part of the domain (mean deviation of approximately 0.19 m; wells 60049, 41203, 40024, 40045, 40691, 41140) compared with results for wells in the northeastern part (mean deviation of approximately 1.5 m; wells 41235, 41236, 40023, 60048). This deviation may stem from the fact that the aquifer in the northeastern part is not homogeneous but consists of sandy material with scattered clay lenses [NIBIS, 2017]. Results of the calibration in form of

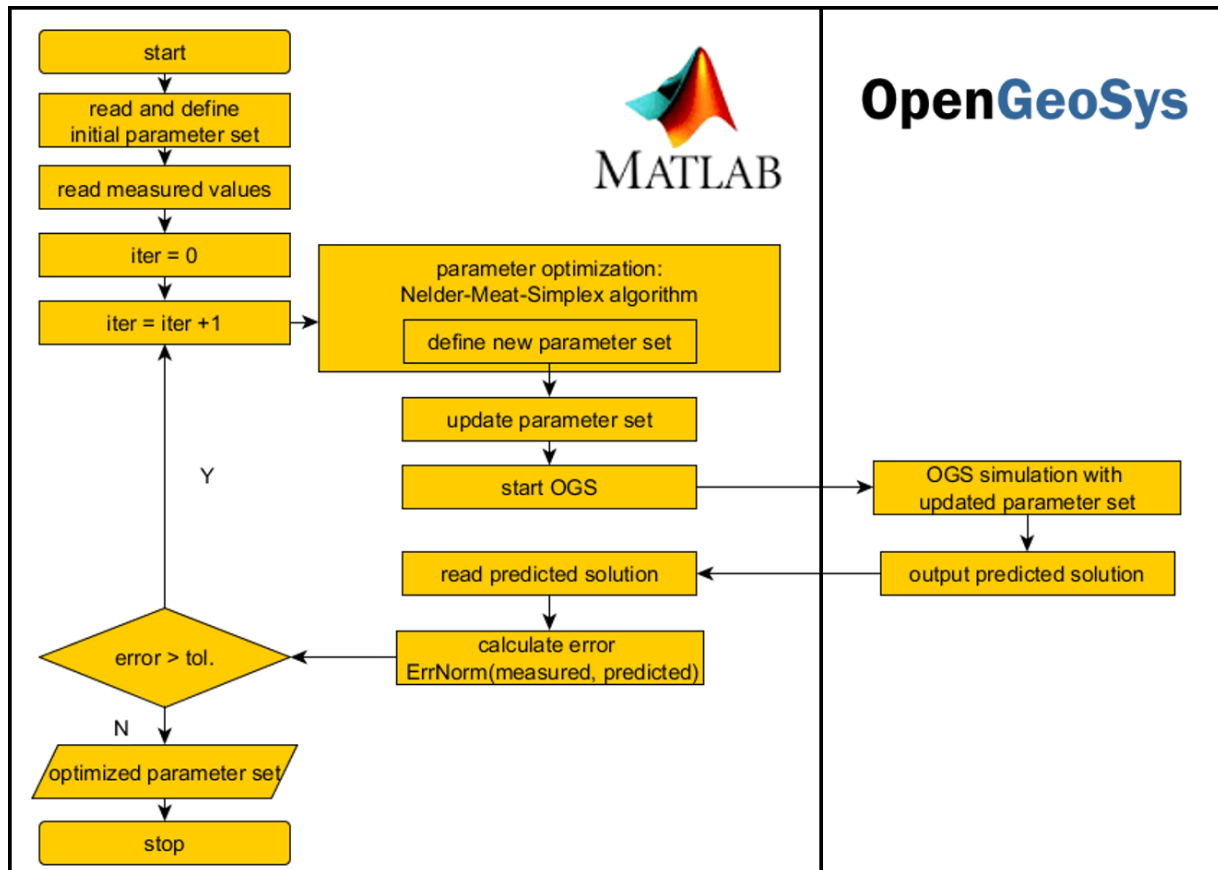


Figure 5.5: Flow chart of the coupled OGS-MATLAB calibration procedure.

κ -values for the intrinsic permeability zones [as displayed in Figure 5.4 (a)] are given in Table 5.1. The calibrated GW model is used for all scenarios described in section 5.6.

A sensitivity analysis was carried out in order to determine model result sensitivity to the input parameters κ_0 , κ_1 , κ_2 , κ_3 , κ_4 , and q_{recharge} . For the sensitivity analysis, each input parameter was multiplied with 1/2 and 3/2 followed by a simulation until steady-state. In order to quantify parameter sensitivity, the Euclidean norm (L^2 -norm) of calculated GW levels at the observation wells were compared with GW levels calculated with the optimized parameter set. Results of the sensitivity analysis are visualized in Figure 5.7.

Table 5.1: Permeabilities of the calibrated model and initial permeabilities used for the calibration.

Intrinsic permeability zone	κ [m ²]	κ_{ini} [m ²]
0	$1.245 \cdot 10^{-10}$	10^{-12}
1	$1.126 \cdot 10^{-9}$	10^{-10}
2	$8.975 \cdot 10^{-10}$	10^{-10}
3	$1.991 \cdot 10^{-12}$	10^{-12}
4	$2.177 \cdot 10^{-12}$	10^{-12}

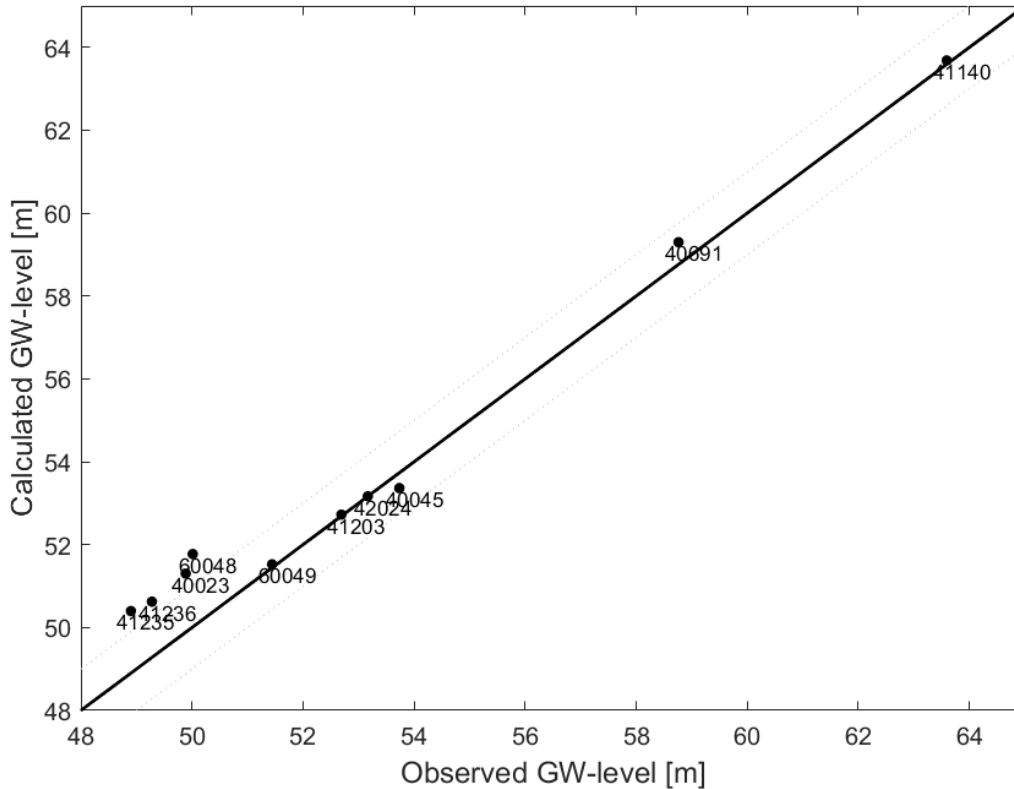


Figure 5.6: Results of the GW model calibration.

Clearly, result deviation is smallest ($L^2 < 1$ m) for variations in κ_1 , κ_2 , κ_3 . The modification of the (area-wise) largest permeability zones κ_0 and κ_4 leads to largest changes of the hydraulic head distribution, which are in the m range. The modification of κ_1 , κ_2 and κ_3 leads to changes in the hydraulic head distribution in the mm and cm range. This sensitivity with regards to permeabilities depends on both, the size of the permeability zone and the number of observation points (groundwater wells) in the permeability zone. The modification of q_{recharge} leads to largest result deviation ($L^2 > 10$ m), leading to the conclusion that this value should be chosen judiciously and with large confidence. Annual GW recharge in the present study stems from NIBIS [2017], was verified against lysimeter measurements [Lemke and Elbracht, 2008], and is assumed to be accurate.

5.6 Scenario definition

A total of 27 transient scenarios were simulated that investigate different aspects of SPL under various conditions. All scenarios are based on the conceptual model described in section 5.4. That model was modified within the scenarios by assigning rain events as source terms to the pipe flow model (Figure 5.8), and by modifying the size of the statistical

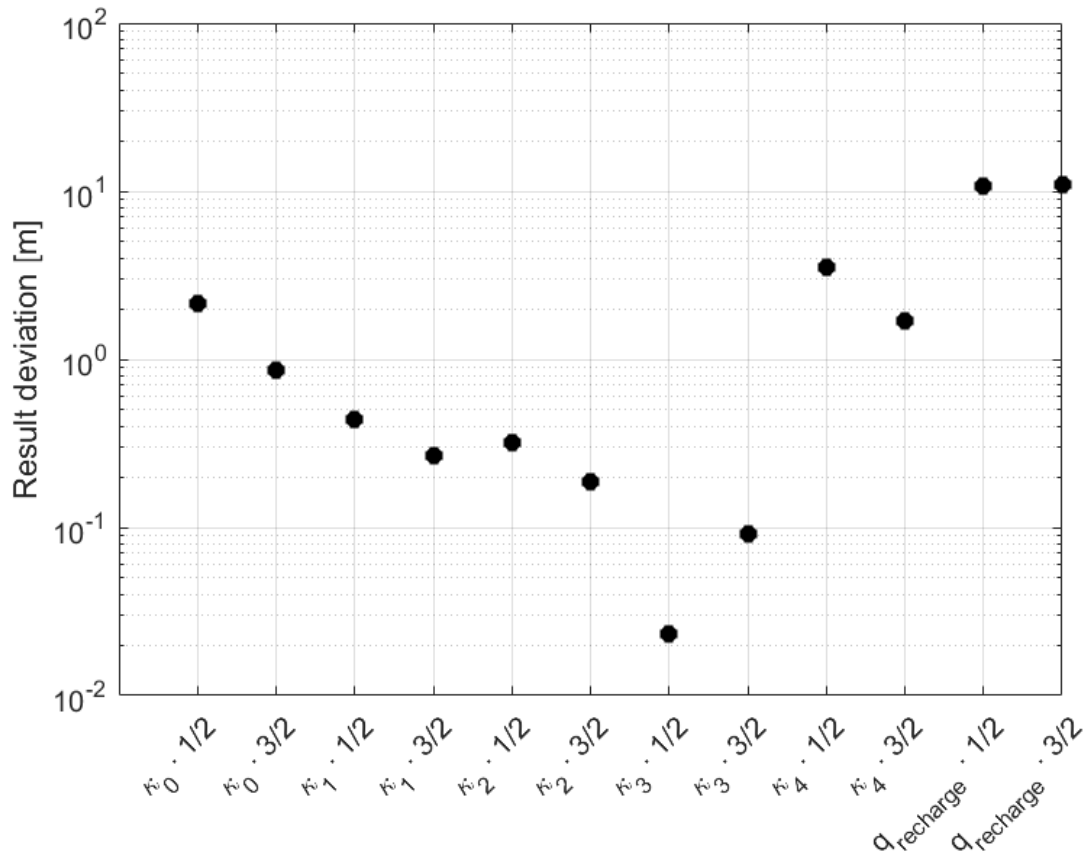


Figure 5.7: Results from the GW model sensitivity analysis.

standard defect per m pipe. The 27 scenarios include 6 scenarios for dry-weather flow conditions with pipe networks of different condition. The remaining 21 scenarios simulate the effect of various rain events on SPL. The model setup for both scenarios is described in the following:

Dry-weather flow scenarios:

A simulation of dry-weather flow over a time interval of 5 days was conducted. The term “dry-weather flow” is meant in the sense that no urban flood occurs. Therefore, no rainwater enters the manholes of the stormwater pipe network. Accordingly, no rain was assigned as source term to the stormwater pipe flow model and exchange fluxes only occur through pipe defects in the subsurface. Exchange fluxes are GW infiltration and pipe water exfiltration for pipe water levels below and above groundwater level, respectively. Water levels in the pipe network stem from GW infiltration. The GW recharge $q_{recharge} = 3 \cdot 10^{-9}$ m/s was assigned as a source term to the land surface of the groundwater model. The unknown parameter A_{defect} was varied in the range of $A_{defect} = 10^{-7}$ m² to $A_{defect} = 10^{-4}$ m² per m pipe. These values were estimated from Wolf et al. [2007] and Karpf [2012], and they represent defect pipes with ages from very few years (10^{-7} m² per m pipe) to 100 years

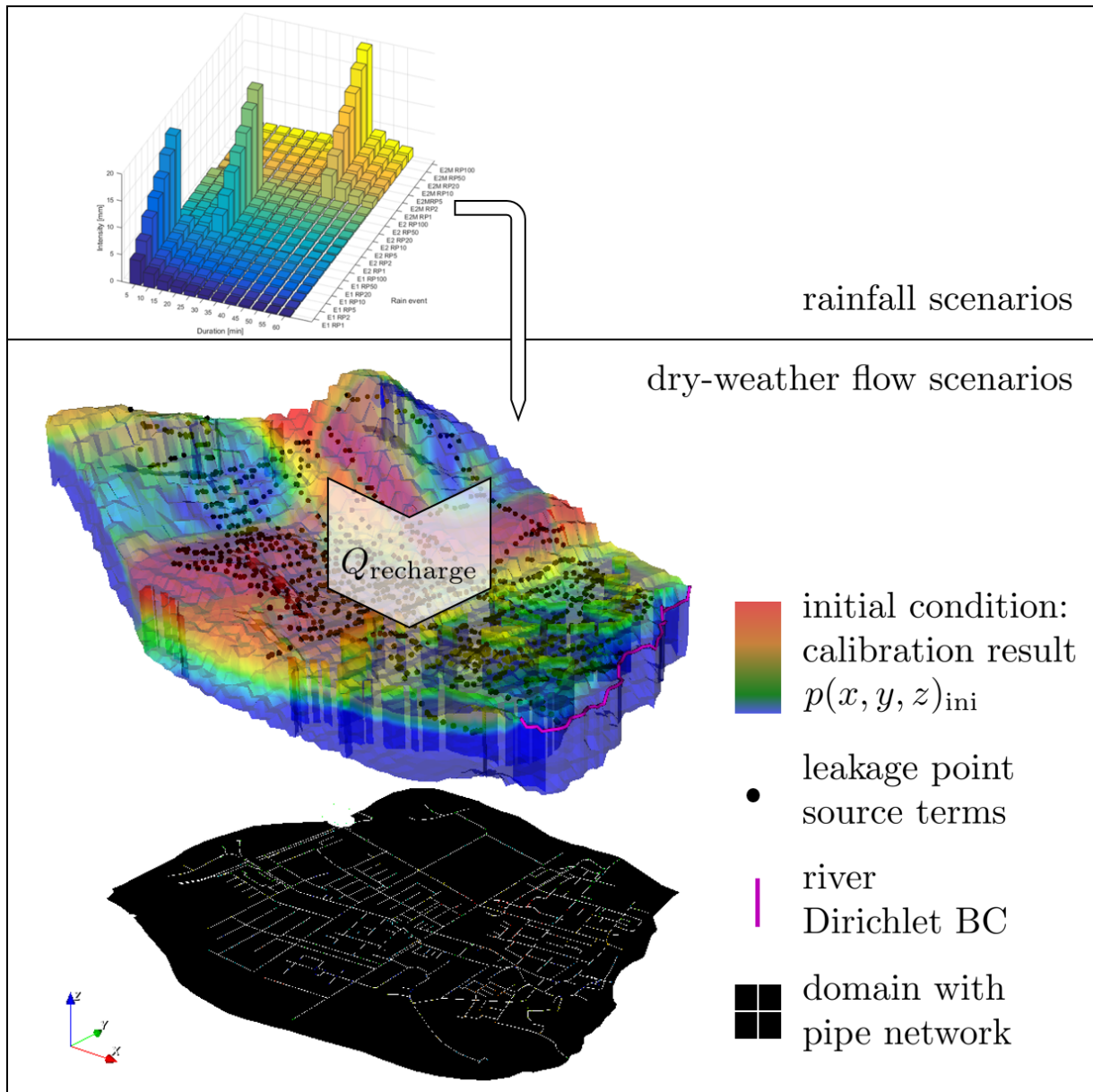


Figure 5.8: Conceptual model for catchment scale simulations. Note that the z -coordinate of the 3D domain is exaggerated by a factor of 60. In order to show pipe network and delineated catchment, the domain with pipe network is visualized.

(10^{-4} m² per m pipe). The simulation time of 5 days was chosen such that both exchange fluxes, stormwater exfiltration and groundwater infiltration have converged. Convergence plots for all standard defect sizes are given in Figure 7.10 in the Appendix. Values for leakage after 5 days simulation time were used as results, which are described in sections 5.7.1, 5.7.2, 5.7.3.

Rainfall scenarios:

The dry-weather flow scenario with the standard defect size $A_{\text{defect}} = 4 \cdot 10^{-7}$ m² per m pipe was modified by assigning rain events with different temporal distribution and return

period (RP) as source terms to the pipe flow model. Temporal distributions were set to Euler 1-type (E1), Euler 2-type (E2), and a mirrored Euler 2-type (E2M). For each of the temporal distributions, the RP was varied between 1, 2, 5, 10, 20, 50, and 100 years. All events have a duration of 1 hour and are visualized in Figure 5.9. A uniform spatial

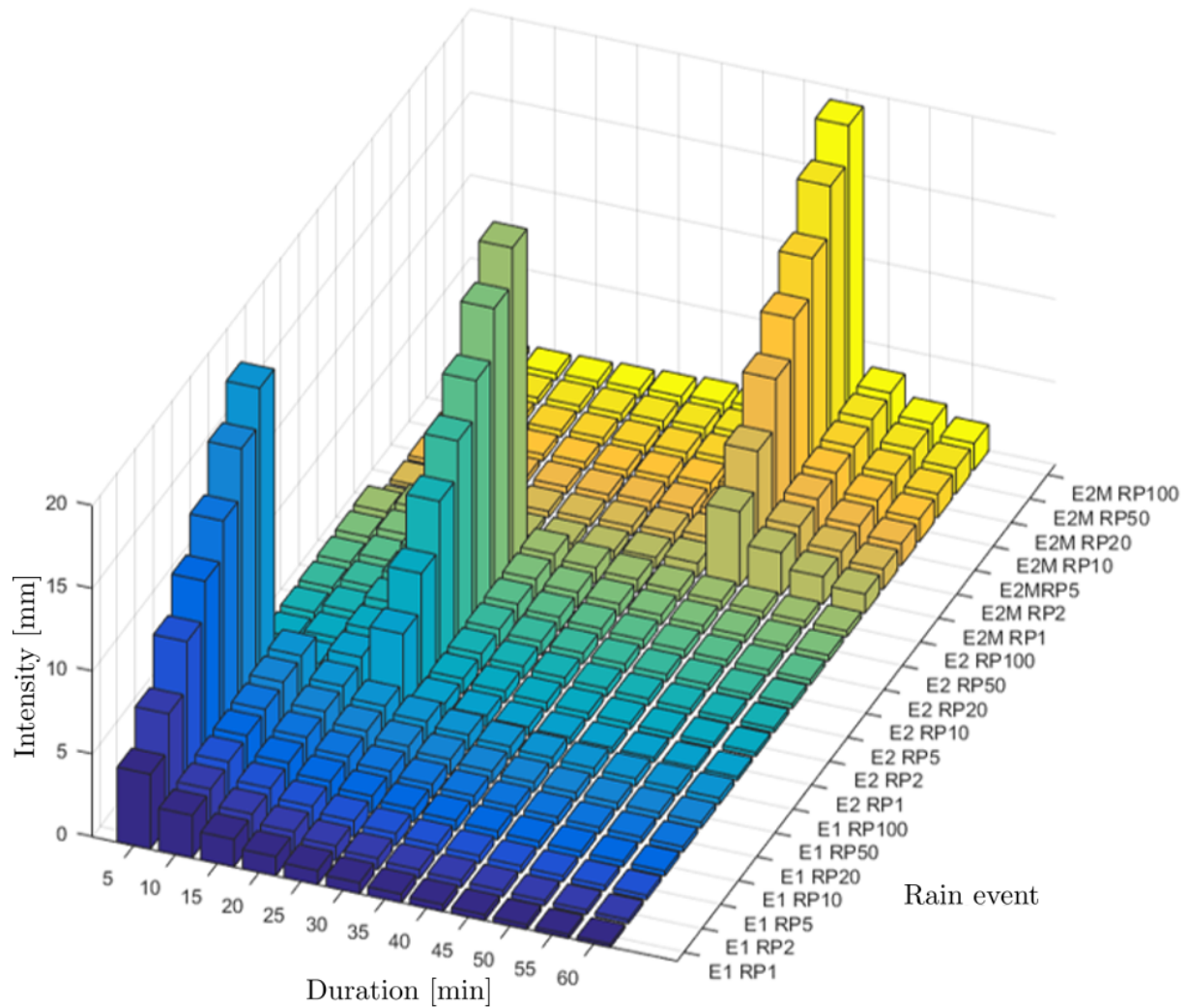


Figure 5.9: Rain events used as source terms in the pipe flow model. Each rain event is characterized by its temporal distribution [Euler 1-type (E1), Euler 2-type (E2), Euler 2-type, mirrored (E2M)] and return period (RP) in years.

distribution of rain intensity was chosen for all simulations. Simulation time was set to 3.5 hours, where the rain event occurs after 30 minutes, and associated rainwater drainage by pipe network occurs in the remaining two hours. Results are given in section 5.7.4.

5.7 Results

5.7.1 Reduction of annual GW recharge by leakage under dry-weather flow conditions

Pipe leakage may change GW recharge in an urban catchment [Lerner, 1986, 1990]. Stormwater exfiltration may increase GW recharge while GW infiltration may reduce GW recharge. As shown by Kidmose et al. [2015], the impact of stormwater exfiltration on GW recharge (leading to GW level increase) is significantly smaller than the impact of GW infiltration on GW recharge (leading to GW level decrease). This different impact stems from the presence of a colmation layer, and from the small relative permeabilities under unsaturated conditions during stormwater exfiltration.

The reduction of annual GW recharge by SPL is quantified for pipe domains with different standard defect sizes. The term “standard defect” refers to the average defect size in a given pipe network and represents the condition of the pipe network as described in Karpf [2012]. In the present study, the standard defect is characterized by a quadratic defect area and a location at the pipe invert. The parameter A_{defect} was varied in the range of $A_{\text{defect}} = 10^{-7} \text{ m}^2$ per m pipe to 10^{-4} m^2 per m pipe. These values were estimated from Wolf et al. [2007] and Karpf [2012], and they represent defect pipes with ages from very few years (10^{-7} m^2 per m pipe) to 100 years (10^{-4} m^2 per m pipe).

The net cumulative dry-weather flow leakage for all pipes was calculated using $Q_{\text{leak,net,dry-weather}} = |Q_{\text{leak,in,dry-weather}}| - |Q_{\text{leak,ex,dry-weather}}|$, as visualized in Figure 5.10. It should be noted that $|Q_{\text{leak,ex,dry-weather}}|$ was always much smaller than $|Q_{\text{leak,in,dry-weather}}|$. The ratio of $Q_{\text{leak,net,dry-weather}}$ to the imposed constant Q_{recharge} was calculated for each defect size, and results are visualized in Figure 5.11. The threshold value of 1% denotes the maximum allowed reduction of GW recharge by leakage (Figure 5.11). Clearly, $Q_{\text{leak,net,dry-weather}}$ strongly depends on the defect size, and it is equal to the chosen threshold of 1% of GW recharge at the standard defect size $A_{\text{defect}} = 4 \cdot 10^{-7} \text{ m}^2$ per m pipe. This corresponds to GW infiltration of 15 l/day per 50 m pipe segment. Larger defect sizes result in a significantly larger reduction of annual GW recharge by leakage. For example, the defect size of $A_{\text{defect}} = 1 \cdot 10^{-5} \text{ m}^2$ per m pipe leads to a reduction of GW recharge by GW infiltration into pipes of 23%. This corresponds to GW infiltration of 340 l/day per 50 m pipe segment, which is in the same order of magnitude as results from Kidmose et al. [2015]. This result shows that urbanization may significantly reduce GW recharge [Lerner, 1990]. Another important result is that, if defects are larger than $4 \cdot 10^{-7} \text{ m}^2$ per m pipe, and GW levels are shallow, the process of pipe leakage must be included in the calibration of an urban GW model.

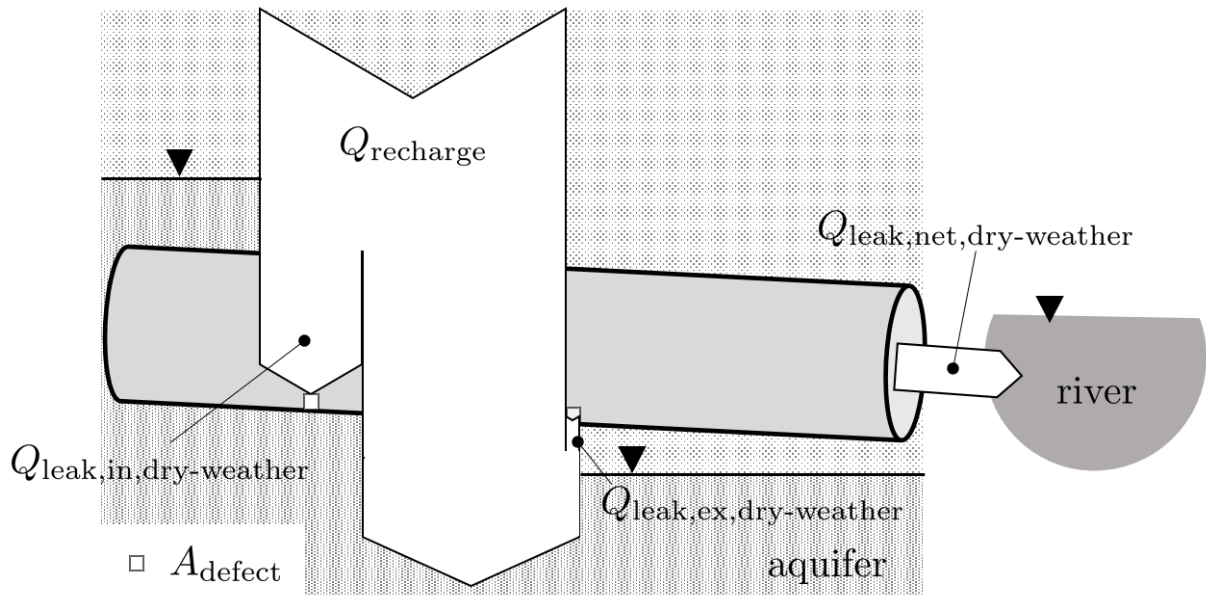


Figure 5.10: Reduction of Q_{recharge} by $Q_{\text{leak,net,dry-weather}}$.

For urban GW model calibration, net leakage can either be quantified with a coupled model as is demonstrated here. Alternatively, in the absence of a coupled model, net leakage can be estimated using Eq. (5.1) with backfill sand intrinsic permeability and fluid properties. The hydraulic gradient can be estimated by reading the local GW head and estimating pipe water levels from dry-weather flow measurements. The thickness of the colmation layer is usually between 0.01 m and 0.02 m, and can be restricted to the pipe wall thickness in the absence of biofilm growth [Ellis et al., 2009]. Because net leakage is mainly controlled by GW infiltration ($|Q_{\text{leak,in,dry-weather}}| \gg |Q_{\text{leak,ex,dry-weather}}|$), stormwater exfiltration can be neglected for the calibration of an urban GW model.

5.7.2 Reduction of GW levels by leakage under dry-weather flow conditions

SPL may significantly reduce groundwater levels in an urban catchment [Lerner, 1986]. To investigate this effect, the parameter A_{defect} was varied in the range of $A_{\text{defect}} = 10^{-7}$ m² per m pipe to 10^{-4} m² per m pipe, as in section 5.7.1. The mean GW level change in the vicinity of all pipe defects, as well as maximum GW level increase and decrease over the entire model domain were calculated for each defect size, and results are visualized in Figures 5.12.

Clearly, GW levels decrease with increasing defect size up to several meters. For example, a large standard defect of $A_{\text{defect}} = 1 \cdot 10^{-4}$ m² per m pipe (which is smaller than the statistical standard defect for the German city of Dresden of $9 \cdot 10^{-4}$ m² per m pipe calculated by Karpf [2012]) leads to a mean decrease in GW level of 0.16 m, and a maximum decrease

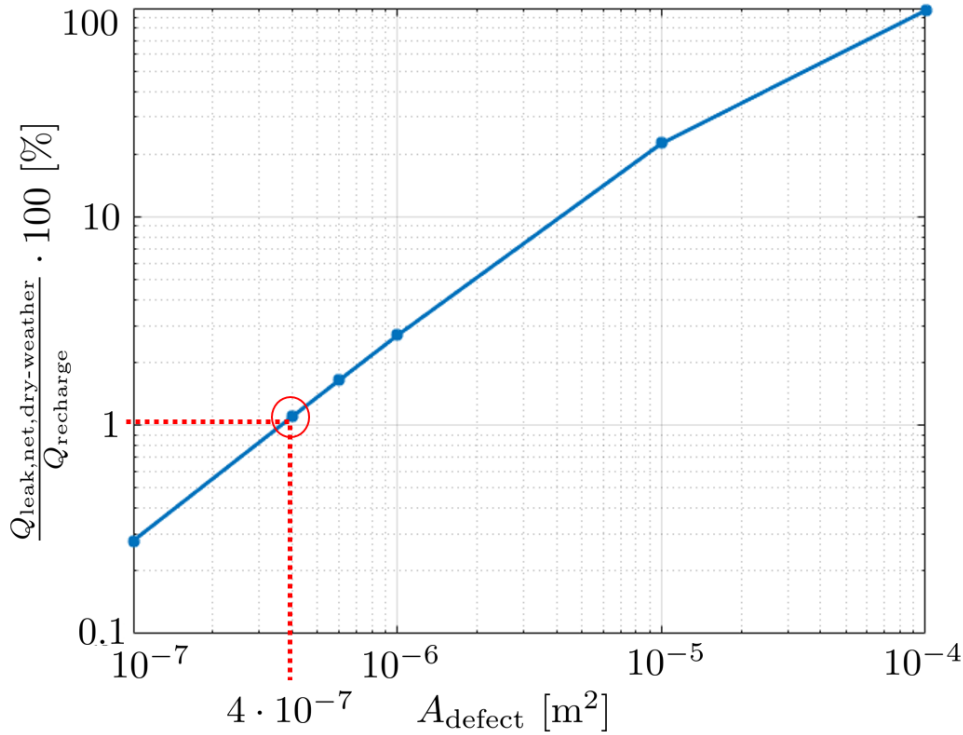


Figure 5.11: Effect of $Q_{\text{leak,net,dry-weather}}$ on Q_{recharge} for different standard defect sizes.

of 3 m. This result illustrates the dependence of urban GW levels on the condition of the pipe system. In reverse conclusion, it supports statements by Herringshaw [2007] and Thorndahl et al. [2016a] saying that a sudden decrease of pipe defects (caused by e.g. a pipe rehabilitation) can result in a significant rise of the GW level. Therefore, while pipe rehabilitation is an important measure to avoid GW pollution by contaminated stormwater leakage, resulting rising GW levels may lead to mobilization of pollutants, and to urban infrastructure damages such as flooded basements or to unstable conditions of buildings by increased buoyancy.

The spatial distribution of GW level reduction from initial condition to steady-state for standard defects larger $A_{\text{defect}} = 6 \cdot 10^{-7} \text{ m}^2$ per m pipe are visualized in Figures 5.13 and 5.14. The spatial distribution of GW level reduction for standard defects smaller $A_{\text{defect}} = 1 \cdot 10^{-6} \text{ m}^2$ per m pipe is not visualized because it was found to be insignificant. Also, GW level increase (by pipe water exfiltration) was found to be insignificant and is therefore not given in Figures 5.13 and 5.14. Clearly, GW level reduction can only occur where GW has been above pipe water at the initial condition. A Figure illustrating soil pressures at pipe invert depth (as a measure of initial GW levels above and below pipe invert) is given as Figure 7.9 in the Appendix. Thus, part of the pipe network in the northern, eastern and southwestern part are prone to GW infiltration and GW level

reduction. For a standard defect of $A_{\text{defect}} = 1 \cdot 10^{-4} \text{ m}^2$ per m pipe, GW level reduction is rather small ($< 0.2 \text{ m}$) in the eastern part of the domain, while local GW level reduction is large ($> 2 \text{ m}$) in the western part. This result correlates to initial GW levels above the pipe network in the the catchment and all GW above the pipe system is drained away by the defect pipe system. Large GW level reduction occurs at locations where the GW above pipes has been large initially. This result indicates that large defects in a pipe network reduce the GW levels to the depth of the pipe network. It further indicates that, despite larger standard defects per m pipe, GW level reduction will not increase, because the GW volume above the pipe network is limited. Clearly, Figure 5.13 further indicates that the spatial distribution of GW level reduction follows the spatial distribution of the pipe network and GW reduction resembles a drawdown of horizontal pumping well systems as described in e.g. Grubb [1993] and Rushton [2004]. Finally, GW level reduction zones are larger at locations where the pipe network is more dense.

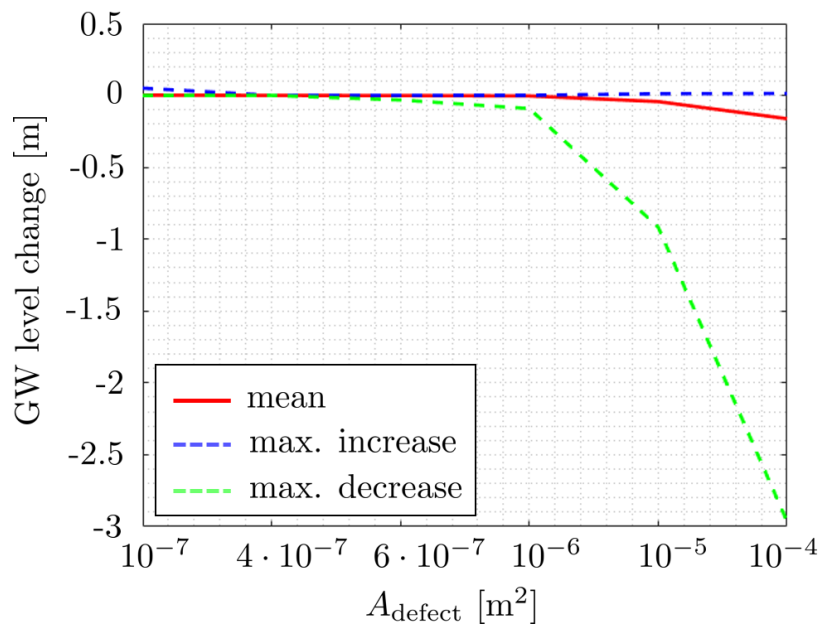


Figure 5.12: Effect of standard defect size on GW level change.

5.7.3 Generation of a leakage severity map under dry-weather flow conditions

GW infiltration decreases the capacity of a stormwater pipe network. The drainage capacity of old pipe networks can be improved by reducing leaks [Stephenson, 2012], especially in pipe sections where the pipe capacity is reduced by GW infiltration. The result of the dry-weather flow scenario with a standard defect size of $4 \cdot 10^{-7} \text{ m}^2$ per m pipe was used for mapping leakage in the pipe system with SPL classified into severity categories. The spatial distribution of SPL (including GW infiltration and stormwater exfiltration) was

plotted on a map by defining leakage flow classes. Such a map can be used as a decision making tool for a pipe rehabilitation plan. The leakage severity map is visualized in Figure 5.15. Parts of the pipe network located in the southern and central part of the study area have a severity class of 0 (and are not subject to leakage under dry-weather flow conditions). Such pipes can be disregarded for rehabilitation. Parts of the pipe system in the eastern, western and northern part have a severity class that is nonzero. Such pipes are subject to potentially large leakage and can be prioritized for pipe rehabilitation. A rehabilitation of only pipes prone to GW infiltration would result in an increased pipe system capacity and decreased manhole surcharge in case of strong rain events. However, as shown in section 5.7.2, such a rehabilitation may lead to a significant rise in groundwater levels and to associated problems such as flooded basements.

5.7.4 Impact of rain return period and temporal rainfall distribution on stormwater pipe leakage

The rainfall scenarios aim at evaluating the impact of rain return period and temporal rainfall distribution on SPL. Differently distributed rain events with different RPs were assigned as source terms to the manholes of the pipe flow model. The cumulative GW infiltration $Q_{\text{leak,in}}$ and the cumulative stormwater exfiltration $Q_{\text{leak,ex}}$ of the whole pipe network during the simulation time of 3.5 h were calculated for all RPs and for all temporal rainfall distributions. Results are given in Figure 5.16. Clearly, cumulative GW infiltration decreases in absolute numbers with increasing return period, which is due to larger pipe water levels and thus smaller hydraulic gradients as mathematically described by Eq. (5.1). Conversely, stormwater exfiltration increases with increasing return period, which is due to larger pipe water levels and larger hydraulic gradients in the colmation layer.

Regarding the temporal distributions of rain events, an early peak of rain leads to a small increase of GW infiltration in absolute numbers, but only for events with small return periods. Results also indicate that cumulative stormwater exfiltration is not affected by the temporal distribution of rain. No temporal distribution of rain events with significantly higher GW infiltration or stormwater exfiltration can be identified. This important result leads to the conclusion that temporal distribution of rain has an insignificant impact on SPL.

Model results for an E1 RP100 rain event are visualized in Figure 5.17. Results for such an extreme rain event show that the pipe network is nearly completely drained after two hours. Pipe water drains towards the eastern part of the catchment, where large pipe water levels last longer than in the western part of the catchment. Figure 5.17 visualizes leakage over time for an exemplary pipe which is prone to stormwater exfiltration.

Clearly, the temporal distribution of leakage does not fit to the temporal distribution of the rain event, which is due to specific flow characteristics in the catchment including different pipe slopes, retention times on the land surface, and manhole surcharge. Pressures at this pipe vary in the range of 10^{-3} Pa, which is rather small. Maximum pressure changes in the whole domain are in the range of 10^1 Pa for long pipes with large leakage.

5.8 Conclusions

The study in this chapter demonstrates the application of OGS-HE for the simulation of stormwater pipe leakage on the scale of a typical northern German urban catchment. The successful calibration of the catchment-scale groundwater model is carried out using a coupled MATLAB-OGS procedure. Finally, the coupled model is applied to scenarios of dry-weather flow leakage and to scenarios of synthetic rain events to investigate the leakage response. In summary, novel key contributions and findings of the present study are given below.

- In the present chapter, the successful application of a coupled physically based model for the simulation of stormwater pipe leakage in an urban catchment is presented. Pipe flow could not be calibrated due to lack of observation data. This leads to questionable accuracy of the model. However, a thorough calibration of urban flow models is typically difficult [Thorndahl et al., 2016b]. Continuous monitoring with several observation points in the pipe network (and not only one discharge measurement at an outlet) is recommended for the accurate calibration of a pipe flow model [Fraga et al., 2017]. Such a flow monitoring is related to large expense and was not possible in the present study. However, a successfully stationary calibration of a GW model was carried out using the Nelder-Mead-Simplex method in an automated OGS-MATLAB procedure. A sensitivity analysis showed that changes in the imposed GW recharge lead to largest deviations in the hydraulic head distribution. Thus, the value for GW recharge should be chosen judiciously and with large confidence.

In model described in the present chapter, the process of (precipitation-driven) land surface infiltration is not simulated. It is assumed that the propagation of the wetting front up to a point where pipe leakage will be influenced (at defect depth of several meters) takes more time than the simulation time (3.5 hours simulation time; 1 hour rain event). This simplification stems from wetting front propagation studies with similar soil types, initial conditions and boundary conditions [Ma et al., 2010; Herrada et al., 2014]. The validity of this simplification may be questionable for rain events of larger duration and larger intensity. It is recommended to include

the process of surface infiltration into similar model setups with rain events of large duration and large intensity, especially since the model has proven to be largely sensitive to GW recharge.

- A parameter study on dry-weather flow leakage with different standard pipe defect sizes per meter pipe was conducted. Results demonstrate the strong dependence of urban groundwater on the condition of the stormwater pipe system. Net leakage for a standard defect larger than $A_{\text{defect}} = 4 \cdot 10^{-7} \text{ m}^2$ per m pipe may exceed 1% of groundwater recharge. Standard defects larger than $A_{\text{defect}} = 1 \cdot 10^{-5} \text{ m}^2$ per m pipe can lead to net leakage exceeding 20% of annual groundwater recharge. These findings are in the similar range of results described in Lerner and Harris [2009]. It is shown that standard defect sizes larger than $A_{\text{defect}} = 1 \cdot 10^{-5} \text{ m}^2$ (which is by an order of magnitude smaller than a standard defect for the German city of Dresden derived by Karpf [2012]) lead to a mean decrease of the groundwater level in the range of several centimeters, which correlates with findings from Thorndahl et al. [2016a]. The maximum local decrease of groundwater levels was found to be in the range of several meters. Further, results indicate that the entire initial GW water volume above the pipe network is drained away by GW infiltration.
- A systematic study investigating the effect of rain events of different return periods and temporal distributions on leakage was conducted. Results show that groundwater infiltration decreases in absolute numbers during rain events and that stormwater exfiltration increases during rain events (both due to larger pipe water levels). Larger return periods result in larger stormwater exfiltration and smaller groundwater infiltration in absolute numbers. The temporal distribution of rain does not significantly affect SPL. However, leakage-driven soil water pressure changes can be considered small for our scenarios. The effect would be more significant for a case study with larger rain duration, larger standard defects and larger leakage as the scenarios regarded here.

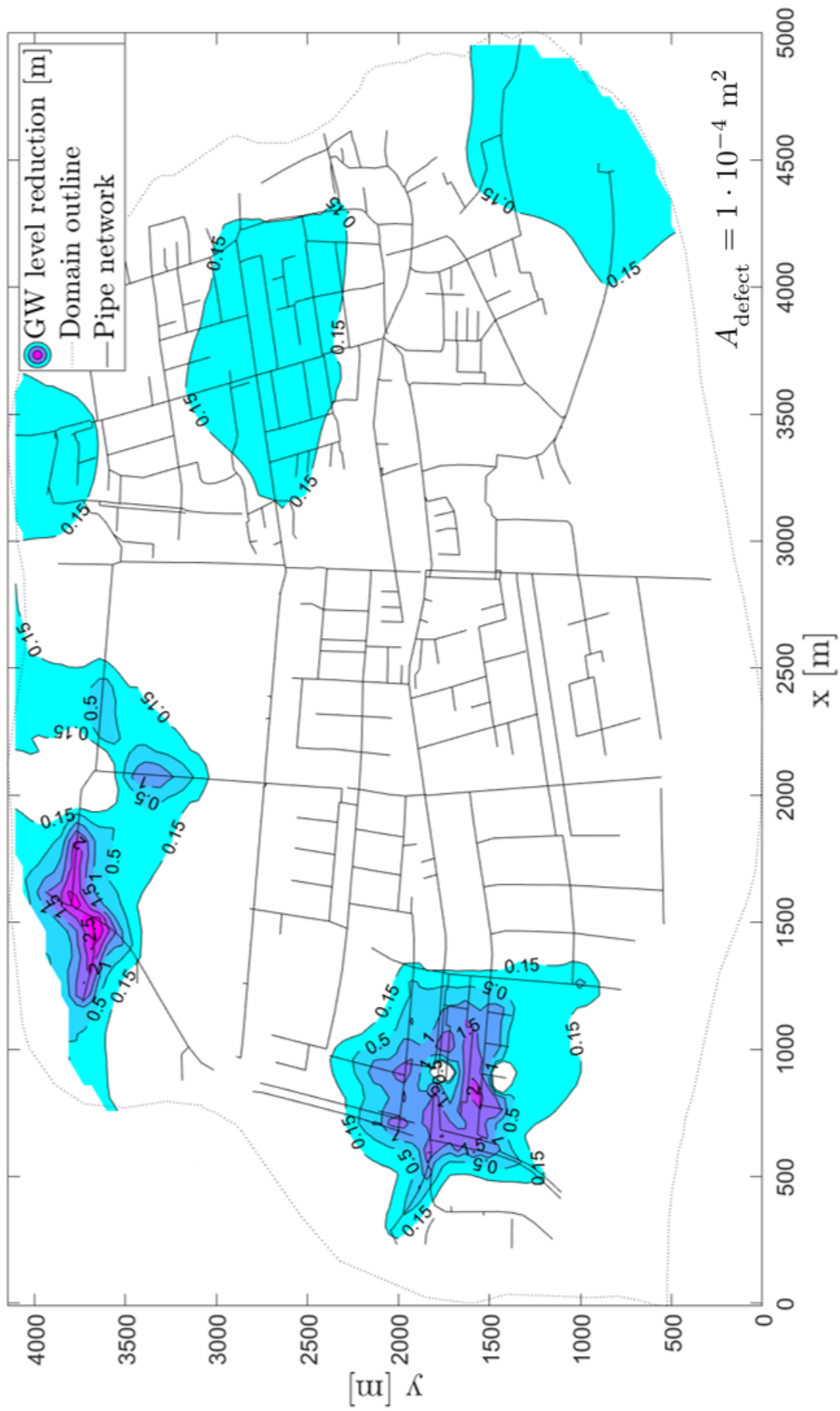


Figure 5.13: Spatial distribution of GW level reduction for a standard defect of $A_{\text{defect}} = 1 \cdot 10^{-4} \text{ m}^2$ per m pipe.

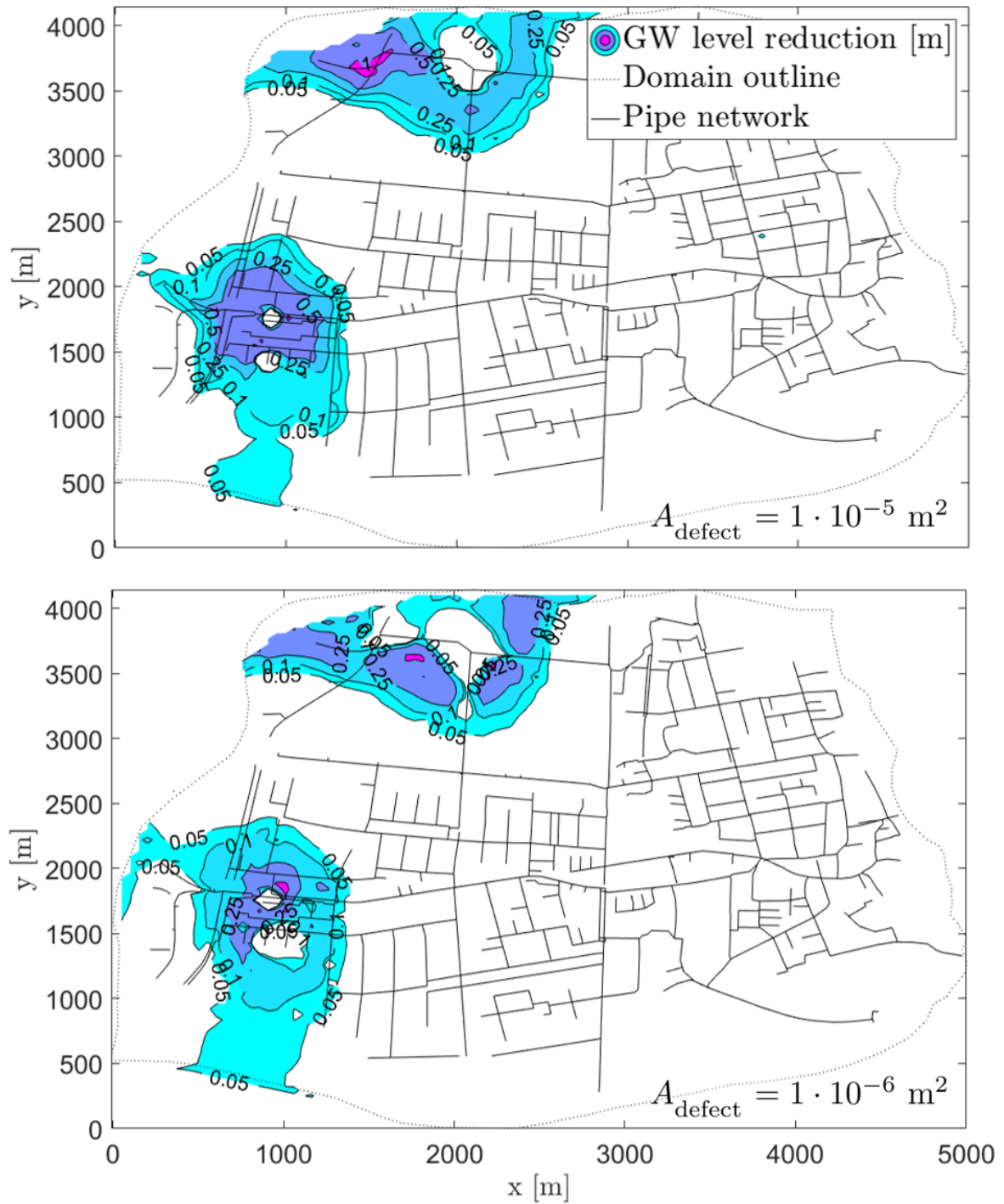


Figure 5.14: Spatial distribution of GW level reduction for standard defects of $A_{\text{defect}} = 1 \cdot 10^{-5} \text{ m}^2$ (above) and $A_{\text{defect}} = 1 \cdot 10^{-6} \text{ m}^2$ (below) per m pipe.

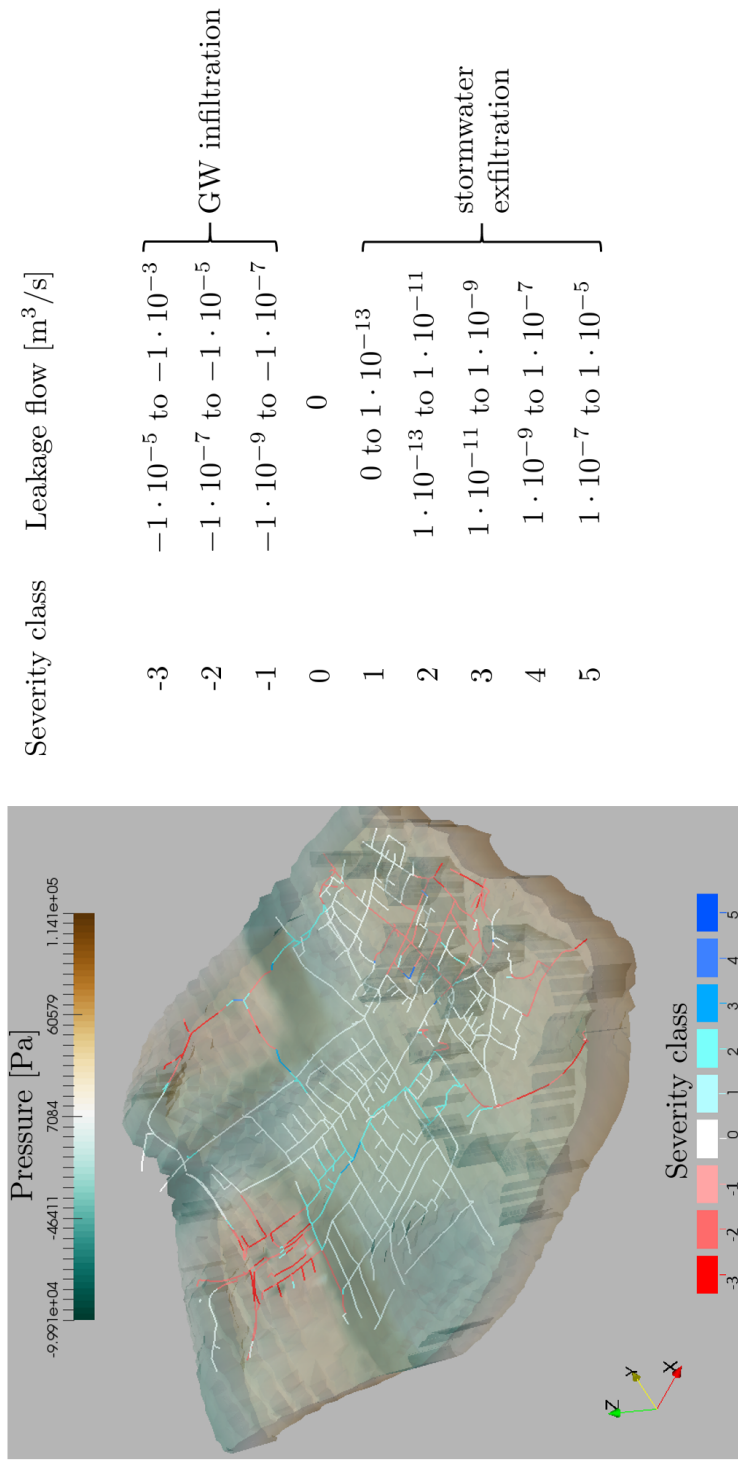


Figure 5.15: Leakage severity map for a standard defect $A_{\text{defect}} = 4 \cdot 10^{-7} \text{ m}^2$ per m pipe. Classes representing GW infiltration are visualized in reddish colors, classes for stormwater exfiltration in blueish colors. Note that the model domain is vertically exaggerated with a factor of 50 for better visualization.

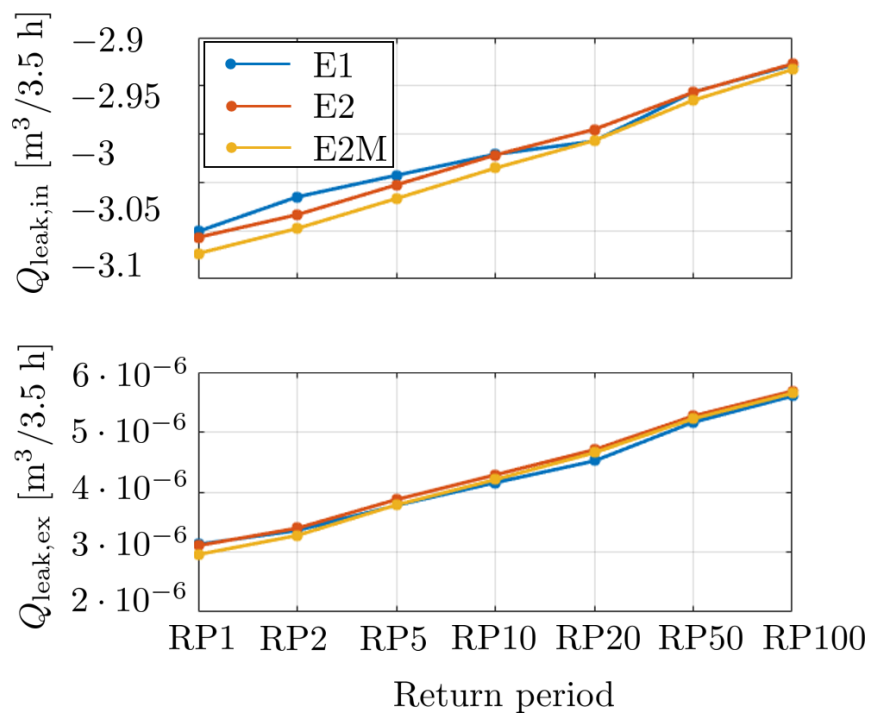


Figure 5.16: Cumulative GW infiltration (above) and cumulative stormwater exfiltration for rain events with different temporal distribution [Euler 1-type (E1), Euler 2-type (E2), Euler 2-type, mirrored (E2M)] and rain event return periods (RP).

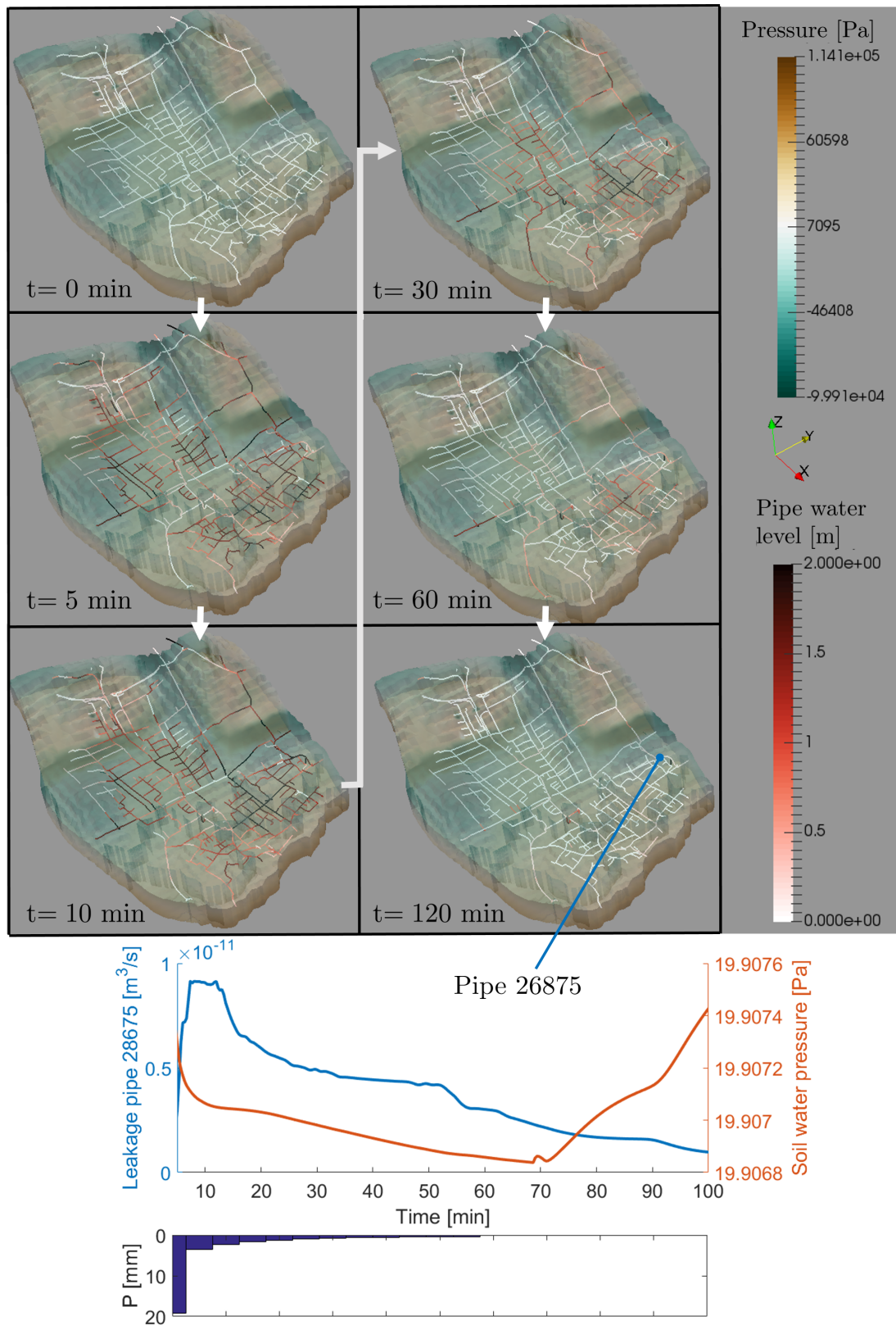


Figure 5.17: Model result for an Euler 1-type rain with a return period of 100 years in form of water level and soil water pressure distribution as well as leakage over time for an exemplary pipe in the catchment. Note that the model domain is vertically exaggerated with a factor of 50 for better visualization.

6 Summary and outlook

Summary

The objective of the present dissertation was divided into three key objectives. First key objective was to generate a validated and verified numerical model for the simulation of pipe leakage in variably-saturated soil. Second key objective was the development of a strategy for upscaling pipe leakage. Last, the third key objective was to successfully apply the leakage model in urban case studies on different spatial scales in order to investigate the pipe leakage process and its impact on urban GW.

Firstly, the present dissertation describes a newly developed model for the physically-based simulation of pipe leakage in variably-saturated soil. The model consists of a groundwater flow simulator and a pipe flow simulator, which are bi-directionally coupled. The newly implemented shared-memory coupling based on updating of boundary conditions and source terms is described. Further, the successful validation and verification of the novel pipe leakage model is demonstrated and a novel benchmark library for pipe leakage models is presented. Benchmarks are based on two physical experiments and two newly derived analytical solutions.

Further, the present dissertation describes a novel method for upscaling pipe leakage. This method is based on transfer functions, called leakage function and relating pipe water level, soil water pressure and pipe leakage flux. The use of this upscaling enables the time-efficient simulation of numerous pipe defects. In total two leakage functions for sewer leakage and stormwater pipe leakage are presented. Further, the source code modifications implemented for this upscaling method are validated and time-efficiency of the method is demonstrated.

Additionally, the present dissertation describes the application of the leakage model in a case study of sewer leakage of a 30 m leaky pipe in order to investigate the response of pipe water exfiltration to various pipe flow events. The impact of total volume of pipe flow, duration of pipe flow, and peak position in time of pipe flow on pipe water exfiltration is investigated systematically.

Finally, the present dissertation describes the application of the leakage model in a case

study of stormwater pipe leakage in an urban subcatchment. The effect of pipe leakage on urban GW under dry-weather conditions is investigated using various model setups with stormwater pipe networks of different ages and conditions (young [largely intact] to old [largely defect]). Further, the impact of rain return period and temporal rainfall distribution on leakage is investigated.

Key contributions and findings

In summary, key contributions and key findings stemming from the present dissertation are

- Main contribution of the present dissertation is the newly developed leakage model for the simulation of pipe leakage in variably-saturated soil. With regards to the included flow processes, the newly developed model is unique. Unlike previous models (see Table 1.1), the model incorporates the flow processes pipe flow, unsaturated-saturated flow, and pipe leakage in a coupled and physically-based manner, where transient pipe flow is simulated in one spatial dimension and transient unsaturated-saturated flow can be simulated in three spatial dimensions.
- Further contribution is the development of a novel benchmark library for the validation and verification of pipe leakage models. The benchmark library consists of in total four benchmark cases. Benchmark cases are based on two physical experiments by Skaggs et al. [1970] and Siriwardene et al. [2007] describing transient pipe leakage driven by constant and time-variable pipe water level into a vertical one-dimensional soil column. Further, the benchmark library consists of two newly developed analytical solutions describing steady-state pipe leakage in one and two spatial dimensions.
- Another key contribution is a newly developed method for upscaling pipe leakage. This novel method is based on leakage functions and enables the simulation of pipe leakage on a large spatial scale with numerous pipe defects and a significantly reduced amount of mesh elements and computation time. In the present dissertation, the method is successfully applied on (otherwise costly) case studies representing a 30 m leaky pipe and an urban catchment with a 53 km leaky pipe network.
- A key finding of the present dissertation is that sinking GW levels lead to the hydraulic disconnection of a leaky pipe with exfiltrating pipe water. As soil water pressure becomes more negative, pipe water exfiltration converges for a given pipe water level. This is due to the evolution of a constant soil saturation (as expressed by κ_r) below the colmation layer. In the state of hydraulic disconnection, pipe water

exfiltration depends only on pipe water level. Although this process is well described for river-GW interaction [e.g. Sophocleous, 2002; Brunner et al., 2009, 2011], it is firstly described for pipe water-GW interaction in the present work.

- A further finding is that pipe flow events of large intensity and/or duration lead to largest pipe water exfiltration, while the temporal distribution of a pipe flow event is irrelevant for pipe water exfiltration. Regarding the significance of pipe flow duration on leakage, this result highlights the effect of time scale dissimilarity of pipe flow and unsaturated-saturated flow. The time scale until the unsaturated-saturated flow system reacts to a pipe flow event may easily be exceeded by the time scale of the pipe flow event itself. In other words, short but very intensive pipe flow events do not evoke large leakage because the increase in soil saturation (and κ_r) is of longer duration than the pipe flow event. Such a time scale dissimilarity is described for surface water-GW interaction in Swain and Wexler [1996] and Singh and Frevert [2003]. It is concluded that large pipe flow events with a small duration evoke small leakage while small pipe flow events with large duration evoke large leakage.
- Another key finding of the present dissertation is that leakage in form of GW infiltration may be in the order of effective annual GW recharge. This result supports findings by Lerner [1986, 1990] who stated that urbanization may significantly reduce GW recharge. Further key finding is that GW infiltration may reduce urban GW levels by several meters. This result supports findings by Lerner [1986] who stated that leakage may lower urban GW levels and Thorndahl et al. [2016a] who found that leakage may reduce urban GW levels by several dozens of centimeters.

Outlook

In future applications, the newly developed leakage model may be coupled to a contaminant transport model [e.g. Sämman et al., 2018] in order to investigate leakage driven-contaminant spreading in an urban flow system. In such an application, both, pipe water exfiltration-driven subsurface contamination and GW-bound contaminant loads in pipe flow could be studied.

Further, the leakage model may be coupled to a numerical model of cavity growth [e.g. Al-Halbouni et al., 2018]. Such a model could be used in order to investigate pipe leakage-driven cavity growth and cavity collapse in form of a sinkhole event. The model could be further used for contributing to the risk assessment and damage mitigation related to urban sinkhole events.

In another future application, the pipe leakage model may be used in order to investigate

the reduction in river and stream baseflow caused by GW infiltration-driven reduced GW levels. This model application may enable to calculate baseflow reduction which enables to investigate environmental consequences such as redistribution of fauna and flora and reduction of biodiversity [King et al., 2016].

Further, the leakage model may be coupled to a heat transport model [e.g. Hein et al., 2016] to investigate the contribution of pipe leakage to warming of urban GW (which is known to be significant [Benz et al., 2015]). Warming of urban GW is related to economic and ecological advantages for the use of shallow geothermal systems [Allen et al., 2003]. In future applications, a coupled pipe leakage-heat transport model may be used to assess consequences of pipe rehabilitation measures to the effectiveness of shallow geothermal systems.

At present stage, no leakage model is able to capture the temporal variability of colmation layers. Especially the breaking-up effect of colmation layers at large pipe flow is known to lead to short-term large leakage [Ellis et al., 2009]. Such large leakage may evoke effects and associated problems such as large contaminant input into the subsurface which may cause GW contamination or short-term changes of the local subsurface flow regime (which may cause damage to underground structures such as cellars). These effects may be investigated with an extended version of the newly developed pipe leakage model, which is able to capture breaking-up of colmation layers.

As described in chapter 1, associated problems related to the pipe leakage process may affect public health and the integrity of urban subsurface structures such as cellars and tunnels. Therefore, pipe leakage represents a risk to humankind and monetary values. A detailed understanding of the pipe leakage process is needed to mitigate this risk. The model developed and presented in the present dissertation has shown to be a useful tool in order to advance the understanding of the pipe leakage process. Its future use may be beneficial for further process understanding and risk mitigation.

7 Appendix

Source code 7.1: MATLAB numerical model example: Richards' flow linearized with a Newton-Raphson scheme. Example problem given is the Celia et al. [1990] problem.

```

1 clear all;
  clc;
  tic;
  // Richards eq. implicitly weighted FD scheme, Aaron Peche. ...
  ...This code was parallelized by Simon Berkhahn.
  // Benchmark problem simulated here: Unsaturated flow problem ...
  ...from Celia et al. (1990)

6
  // Spatial discretization
  Z = 1; // total column length in m
  dz = .025; // spatial increment
  nn = Z/dz;

11 // Soil parameters
  Ks = .922e-4; // saturated hydr. cond. in m/s
  phi = .368; // porosity
  Cs = 1e-10; // storage term - water ...
  ...capacity in 1/m
  // Van Genuchten water retention curve parameter

16 n = 2;
  m = 1-(1/n);
  alpha = 3.35;
  Sr = .277;
  Ss = 1;

21 thetas = phi;
  thetar = Sr*phi/Ss;
  // Initial and Boundary Conditions
  h_new(1:nn,1) = -10;
  h(:,1)=h_new;

26 h_t_old = h_new;
  h_top=-.75; // Top Dirichlet BC
  h_bottom=-10; // Bottom Dirichlet BC
  h_new(1,1)=h_top;
  h_new(nn,1)=h_bottom;

31 h_old(1:nn,1) = -10; // Initialize Old matrix ...
  ...potentials
  // Temporal discretization
  lambda = .5; // For Neumann criterion
  dt = getTimestep( Ks, Cs, lambda, dz); // initialization of ...
  ...time step length
  T =86400; // 1 day simulation time in ...
  ...s

36 // Newton Iteration Parameters
  epsilon = 1e-4;
  tolerance = 1e-5;
  error = 1;
  f = zeros(nn,1); // Initialization of f

```

```

41 J = zeros(nn,nn);           // Initialization of Jacobian

    T_temp = 0;
    k = 1;                     // Time indice
    // Time loop
46 tic
    while T_temp < T
        r = 1;                 // Newton Iteration Counter
        k=k+1;                 // Increase time indice
        error = 1;
51 // Newton Iteration
        while error > tolerance
            h_old=h_new;
            theta=getTheta( phi, thetar, alpha, h_old, n, m);
            Se = getSe( theta, thetar, phi );
56 C = getC( phi, thetar, n, m, alpha, h_old, Cs );
            // Newton-Raphson
            // Generate f-vector - top and bottom boundary node
            f(1) = h_old(1) - h_top;
            f(nn) =h_old(nn) - h_bottom;
61 // Generate JACOBIAN - top and bottom boundary node
            J(1,1) = 1;
            J(nn,nn) = 1;
            parfor i = 2 : nn-1
                // Generate f-vector
66 hi = h_old(i-1);
                hj = h_old(i);
                hk = h_old(i+1);
                h_t_old_i=h_t_old(i);
                f(i) = getf (i, hi, hj, hk, dz, dt, C, h_t_old_i, Ks, ...
                    ...Se, m );
71 // Generate Jacobian
                J_v(i).u=(getf(i, hi+epsilon, hj, hk, dz, dt, C, ...
                    ...h_t_old_i, Ks, Se, m )-f(i))/epsilon;
                J_v(i).h=(getf(i, hi, hj+epsilon, hk, dz, dt, C,...
                    ...h_t_old_i, Ks, Se, m )-f(i))/epsilon;
                J_v(i).o=(getf(i, hi, hj, hk+epsilon, dz, dt, C, ...
                    ...h_t_old_i, Ks, Se, m )-f(i))/epsilon;
            end
76 for i = 2 : nn-1
            hi = h_old(i-1);
            hj = h_old(i);
            hk = h_old(i+1);
            h_t_old_i=h_t_old(i);
81 // Generate Jacobian
            J(i,i-1) = J_v(i).u;
            J(i,i) = J_v(i).h;
            J(i,i+1) = J_v(i).o;
            end
86 // Update solution
            dh = J^(-1)*f;
            dh(1) = 0;
            dh(nn) = 0;
            h_new = h_old-dh;
91 r=r+1;
            error = abs(max(h_new - h_old));
        end

```

```

T_temp = T_temp + dt;           // Current time
96 h_t_old=h_new;
   // Adaptive time stepping scheme
   h_criter = 20;                // No iterations
   time_step_multiplier = (h_criter/r);
   if time_step_multiplier > 2
101   time_step_multiplier = 2;
   elseif time_step_multiplier < 1e-4
       time_step_multiplier = 1e-4;
   end
   dt = dt * time_step_multiplier;
106 if dt >= 60*2
       dt = 60*2;
   end
   end
   figure(3)
111 rho=1000;
   g=9.81;
   plot(dz:dz:Z,h_new*(rho*g), 'LineWidth', 2)
   xlabel(['depth [m]'])
   ylabel(['pressure [kPa]'])
116 title(['Celias problem - FD scheme,weighting:central_{space},...
         ...implicit_{time}'])
   legend(['dt_{max}=60 s, dx=1e-3 m'])
   hold all
   toc

121 // Function - storage term:

   function [ C ] = getC( phi, thetar, n, m, alpha, h, Cs )

   C = (((phi - thetar) * n * m * alpha * (-alpha * h).^ (n - 1)))...
       .... / ...
126   ((1 + (-alpha * h).^ (n)).^ (m + 1)) + Cs;
   C (h>=0) = Cs;

   end
   // Function - f-vector
131 function [ f ] = getf( i, hi, hj, hk, dz, dt, C, h_t_old, Ks, ...
       ...Se, m )

   a = (-( getKr(hi, hj, hk, Ks, Se(i+1), m, dz) - getKr(hi, hj, ...
       ...hk, Ks, Se(i-1), m, dz) ) ...
       / (4*dz^2) ) + (getKr(hi, hj, hk, Ks, Se(i), m, dz)/(dz^2))...
       ... ) * (dt/C(i));
136 b = -(1+(2*(getKr(hi, hj, hk, Ks, Se(i), m, dz))/dz^2)*dt/C(i)...
       ... ));
   c = (( getKr(hi, hj, hk, Ks, Se(i+1), m, dz) - getKr(hi, hj, ...
       ...hk, Ks, Se(i-1), m, dz) ) ...
       / (4*dz^2) ) + (getKr(hi, hj, hk, Ks, Se(i), m, dz)/(dz^2))...
       ... ) * (dt/C(i));
   d = h_t_old+ (0-(getKr(hi, hj, hk, Ks, Se(i+1), m, dz) - getKr...
       ... (hi, hj, hk, Ks, Se(i-1), m, dz) ) ...
       / (2*dz)) * (dt/C(i));
141 f = a * hi + b * hj + c * hk + d;

```

```

    end
    // Function - relative hydraulic conductivity
146 function [ Kr ] = getKr( hi, hj, hk, Ks, Se, m, dz )

    Kr = Ks*sqrt(Se)*((1-(1-(Se^(1/m))))^(m))^2);
    Kr (Se>=1) = Ks;

151 end
    // Function - effective saturation

    function [ Se ] = getSe( theta, thetar, phi )

156 Se = (theta-thetar)/(phi-thetar);

    end
    // Function - water content

161 function [ theta ] = getTheta ( phi, thetar, alpha, h, n, m)

    theta = thetar+(phi-thetar)*((1+(-alpha*h).^n).^(-m));
    theta(h>=0) = phi;

166 end
    // Function - Neumann time step criterion

    function [ functionvalue ] = getTimestep( Ks, Cs, lambda, dz )

171 Ds = Ks/Cs;
    functionvalue = lambda*((dz^2)/Ds);

    end

```

Source code 7.2: C++ source code example for NamedPipes-based interprocess data transfer. Modified from Bloomfield, P. R. [2012].

```

1  ///// SERVER PROGRAM /////

    #include <iostream>
    #include <windows.h>

6  using namespace std;
    int main(int argc, const char **argv)
    {
        wcout << "Creating instance of NamedPipe..." << endl;

11     // Create a pipe to send data
        HANDLE pipe = CreateNamedPipe(
            "\\.\pipe\\_pipe", // declare name of pipe
            PIPE_ACCESS_OUTBOUND, // this is a one-way pipe
            PIPE_TYPE_BYTE, // data will be send as byte stream
16            1, // only allow 1 instance of this pipe
            0, // no outbound buffer
            0, // no inbound buffer
            0, // use default wait time
            NULL // use default security attributes

```



```

21     );

    if (pipe == NULL || pipe == INVALID_HANDLE_VALUE) {
        wcout << "Failed to create outbound pipe instance.";
        // look up error code here using GetLastError()
26     system("pause");
        return 1;
    }

    wcout << "Waiting for a client to connect to the pipe..." ...
        ...<< endl;
31    // This call blocks until a client process connects to the ...
        ...pipe
    BOOL result = ConnectNamedPipe(pipe, NULL);
    if (!result) {
        wcout << "Failed to make connection on named pipe." << ...
            ...endl;
        // look up error code here using GetLastError()
36    CloseHandle(pipe); // close the pipe
        system("pause");
        return 1;
    }

41    wcout << "Sending data to pipe..." << endl;
    // This call blocks until a client process reads all the ...
        ...data
    //     wcout << "Enter something..." << endl;
    //     wchar_t *ch;
    //     wcin >> *ch;
46    const wchar_t *data = L"Das ist ein Loewe! Na logo, endlich...
        ... kein Schneider mehr. This entire string including a ...
        ...charming reference to H. Gallig and H. Hennings is ...
        ...transferred via a NamedPipe.";
    wcout << "String being transferred is: " << data << endl;
    DWORD numBytesWritten = 0;
    result = WriteFile(
        pipe, // handle to our outbound pipe
51    data, // data to send
        wcslen(data) * sizeof(wchar_t), // length of data to ...
            ...send (bytes)
        &numBytesWritten, // will store actual amount of data ...
            ...sent
        NULL // not using overlapped IO
    );
56
    if (result) {
        wcout << "Number of bytes sent: " << numBytesWritten <<...
            ... endl;
    } else {
        wcout << "Failed to send data." << endl;
61    // look up error code here using GetLastError()
    }

    // Close the pipe (automatically disconnects client too)
    CloseHandle(pipe);
66
    wcout << "Done." << endl;

```

```

        system("pause");
        return 0;
71 }

    ////// CLIENT PROGRAM //////

#include <iostream>
76 #include <windows.h>
using namespace std;

int main(int argc, const char **argv)
{
81     wcout << "Connecting to pipe..." << endl;

    // Open the NamedPipe
    HANDLE pipe = CreateFile(
        "\\.\pipe\_pipe",
86     GENERIC_READ, // only need read access
        FILE_SHARE_READ | FILE_SHARE_WRITE,
        NULL,
        OPEN_EXISTING,
        FILE_ATTRIBUTE_NORMAL,
91     NULL
    );

    if (pipe == INVALID_HANDLE_VALUE) {
        wcout << "Failed to connect to pipe." << endl;
96     system("pause");
        return 1;
    }

    wcout << "Reading data from pipe..." << endl;
101

    // The read operation will block until there is data to ...
    ...read
    wchar_t buffer[128];
    DWORD numBytesRead = 0;
    BOOL result = ReadFile(
106     pipe,
        buffer, // data from pipe will be stored here
        127 * sizeof(wchar_t), // number of allocated bytes
        &numBytesRead, // number of bytes that are read will be...
        ... stored here
        NULL // prevents overla in InOut
111 );

    if (result) {
        buffer[numBytesRead / sizeof(wchar_t)] = '\0'; // null ...
        ...terminate the string
        wcout << "Number of bytes read: " << numBytesRead << ...
        ...endl;
116     wcout << "Message: " << buffer << endl;
    } else {
        wcout << "Failed to read data from the pipe." << endl;
    }
}

```

```

121 // Close our pipe handle
    CloseHandle(pipe);

    wcout << "Done." << endl;

126 system("pause");
    return 0;
}

```

Table 7.1: Single pipe defect bottom boundary pressures used for the single defect model.

Pressure [Pa]
0
9807000
19614000
29421000
34324000
36286000
37266000
37757000
38002000
38125000
38275000
39228000
44131000
46584000
49035000

Table 7.2: Total number of elements and colmation layer elements within all meshes used for the grid convergence study with the single pipe defect model.

Mesh no.	Elements	Colmation layer elements
1	7054000	24
2	10203000	43
3	10788000	78
4	14820000	98
5	17672000	124
6	22215000	142

Table 7.3: Total number of elements for the grid convergence study with the single pipe defect leakage function-model.

Mesh no.	Elements
1	3750000
2	5217000
3	6745000
4	9364000
5	11677000
6	23016000

Table 7.4: Total number of elements within all meshes used for the grid convergence study with the 30 m leaky pipe model.

Mesh no.	Elements
1	177000
2	227000
3	249000
4	358000
5	506000
6	1228000

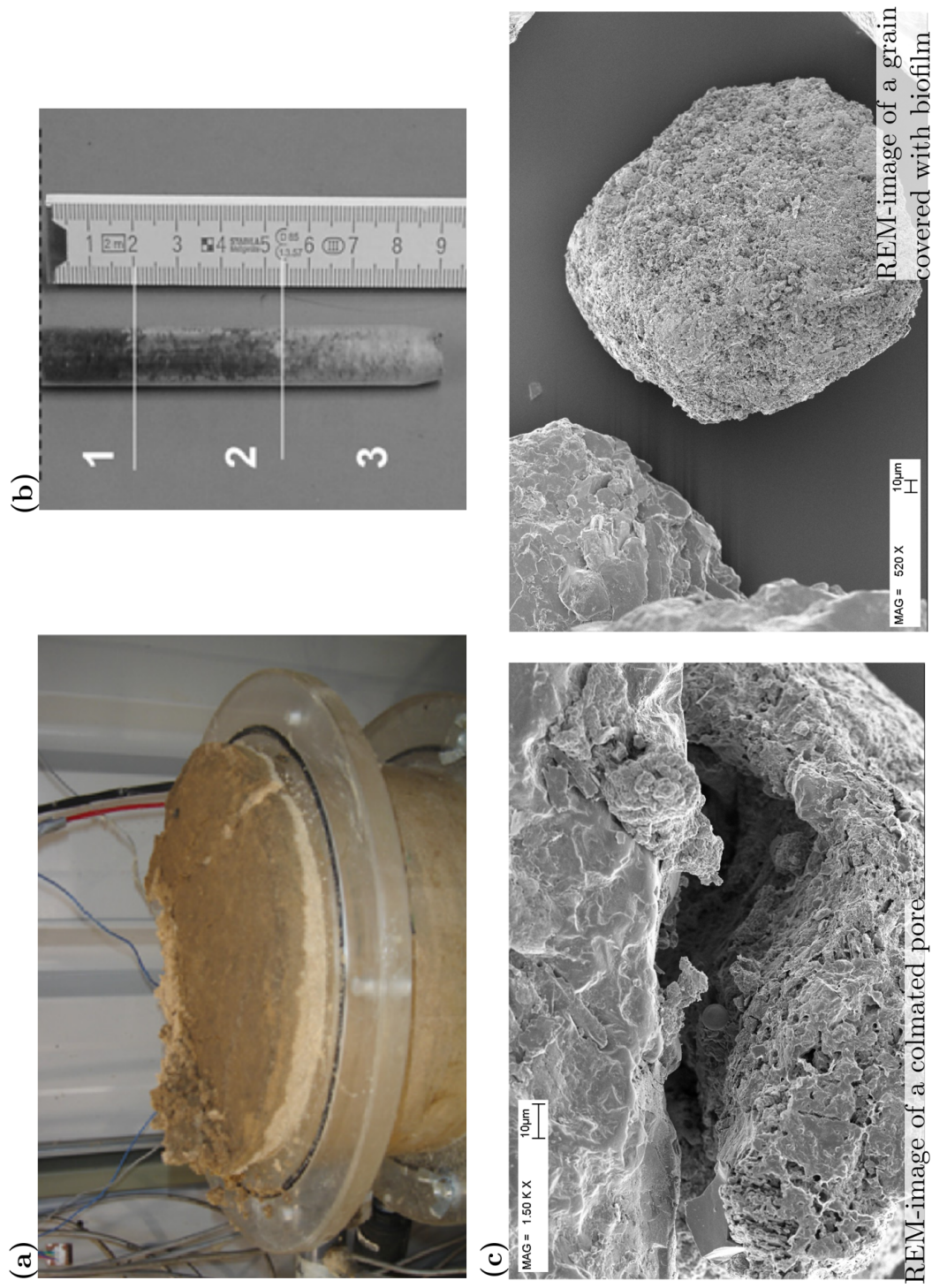


Figure 7.1: (a) Stormwater colmatation layer. Modified from Siriwardene et al. [2007]. (b) Probe taken from a sewer colmatation layer. The label 1 denotes the colmatation layer, and 2 and 3 denote a transition zone. Modified from Klinger et al. [2010]. (c) REM-images of a colmatation layer. Modified from Schwarz [2004].

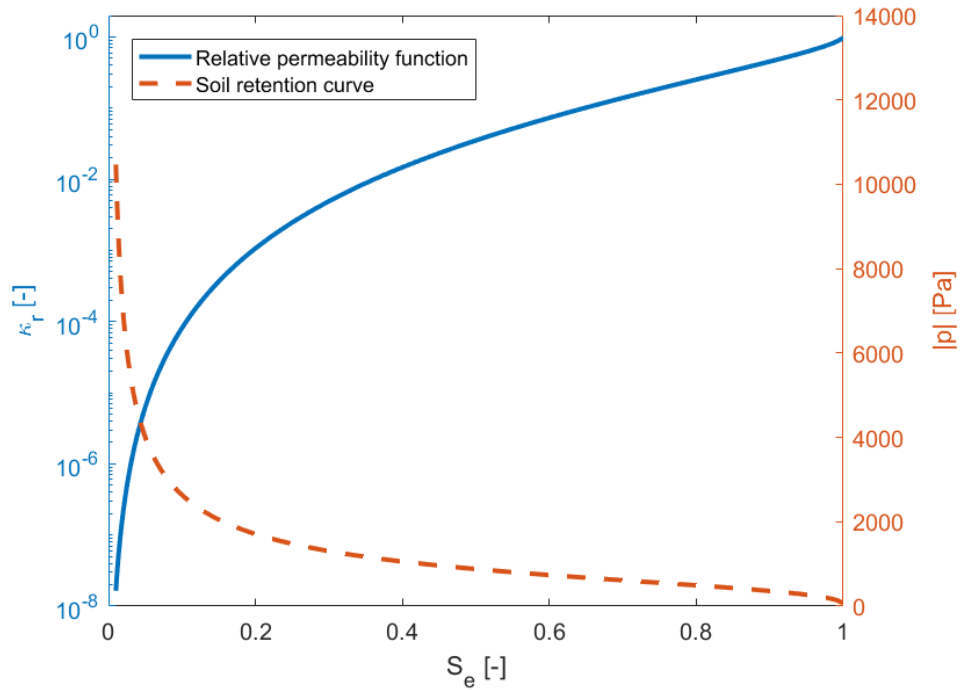


Figure 7.2: van Genuchten [1980] retention curve and relative permeability function representing the trench backfill and aquifer strata given in Table 3.1.

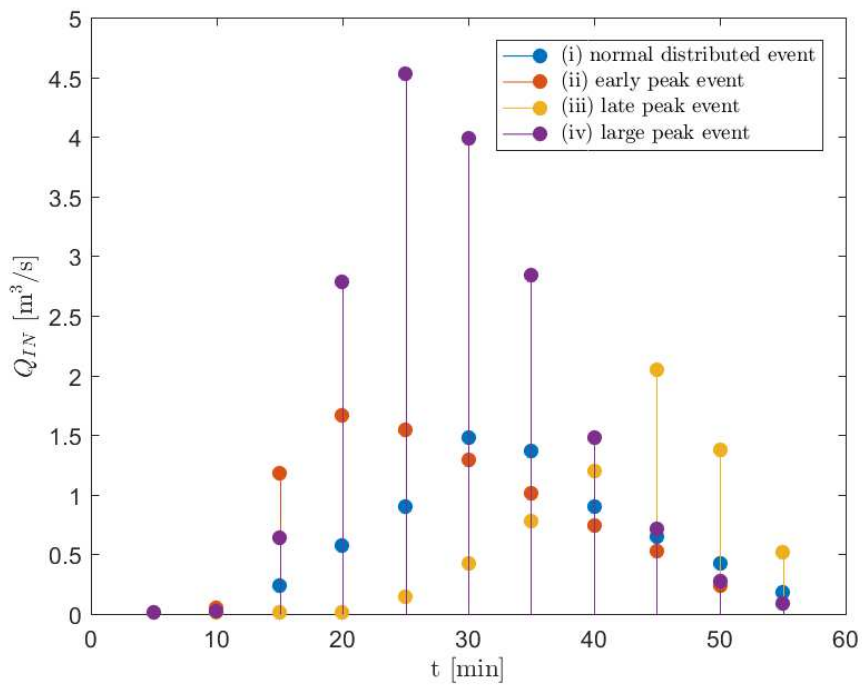


Figure 7.3: Pipe flow events used for the single defect model.

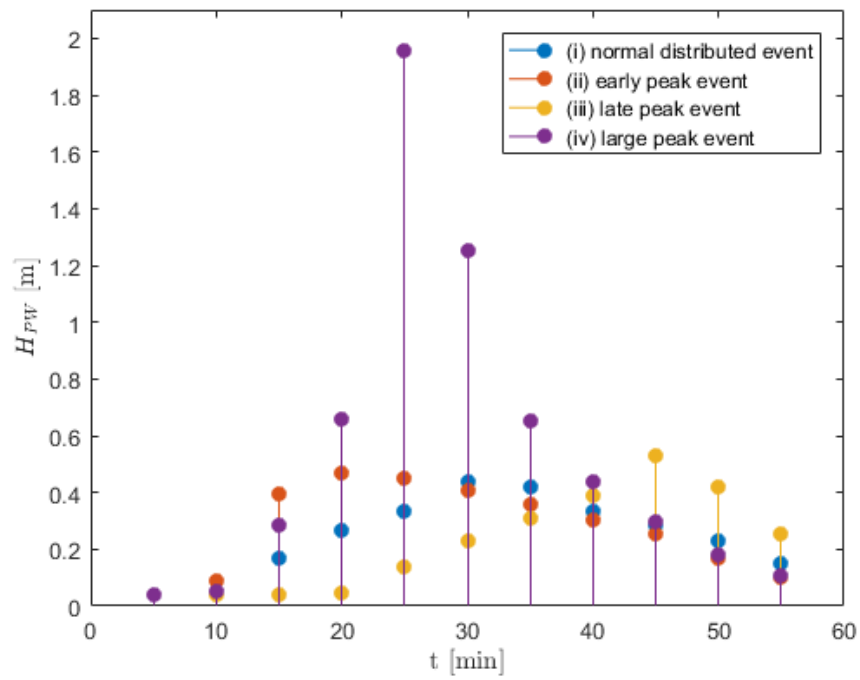


Figure 7.4: Pipe water levels above the defect calculated for the single defect model.

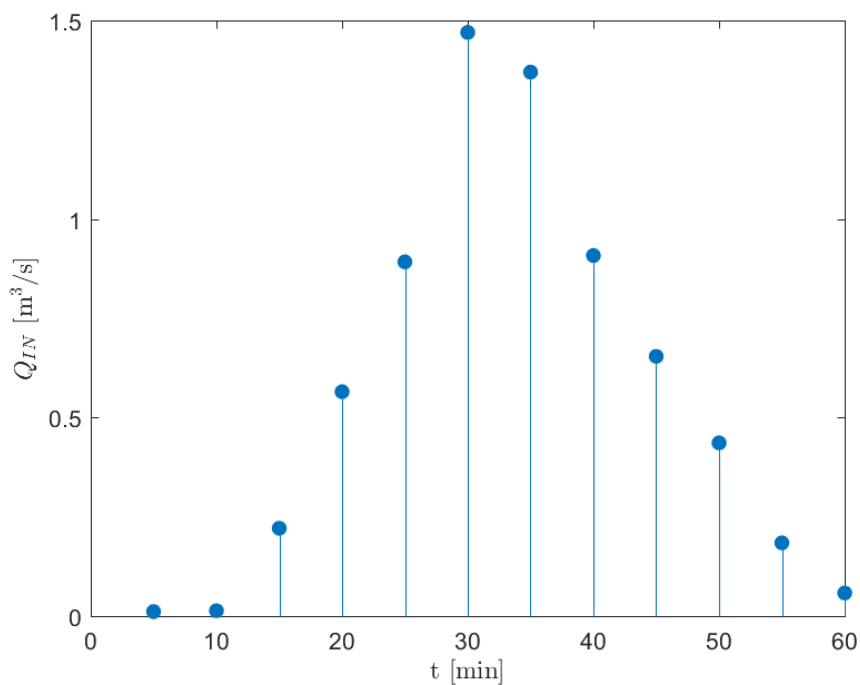


Figure 7.5: Pipe flow event used for the comparison of the fully discretized model with the LF-model.

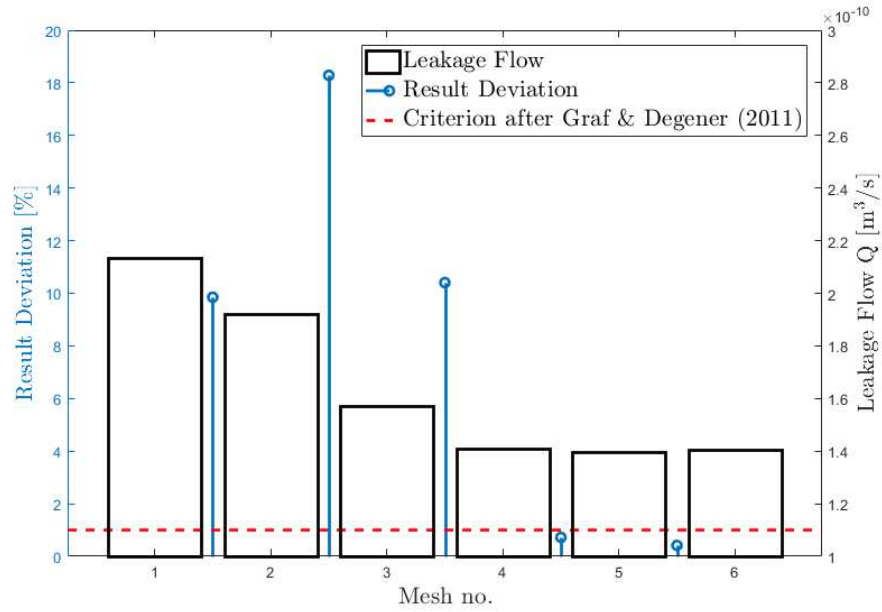


Figure 7.6: Results of the grid convergence study for the fully discretized single pipe defect simulations. Black colors represent colmatation layer flow and blue colors the relative deviation of results compared with the coarser mesh, respectively. The red dashed line represents the 1% result deviation criterion described in Graf and Degener (2011). Information about meshes 1 to 6 is given in table 7.2.

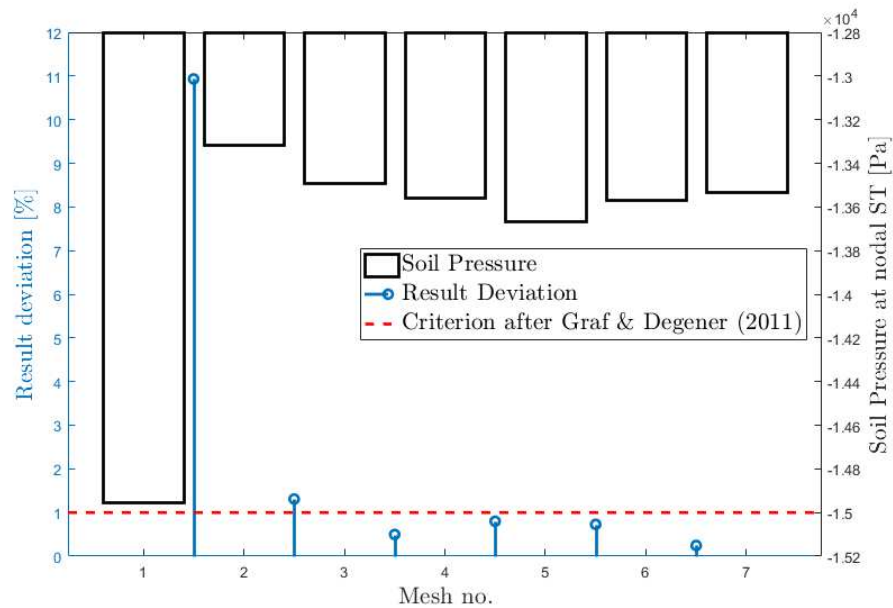


Figure 7.7: Results of the grid convergence study for the LF-model single pipe defect simulations. Black colors represent LF-ST node pressure and blue colors the relative deviation of results compared with the coarser mesh, respectively. The red dashed line represents the 1% result deviation criterion described in Graf and Degener (2011). Information about meshes 1 to 6 is given in table 7.3.

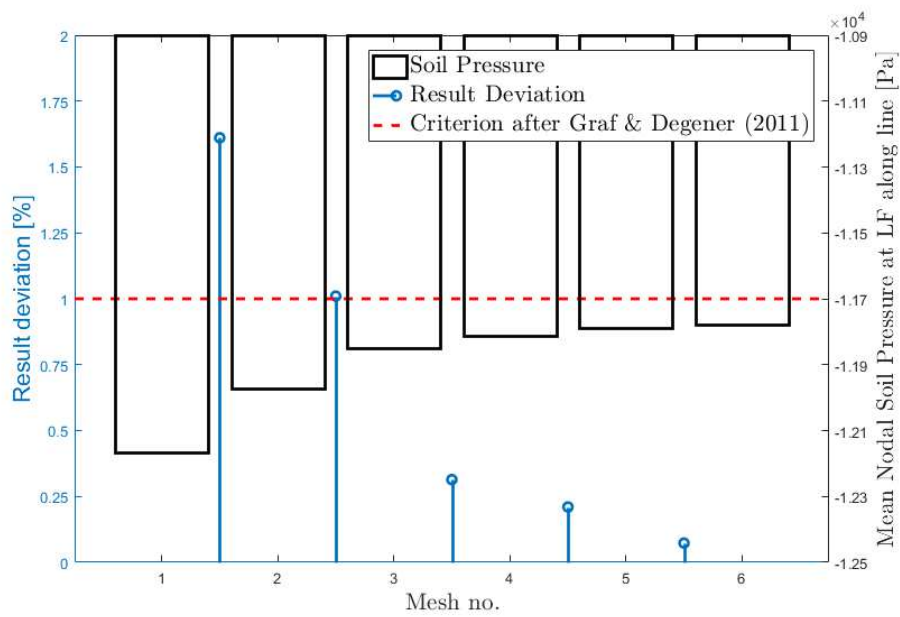


Figure 7.8: Results of the grid convergence study for the 30 m leaky pipe model. Black colors represent water pressure in the soil at nodes which are later used as LF source term nodes. Blue colors represent the relative deviation of results compared with the coarser mesh, respectively. The red dashed line represents the 1% result deviation criterion described in Graf and Degener (2011). Information about meshes 1 to 6 is given in table 7.4.

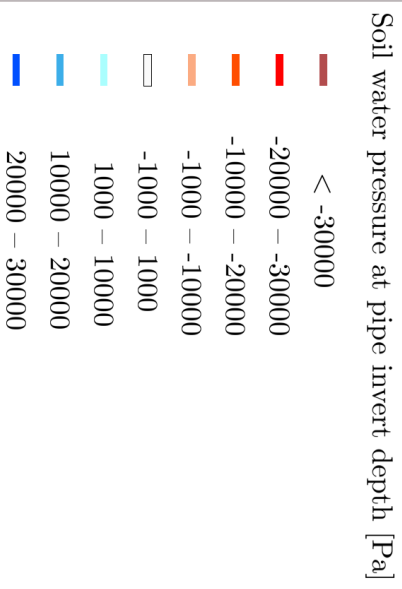


Figure 7.9: Initial spatial distribution of soil water pressure at pipe invert for the urban subcatchment model.

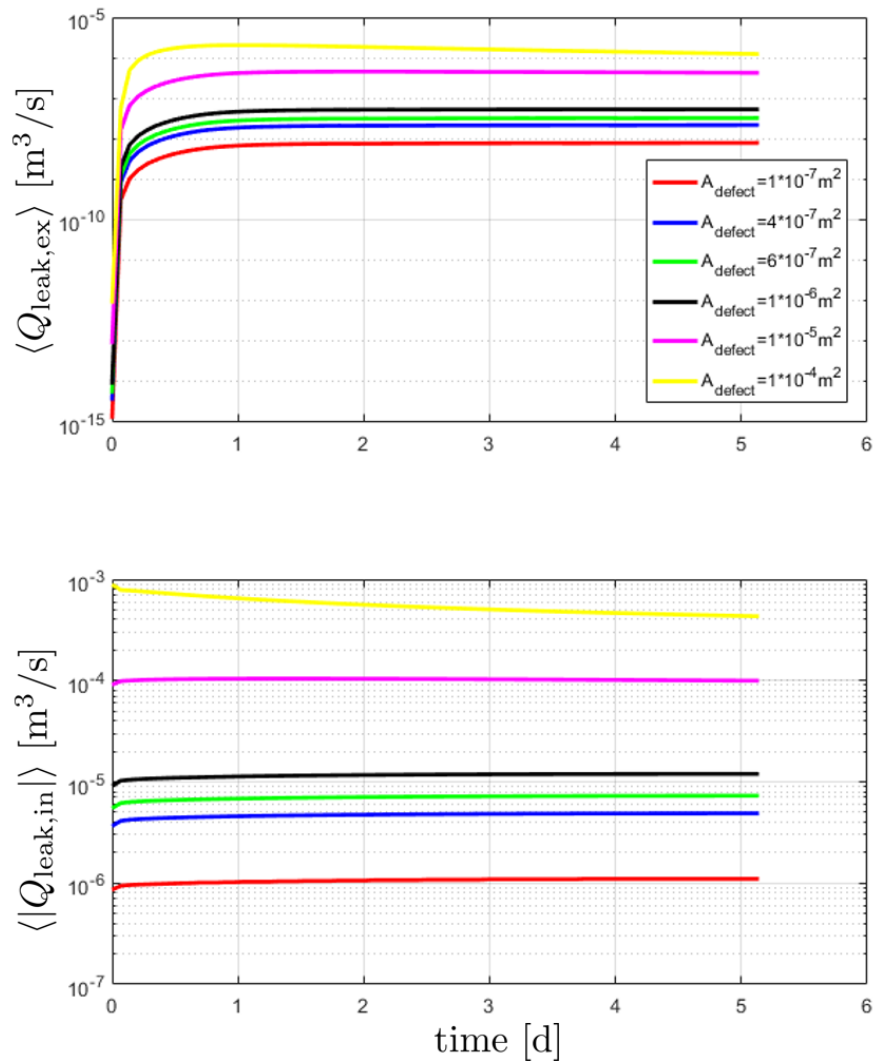


Figure 7.10: Dynamic evolution of dry-weather flow leakage in the catchment scale model. Above: Mean leakage (for all pipes) in form of pipe water exfiltration over time for different standard defect sizes. Below: Mean leakage (for all pipes) in form of absolute values of groundwater infiltration over time.

List of symbols

A	$[L^2]$ cross-sectional area
A_{defect}	$[L^2]$ quadratic standard defect area after Karpf [2012]
dGW	$[L]$ distance between pipe defect and groundwater table
g	$[LT^{-2}]$ gravitational acceleration
η	$[ML^{-1}T^{-1}]$ fluid dynamic viscosity
ρ	$[ML^{-3}]$ fluid density
p	$[ML^{-1}T^{-2}]$ water pressure
p_{int}	$[ML^{-1}T^{-2}]$ water pressure at colmation layer-aquifer interface
ψ	$[L]$ matric potential
ψ_{int}	$[L]$ matric potential at colmation layer-aquifer interface
t	$[T]$ time
Q	$[L^3T^{-1}]$ volumetric flow
q	$[LT^{-1}]$ specific flux
v	$[LT^{-1}]$ flow velocity
r	$[L]$ radius
r_{wf}	$[L]$ radius of a circular wetting front
V_{unit}	$[L^3]$ unit volume
x, y, z	$[L]$ spatial coordinate
∇	$[L^{-1}]$ nabla operator
ϕ	$[-]$ porosity
κ	$[L^2]$ intrinsic permeability
κ_r	$[-]$ relative intrinsic permeability
K_s	$[LT^{-1}]$ saturated hydraulic conductivity
α	$[L^{-1}]$ van Genuchten [1980] parameter: inverse of the capillary rise
m, n	$[-]$ van Genuchten [1980] parameter: pore size distribution related parameter

$\Delta x_c, \Delta y_c$	[L] colmation layer extent
h_c	[L] colmation layer height (z-extent)
S	[-] water saturation
S_e	[-] effective water saturation
S_m	[-] maximum water saturation
S_r	[-] residual water saturation
b	[L] aquifer thickness
H_{PW}	[L] pipe water level
I_s	[-] pipe slope
I_r	[-] pipe friction slope
Δx	[L] pipe length
$\cdot_{a,c}$	subscripts referring to colmation layer and aquifer
a_i	coefficients of the leakage function polynomial

References

- Al-Halbouni, D., Holohan, E. P., Taheri, A., Schöpfer, M. P. J., Emam, S., and Dahm, T. (2018). Geomechanical modelling of sinkhole development using distinct elements: Model verification for a single void space and application to the dead sea area. *Solid Earth Discussions*, 2018:1–53.
- Allen, A., Milenic, D., and Sikora, P. (2003). Shallow gravel aquifers and the urban heat island effect: a source of low enthalpy geothermal energy. *Geothermics*, 32(4-6):569–578.
- Bauer, M., Freeden, W., Jakobi, H., and Neu, T. (2014). *Handbuch Tiefe Geothermie*. Springer.
- Becker, B., Nowack, L., Klauder, W. S., Köngeter, J., and Schüttrumpf, H. (2009). Eine nichtlineare Leakage-Randbedingung für die Modellierung von hochwasserbeeinflusstem Grundwasseranstieg. *WasserWirtschaft*, 99:1–2.
- Benz, S. A., Bayer, P., Menberg, K., Jung, S., and Blum, P. (2015). Spatial resolution of anthropogenic heat fluxes into urban aquifers. *Science of The Total Environment*, 524:427–439.
- Bhaskar, A., Welty, C., Maxwell, R., and Miller, A. (2015). Untangling the effects of urban development on subsurface storage in baltimore. *Water Resources Research*, 51(2):1158–1181.
- Birch, G., Matthai, C., Fazeli, M., and Suh, J. (2004). Efficiency of a constructed wetland in removing contaminants from stormwater. *Wetlands*, 24(2):459–466.
- Bishop, P., Misstear, B., White, M., and Harding, N. (1998). Impacts of sewers on groundwater quality. *Water and Environment Journal*, 12(3):216–223.
- Blackwood, D. J., Gilmour, D., Ellis, J. B., Revitt, D. M., and Stainer, A. (2005). Ex-filtration from sewers: is it a serious problem. In *Proceedings of the 10th International Conference on Urban Drainage, Copenhagen, Denmark*, pages 21–26.
- Bloomfield, P. R. (2012). <http://avidinsight.uk/2012/03/introduction-to-win32-named-pipes-cpp/> (access date: 2018-06-21).
- Booth, D. (2006). *The environmental consequences of growth: steady-state economics as an alternative to ecological decline*. Routledge.
- Boukhemacha, M. A., Gogu, C. R., Serpescu, I., Gaitanaru, D., and Bica, I. (2015). A hydrogeological conceptual approach to study urban groundwater flow in Bucharest city, Romania. *Hydrogeology Journal*, 23(3):437–450.
- Brooks, R. H. and Corey, A. T. (1966). Properties of porous media affecting fluid flow. *Journal of the Irrigation and Drainage Division*, 92(2):61–90.

- Browne, D., Deletic, A., Mudd, G. M., and Fletcher, T. D. (2008). A new saturated/unsaturated model for stormwater infiltration systems. *Hydrological Processes*, 22(25):4838–4849.
- Brunner, P., Cook, P. G., and Simmons, C. T. (2009). Hydrogeologic controls on disconnection between surface water and groundwater. *Water Resources Research*, 45(1).
- Brunner, P., Cook, P. G., and Simmons, C. T. (2011). Disconnected surface water and groundwater: from theory to practice. *Groundwater*, 49(4):460–467.
- Butler, D. and Davies, J. (2003). *Urban drainage*. Crc Press.
- Camporese, M., Paniconi, C., Putti, M., and Orlandini, S. (2010). Surface-subsurface flow modeling with path-based runoff routing, boundary condition-based coupling, and assimilation of multisource observation data. *Water Resources Research*, 46(2).
- Carsel, R. and Parrish, R. (1988). Developing joint probability distributions of soil water retention characteristics. *Water Resources Research*, 24(5):755–769.
- Celia, M. A., Bouloutas, E. T., and Zarba, R. L. (1990). A general mass-conservative numerical solution for the unsaturated flow equation. *Water resources research*, 26(7):1483–1496.
- Chisala, B. and Lerner, D. (2008). Distribution of sewer exfiltration to urban groundwater. In *Proceedings of the Institution of Civil Engineers-Water Management*, volume 161, pages 333–341. Thomas Telford Ltd.
- Clemens, F., Stanić, N., Van der Schoot, W., Langeveld, J., and Lepot, M. (2015). Uncertainties associated with laser profiling of concrete sewer pipes for the quantification of the interior geometry. *Structure and Infrastructure Engineering*, 11(9):1218–1239.
- Coppola, D. (2015). *Introduction to international disaster management*. Elsevier, third edition.
- Davies, J., Clarke, B., Whiter, J., and Cunningham, R. (2001). Factors influencing the structural deterioration and collapse of rigid sewer pipes. *Urban water*, 3(1-2):73–89.
- Davis, A. P. and McCuen, R. H. (2005). *Stormwater management for smart growth*. Springer Science & Business Media.
- de Saint-Venant, A. (1871). Théorie et equations générales du mouvement non permanent des eaux courantes. *Comptes Rendus des séances de l'Académie des Sciences*, 73:147–154.
- delta h Ingenieurgesellschaft GmbH (2017). *SPRING Simulation of Processes in Groundwater - User Manual*. delta h Ingenieurgesellschaft GmbH Witten.
- DeSilva, D., Burn, S., Moglia, M., Tjandraatmadja, G., Gould, S., and Sadler, P. (2007). Chapter. 2 the models: Network exfiltration and infiltration model neimo. *Urban Water Resources Toolbox-Integrating Groundwater into Urban Water Management*, pages 34–50.
- DeSilva, D., Burn, S., Tjandraatmadja, G., Moglia, M., Davis, P., Wolf, L., Held, I., Vollertsen, J., Williams, W., and Hafskjold, L. (2005). Sustainable management of leakage from wastewater pipelines. *Water science and technology*, 52(12):189–198.

- DHI (2017). *MIKE 1D - DHI Simulation Engine for 1D river and urban modelling, Reference Manual*. MIKE powered by DHI, Hørsholm, Denmark.
- DHI (2017b). *MIKE SHE. Volume 2: Reference Guide*. MIKE powered by DHI, Hørsholm, Denmark.
- Dohmann, M., editor (2013). *Wassergefährdung durch undichte Kanäle: Erfassung und Bewertung*. Springer-Verlag.
- Ehlers, J. and Gibbard, P. L. (1996). *Allgemeine und historische Quartärgeologie*. John Wiley & Sons.
- Eiswirth, M. and Hötzl, H. (1997). The impact of leaking sewers on urban groundwater. *Groundwater in the urban environment*, 1:399–404.
- Elliott, H., Liberati, M., and Huang, C. (1986). Competitive adsorption of heavy metals by soils 1. *Journal of Environmental Quality*, 15(3):214–219.
- Ellis, B. and Bertrand-Krajewski, J.-L. (2010). *Assessing infiltration and exfiltration on the performance of urban sewer systems*. IWA Publishing.
- Ellis, J. (2001). *Sewer Infiltration/exfiltration and Interactions with Sewer Flows and Groundwater Quality. Interactions between Sewers, Treatment Plants and Receiving Waters in Urban Areas - INTERUBA II*, pages 311–319. cited By 1.
- Ellis, J., Revitt, D., Vollertsen, J., and Blackwood, D. (2009). Sewer exfiltration and the colmation layer. *Water Science and Technology*, 59(11):2273–2280.
- Eriksson, E., Baun, A., Scholes, L., Ledin, A., Ahlman, S., Revitt, M., Noutsopoulos, C., and Mikkelsen, P. S. (2007). Selected stormwater priority pollutants: a european perspective. *Science of the total environment*, 383(1-3):41–51.
- Fenner, R. A. (2000). Approaches to sewer maintenance: a review. *Urban water*, 2(4):343–356.
- Fraga, I., Cea, L., and Puertas, J. (2017). Validation of a 1d-2d dual drainage model under unsteady part-full and surcharged sewer conditions. *Urban Water Journal*, 14(1):74–84.
- Fuchs, L. and Beeneken, T. (2005). Development and implementation of a real-time control strategy for the sewer system of the city of Vienna. *Water Science and Technology*, 52(5):187–194.
- Fuchs, L., Beeneken, T., Spönemann, P., and Scheffer, C. (1997). Model based real-time control of sewer system using fuzzy-logic. *Water science and technology*, 36(8-9):343–347.
- Fuchs-Hanusch, D., Steffelbauer, D., Günther, M., and Muschalla, D. (2016). Systematic material and crack type specific pipe burst outflow simulations by means of EPANET2. *Urban water journal*, 13(2):108–118.
- Gironás, J., Roesner, L. A., Rossman, L. A., and Davis, J. (2009). Software, Data and Modelling News A new applications manual for the Storm Water Management Model (SWMM). *Environmental Modelling and Software*, 25:813–814.

- Gogu, C., Gaitanaru, D., Boukhemacha, M., Serpescu, I., Litescu, L., Zaharia, V., Moldovan, A., and Mihailovici, M. (2017). Urban hydrogeology studies in Bucharest city, Romania. *Procedia Engineering*, 209:135–142.
- Graf, T. and Degener, L. (2011). Grid convergence of variable-density flow simulations in discretely-fractured porous media. *Advances in water resources*, 34(6):760–769.
- Grubb, S. (1993). Analytical model for estimation of steady-state capture zones of pumping wells in confined and unconfined aquifers. *Groundwater*, 31(1):27–32.
- Gujer, W. (2007). Technik der Siedlungsentwässerung. *Siedlungswasserwirtschaft*, pages 245–286.
- Guo, S., Shao, Y., Zhang, T., Zhu, D. Z., and Zhang, Y. (2013). Physical modeling on sand erosion around defective sewer pipes under the influence of groundwater. *Journal of Hydraulic Engineering*, 139(12):1247–1257.
- Gustafsson, L.-G. (2000). Alternative drainage schemes for reduction of inflow/infiltration-prediction and follow-up of effects with the aid of an integrated sewer/aquifer model. In *1st International Conference on Urban Drainage via Internet*, pages 21–37.
- Harbaugh, A. W., Banta, E. R., Hill, M. C., and McDonald, M. G. (2000). MODFLOW 2000, the U. S. Geological Survey modular ground-water model-user guide to modularization concepts and the ground-water flow process. *Open-file Report. U. S. Geological Survey*, (92):134.
- Harvey, R. and McBean, E. (2014). Understanding stormwater pipe deterioration through data mining. *Journal of Water Management Modeling*.
- Hein, P., Kolditz, O., Görke, U.-J., Bucher, A., and Shao, H. (2016). A numerical study on the sustainability and efficiency of borehole heat exchanger coupled ground source heat pump systems. *Applied Thermal Engineering*, 100:421–433.
- Hermosilla, R. G. (2012). The Guatemala city sinkhole collapses. *Carbonates and evaporites*, 27(2):103–107.
- Herrada, M., Gutiérrez-Martín, A., and Montanero, J. (2014). Modeling infiltration rates in a saturated/unsaturated soil under the free draining condition. *Journal of Hydrology*, 515:10–15.
- Herringshaw, L. (2007). *Urban groundwater management and sustainability*, volume 74. Springer Science & Business Media.
- Hornef, H. (1983). Menaces to the quality of groundwater due to leaky public sewers and house drainage systems. *Korrespondenz Abwasser*, 12(83):896–903.
- Huang, G. and Yeh, G.-T. (2009). Comparative study of coupling approaches for surface water and subsurface interactions. *Journal of Hydrologic Engineering*, 14(5):453–462.
- itwh (2010). *Kanalnetzrechnung - Hydrodynamische Abfluss-Transport- und Schmutzfrachtberechnung. HYSTEM-EXTRAN 7 Modellbeschreibung*. Institut für technisch-wissenschaftliche Hydrologie GmbH Hannover.
- Iwalewa, T. M., Elamin, A. S., and Kaka, S. I. (2016). A coupled model simulation

- assessment of shallow water-table rise in a saudi arabian coastal city. *Journal of Hydro-environment Research*, 12:46–58.
- Jahanbazi, M. and Egger, U. (2014). Application and comparison of two different dual drainage models to assess urban flooding. *Urban Water Journal*, 11(7):584–595.
- Jones, J. P., Sudicky, E. A., and McLaren, R. G. (2008). Application of a fully-integrated surface-subsurface flow model at the watershed-scale: A case study. *Water Resources Research*, 44(3).
- Kalbacher, T., Delfs, J.-O., Shao, H., Wang, W., Walther, M., Samaniego, L., Schneider, C., Kumar, R., Musolff, A., Centler, F., et al. (2012). The IWAS-ToolBox: software coupling for an integrated water resources management. *Environmental Earth Sciences*, 65(5):1367–1380.
- Karpf, C. (2012). *Modellierung der Interaktion zwischen Grundwasser und Kanalisation*. PhD thesis, TU Dresden.
- Karpf, C. and Krebs, P. (2005). Application of a leakage model to assess exfiltration from sewers. *Water science and technology*, 52(5):225–231.
- Karpf, C. and Krebs, P. (2011). A new sewage exfiltration model – parameters and calibration. *Water Science and Technology*, 63(10):2294–2299.
- Karpf, C. and Krebs, P. (2013). Modelling of groundwater infiltration into sewer systems. *Urban Water Journal*, 10(4):221–229.
- Karpf, C., Traenckner, J., and Krebs, P. (2009). Hydraulic modelling of sewage exfiltration. *Water Science and Technology*, 59(8):1559–1565.
- Kidmose, J., Troldborg, L., Refsgaard, J., and Bischoff, N. (2015). Coupling of a distributed hydrological model with an urban storm water model for impact analysis of forced infiltration. *Journal of Hydrology*, 525:506–520.
- King, R. S., Scoggins, M., and Porras, A. (2016). Stream biodiversity is disproportionately lost to urbanization when flow permanence declines: evidence from southwestern north america. *Freshwater Science*, 35(1):340–352.
- Klinger, J., Thoma, R., and Wolf, L. (2010). Untersuchungen zur Quantifizierung und qualitativen Bewertung der Abwasserexfiltration. In *2. Deutscher Tag der Grundstücksentwässerung; Grundstücksentwässerung - quo vadis?*
- Knudsen, L., Andersen, U., Ørskov, P., and Pedersen, C. (1996). Undgå forurening af drikkevandet. *Stads og havneingeniøren*, 10:34–36.
- Kolditz, O., Bauer, S., Bilke, L., Böttcher, N., Delfs, J.-O., Fischer, T., Görke, U. J., Kalbacher, T., Kosakowski, G., McDermott, C., et al. (2012a). OpenGeoSys: an open-source initiative for numerical simulation of thermo-hydro-mechanical/chemical (THM/C) processes in porous media. *Environmental Earth Sciences*, 67(2):589–599.
- Kolditz, O., Nagel, T., Shao, H., Wang, W., and Bauer, S. (2018). *Thermo-Hydro-Mechanical-Chemical Processes in Fractured Porous Media: Modelling and Benchmarking - From Benchmarking to Tutoring*. Springer.

- Kolditz, O., Shao, H., and Wang, W. (2012b). *Thermo-Hydro-Mechanical-Chemical Processes in Fractured Porous Media*. Springer Publishing Company, Incorporated.
- Kolditz, O., Shao, H., Wang, W., and Bauer, S. (2015). *Thermo-hydro-mechanical Chemical Processes in Fractured Porous Media: Modelling and Benchmarking - Closed Form Solutions*. Springer.
- Kolditz, O., Shao, H., Wang, W., and Bauer, S. (2016). *Thermo-hydro-mechanical Chemical Processes in Fractured Porous Media: Modelling and Benchmarking - Benchmarking Initiatives*. Springer.
- Laszewski, T. and Nauduri, P. (2012). Migrating to the Cloud: Client/Server Migrations to the Oracle Cloud. In *Migrating to the Cloud*, pages 1–19. Elsevier.
- Le Coustumer, S., Fletcher, T., Deletic, A., Barraud, S., and Poelsma, P. (2012). The influence of design parameters on clogging of stormwater biofilters: A large-scale column study. *Water Research*, 46(20):6743–6752.
- Lehmann, C., Kolditz, O., and Nagel, T. (2017). *Models of Thermochemical Heat Storage*, volume 1. Springer.
- Lemke, D. and Elbracht, J. (2008). *Grundwasserneubildung in Niedersachsen: ein Vergleich der Methoden Dörhöfer & Josopait und GROWA06V2*. Landesamt für Bergbau, Energie und Geologie.
- Lerner, D. (1986). Leaking pipes recharge ground water. *Groundwater*, 24(5):654–662.
- Lerner, D. and Harris, B. (2009). The relationship between land use and groundwater resources and quality. *Land Use Policy*, 26:S265–S273.
- Lerner, D. N. (1990). Groundwater recharge in urban areas. *Atmospheric Environment. Part B. Urban Atmosphere*, 24(1):29–33.
- Liu, X., Chen, Y., and Shen, C. (2016). Coupled two-dimensional surface flow and three-dimensional subsurface flow modeling for drainage of permeable road pavement. *Journal of Hydrologic Engineering*, 21(12):04016051.
- Ly, D. K. and Chui, T. F. M. (2012). Modeling sewage leakage to surrounding groundwater and stormwater drains. *Water Science and Technology*, 66(12):2659–2665.
- Ma, Y., Feng, S., Su, D., Gao, G., and Huo, Z. (2010). Modeling water infiltration in a large layered soil column with a modified green-ampt model and hydrus-1d. *Computers and Electronics in Agriculture*, 71:S40–S47.
- Martinez, S., Escolero, O., and Wolf, L. (2011). Total urban water cycle models in semiarid environments quantitative scenario analysis at the area of san luis potosi, mexico. *Water Resources Management*, 25(1):239–263.
- Maxwell, R., Kollet, S., Smith, S., Woodward, C., Falgout, R., Ferguson, I., Baldwin, C., Bosl, W., Hornung, R., and Ashby, S. (2009). Parflow users manual. *International Ground Water Modeling Center Report GWMI*, 1(2009):129.
- Micevski, T., Kuczera, G., and Coombes, P. (2002). Markov model for storm water pipe deterioration. *Journal of infrastructure systems*, 8(2):49–56.

- Mohrlok, U., Wolf, L., and Klinger, J. (2008). Quantification of infiltration processes in urban areas by accounting for spatial parameter variability. *Journal of Soils and Sediments*, 8(1):34–42.
- Musy, A., Hingray, B., and Picouet, C. (2014). *Hydrology: A Science for Engineers*. CRC Press, Taylor and Francis Group.
- Nelder, J. A. and Mead, R. (1965). A Simplex Method for Function Minimization. *The Computer Journal*, 7(4):308–313.
- NIBIS (2017). Huek200 - grundwasserneubildung (mgrowa). nibis.lbeg.de/cardomap3, Accessed: 2017-06-30.
- Ogai, H. and Bhattacharya, B. (2018). *Pipe Inspection Robots for Structural Health and Condition Monitoring*. Springer.
- Okubo, T. and Matsumoto, J. (1983). Biological clogging of sand and changes of organic constituents during artificial recharge. *Water Research*, 17(7):813–821.
- Peche, A., Graf, T., Fuchs, L., and Neuweiler, I. (2017). A coupled approach for the three-dimensional simulation of pipe leakage in variably saturated soil. *Journal of Hydrology*.
- Peche, A., Graf, T., Fuchs, L., and Neuweiler, I. (2019). Physically based modeling of stormwater pipe leakage in an urban catchment. *Journal of Hydrology*.
- Peche, A., Graf, T., Fuchs, L., Neuweiler, I., Maßmann, J., Huber, M., Vassolo, S., Stoeckl, L., Lindenmaier, F., Neukum, C., Jing, M., and Attinger, S. (2018). HH Processes. In Kolditz, O., Nagel, T., Shao, H., Wang, W., and Bauer, S., editors, *Thermo-Hydro-Mechanical-Chemical Processes in Fractured Porous Media: Modelling and Benchmarking: From Benchmarking to Tutoring*, pages 125–144. Springer International Publishing, Cham.
- Pitt, R. (1993). *Investigation of inappropriate pollutant entries into storm drainage systems: a user's guide*. DIANE Publishing.
- Preissmann, A. (1961). Propagation des intumescences dans les canaux et rivires. *Proc. 1st Congres de l'Assoc. Francaise de Calcul*, pages 433–442.
- Rauch, W. and Stegner, T. (1994). The colmation of leaks in sewer systems during dry weather flow. *Water Science and Technology*, 30(1):205–210.
- Read, G. F. and Vickridge, I. (1996). *Sewers: Repair and Renovation*. Butterworth-Heinemann.
- Reichel, F. and Getta, M. (2008). Grundwassermodelle als Werkzeuge zur Fremdwasser-sanierung. *Korrespondenz Wasserwirtschaft (1)*, (12):10–11.
- Richards, L. A. (1931). Capillary conduction of liquids through porous mediums. *Journal of Applied Physics*, 1(5):318–333.
- Rogers, H. R. (1996). Sources, behaviour and fate of organic contaminants during sewage treatment and in sewage sludges. *Science of the total environment*, 185(1-3):3–26.
- Romanova, A., Horoshenkov, K. V., Tait, S. J., and Ertl, T. (2013). Sewer inspection and comparison of acoustic and CCTV methods. *Proceedings of the Institution of Civil Engineers - Water Management*, 166(2):70–80.

- Rosi-Marshall, E., Snow, D., Bartelt-Hunt, S., Paspalof, A., and Tank, J. (2015). A review of ecological effects and environmental fate of illicit drugs in aquatic ecosystems. *Journal of hazardous materials*, 282:18–25.
- Rossi, L., De Alencastro, L., Kupper, T., and Tarradellas, J. (2004). Urban stormwater contamination by polychlorinated biphenyls (PCBs) and its importance for urban water systems in Switzerland. *Science of the total environment*, 322(1-3):179–189.
- Rossmann, L. A. (2006). Storm Water Management Model Quality Assurance Report: Dynamic Wave Flow Routing. Technical Report EPA/600/R-06/097.
- Roth, K. (2006). Soil physics. *Lecture Notes, Institute of Environmental physics, University of Heidelberg*, <http://www.iup.uniheidelberg.de/institut/forschung/groups/ts/students>.
- Rushton, K. and Tomlinson, L. (1979). Possible mechanisms for leakage between aquifers and rivers. *Journal of Hydrology*, 40(1-2):49–65.
- Rushton, K. R. (2004). *Groundwater hydrology: conceptual and computational models*. John Wiley & Sons.
- Rutsch, M., Rieckermann, J., Cullmann, J., Ellis, J. B., Vollertsen, J., and Krebs, P. (2008). Towards a better understanding of sewer exfiltration. *Water Research*, 42(10-11):2385–2394.
- Sämman, R., Graf, T., and Neuweiler, I. (2018). Modeling of contaminant transport during an urban pluvial flood event - The importance of surface flow. *Journal of Hydrology*.
- Schrock, B. (1994). Existing sewer evaluation and rehabilitation. *ASCE Manual and Report on Engineering Practice*, (62).
- Schwarz, M. (2004). *Mikrobielle Kolmation von abwasserdurchsickerten Bodenkörpern: Nucleinsäuren zum Nachweis von Biomasse und Bioaktivität*. Institutsverl. Siedlungswasserwirtschaft.
- Shaad, K. (2015). *Development of a distributed surface-subsurface interaction model for river corridor hydrodynamics*. PhD thesis, ETH Zurich.
- Shaad, K. and Burlando, P. (2018). Monitoring and modelling of shallow groundwater dynamics in urban context: The case study of Jakarta. *Journal of Hydrology*.
- Siegrist, R. L. (1987). Soil clogging during subsurface wastewater infiltration as affected by effluent composition and loading rate. *Journal of Environmental Quality*, 16(2):181–187.
- Simunek, J., Van Genuchten, M. T., and Sejna, M. (2005). The hydrus-1d software package for simulating the one-dimensional movement of water, heat, and multiple solutes in variably-saturated media. *University of California-Riverside Research Reports*, 3:1–240.
- Singh, V. P. and Frevert, D. K. (2003). Watershed models. In *Environmental and Water Resources History*, pages 156–167.
- Siriwardene, N. R., Deletic, A., and Fletcher, T. D. (2007). Clogging of stormwater gravel infiltration systems and filters: Insights from a laboratory study. *Water Research*, 41(7):1433–1440.

- Skaggs, R., Monke, E., and Huggins, L. (1970). An approximate method for determining the hydraulic conductivity of unsaturated soils. Technical Report 2, Water Resources Research Center, Purdue University, Lafayette, Indiana.
- Sommer, T., Karpf, C., Ettrich, N., Haase, D., Weichel, T., Peetz, J.-V., Steckel, B., Eulitz, K., and Ullrich, K. (2009). Coupled modelling of subsurface water flux for an integrated flood risk management. *Natural Hazards and Earth System Sciences*, 9(4):1277–1290.
- Sophocleous, M. (2002). Interactions between groundwater and surface water: the state of the science. *Hydrogeology journal*, 10(1):52–67.
- Stephenson, D. (2012). *Water supply management*, volume 29. Springer Science & Business Media.
- Swain, E. D. and Wexler, E. J. (1996). A coupled surface-water and ground-water flow model (MODBRANCH) for simulation of stream-aquifer interaction. In *Techniques of Water-Resources Investigations, Book 6*. USGS, US Government Printing Office.
- Tang, Y., Zhu, D. Z., and Chan, D. H. (2017). Experimental study on submerged sand erosion through a slot on a defective pipe. *Journal of Hydraulic Engineering*, 143(9):04017026.
- The Mathworks Inc. (2016). MATLAB - MathWorks.
- Thoms, R. B., Johnson, R. L., and Healy, R. W. (2006). User’s guide to the Variably Saturated Flow (VSF) process to MODFLOW. Technical report.
- Thorndahl, S., Balling, J., and Larsen, U. (2016a). Analysis and integrated modelling of groundwater infiltration to sewer networks. *Hydrological Processes*, 30(18):3228–3238. HYP-15-0457.R1.
- Thorndahl, S., Nielsen, J. E., and Jensen, D. G. (2016b). Urban pluvial flood prediction: a case study evaluating radar rainfall nowcasts and numerical weather prediction models as model inputs. *Water Science and Technology*.
- Tian, D. and Liu, D. (2011). A new integrated surface and subsurface flows model and its verification. *Applied Mathematical Modelling*, 35(7):3574–3586.
- Tondera, K., Blecken, G.-T., Chazarenc, F., and Tanner, C. C. (2018). *Ecotechnologies for the Treatment of Variable Stormwater and Wastewater Flows*. Springer.
- Tubau, I., Vázquez-Suñé, E., Carrera, J., Valhondo, C., and Criollo, R. (2017). Quantification of groundwater recharge in urban environments. *Science of the Total Environment*, 592:391–402.
- van Genuchten, M. T. (1980). A closed-form equation for predicting the hydraulic conductivity of unsaturated soils. *Soil Science Society of America Journal*, 44(5):892.
- Vizintin, G., Souvent, P., Veselič, M., and Curk, B. C. (2009). Determination of urban groundwater pollution in alluvial aquifer using linked process models considering urban water cycle. *Journal of hydrology*, 377(3-4):261–273.
- Vogel, T. (1987). SWMII-Numerical model of two-dimensional flow in a variably saturated porous medium. Technical Report 87, Department of Hydraulics and Catchment Hydrology, Agricultural University, Wageningen, Netherlands.

- Vollertsen, J. and Hvitved-Jacobsen, T. (2003). Exfiltration from gravity sewers: a pilot scale study. *Water Science and Technology*, 47(4):69–76.
- Walther, M., Delfs, J.-O., Grundmann, J., Kolditz, O., and Liedl, R. (2012). Saltwater intrusion modeling: verification and application to an agricultural coastal arid region in Oman. *Journal of Computational and Applied Mathematics*, 236(18):4798–4809.
- Weiss, G., Brombach, H., and Haller, B. (2002). Infiltration and inflow in combined sewer systems: long-term analysis. *Water Science and Technology*, 45(7):11–19.
- Wells, T. and Melchers, R. (2015). Modelling concrete deterioration in sewers using theory and field observations. *Cement and Concrete Research*, 77:82–96.
- Wirahadikusumah, R., Abraham, D., and Iseley, T. (2001). Challenging issues in modeling deterioration of combined sewers. *Journal of infrastructure systems*, 7(2):77–84.
- Wittenberg, H. and Aksoy, H. (2010). Groundwater intrusion into leaky sewer systems. *Water Science and technology*, 62(1):92–98.
- Wolf, L., Eiswirth, M., and Hötzl, H. (2006). Assessing sewer–groundwater interaction at the city scale based on individual sewer defects and marker species distributions. *Environmental Geology*, 49(6):849–857.
- Wolf, L., Morris, B., and Burn, S. (2007). *Urban Water Resources Toolbox*. European Water Research Series. IWA Publishing.
- Wriggers, P. (2008). *Nonlinear finite element methods*. Springer Science & Business Media.
- Xu, Z., Yin, H., and Li, H. (2014). Quantification of non-stormwater flow entries into storm drains using a water balance approach. *Science of the Total Environment*, 487:381–388.
- Yang, J., Graf, T., and Ptak, T. (2015). Impact of climate change on freshwater resources in a heterogeneous coastal aquifer of Bremerhaven, Germany: A three-dimensional modeling study. *Journal of Contaminant Hydrology*, 177-178:107–121.
- Zieffe, G., Matray, J.-M., Maßmann, J., and Möri, A. (2017). Coupled hydraulic-mechanical simulation of seasonally induced processes in the Mont Terri rock laboratory (Switzerland). *Swiss Journal of Geosciences*, 110(1):195–212.

List of dissertations in the institute

Institute of Fluid Mechanics and Environmental Physics in Civil Engineering
Gottfried Wilhelm Leibniz Universität Hannover

Previously published publications in this book series:

- 01/1970 **Holz, K.-P.** *Ergänzung des Verfahrens finiter Elemente durch Ecksingularitäten zur verbesserten Berechnung schiefwinkliger Platten.* Dissertation, Techn. Univ. Hannover, 1970
- 02/1971 **Ehlers, K.-D.** *Berechnung instationärer Grund- und Sickerwasserströmungen mit freier Oberfläche nach der Methode finiter Elemente.* Dissertation, Techn. Univ. Hannover, 1971
- 03/1971 **Meißner, U.** *Berechnung von Schalen unter großen Verschiebungen und Verdrehungen bei kleinen Verzerrungen mit Hilfe finiter Dreieckelemente.* Dissertation, Techn. Univ. Hannover, 1971
- 04/1972 **Grotkop, G.** *Die Berechnung von Flachwasserwellen nach der Methode der finiten Elemente.* Dissertation, Techn. Univ. Hannover, 1972
- 05/1973 **Schulze, K.** *Eine problemorientierte Sprache für die Dynamik offener Gerinne (DOG).* Dissertation, Techn. Univ. Hannover, 1973
- 06/1977 **Beyer, A.** *Die Berechnung grossräumiger Grundwasserströmungen mit Vertikalstruktur mit Hilfe der Finite-Element-Methode.* Dissertation, Fortschrittberichte der VDI-Zeitschriften : Reihe 4, Nr. 34, 1977
- 07/1977 **Ebeling, H.** *Berechnung der Vertikalstruktur wind- und gezeitenerzeugter Strömungen nach der Methode der finiten Elemente.* Dissertation, Fortschrittberichte der VDI-Zeitschriften : Reihe 4, Nr. 32, 1977
- 08/1977 **Gärtner, S.** *Zur berechnung von flachwasserwellen und instationären transportprozessen mit der methode der finiten elemente.* Dissertation, Fortschrittberichte der VDI-Zeitschriften : Reihe 4, Nr. 30, 1977
- 09/1977 **Herrling, B.** *Eine hybride formulierung in wasserständen zur berechnung von flachwasserwellen mit der methode finiter elemente.* Dissertation, Fortschrittberichte der VDI-Zeitschriften : Reihe 4, Nr. 37, 1977
- 10/1979 **Herrling, B.** *Aeroelastische Stabilitätsuntersuchung von Linientragwerken.* Dissertation, Fortschrittberichte der VDI-Zeitschriften : Reihe 4, Nr. 37, 1979
- 11/1979 **Kaločay, E.** *Zur numerischen Behandlung der Konvektions-Diffusions-Gleichung im Hinblick auf das inverse Problem.* Dissertation, Univ. Hannover, 1979
- 12/1980 **Januszewski, U.** *Automatische Eichung für ein- und zweidimensionale hydrodynamisch-numerische Flachwassermodelle.* Dissertation, Univ. Hannover, Fortschrittberichte der VDI-Zeitschriften : Reihe 4, Nr. 58, 1980
- 13/1982 **Carbonel Huamán, C.A.A** *Numerisches Modell der Zirkulation in Auftriebsgebieten mit Anwendung auf die nordperuanische Küste.* Dissertation, Univ. Hannover, 1982
- 14/1985 **Tuchs, M.** *Messungen und Modellierung am deep shaft.* Dissertation, Univ. Hannover, 1985
- 15/1985 **Theunert, F.** *Zum lokalen Windstau in Ästuarien bei Sturmfluten: Numerische Untersuchung am Beispiel der Unterelbe.* Dissertation, Univ. Hannover, 1984

- 16/1985 **Perko, H.-D.** *Gasausscheidung in instationärer Rohrströmung.* Dissertation, Univ. Hannover, 1984
- 17/1985 **Crotogino, A.** *Ein Beitrag zur numerischen Modellierung des Sedimenttransports in Verbindung mit vertikal integrierten Strömungsmodellen.* Dissertation, Univ. Hannover, 1984
- 18/1985 **Rottmann-Söde, W.** *Ein halbanalytisches FE-Modell für harmonische Wellen zur Berechnung von Wellenunruhen in Häfen und im Küstenvorfeld.* Dissertation, Univ. Hannover, 1985
- 19/1985 **Nitsche, G.** *Explizite Finite-Element-Modelle und ihre Naturanwendungen auf Strömungsprobleme in Tidegebieten.* Dissertation, Univ. Hannover, 1985
- 20/1985 **Vera Muthre, C.** *Untersuchungen zur Salzausbreitung in Ästuarien mit Taylor'schen Dispersionsmodellen.* Dissertation, Univ. Hannover, 1985
- 21/1985 **Schaper, H.** *Ein Beitrag zur numerischen Berechnung von nichtlinearen kurzen Flachwasserwellen mit verbesserten Differenzenverfahren.* Dissertation, Univ. Hannover, 1985
- 22/1986 **Urban, C.** *Ein Finite-Element-Verfahren mit linearen Ansätzen für stationäre zweidimensionale Strömungen.* Dissertation, Univ. Hannover, 1986
- 23/1987 **Heyer, H.** *Die Beeinflussung der Tidedynamik in Ästuarien durch Steuerung: E. Beitr. zur Anwendung von Optimierungsverfahren in der Wasserwirtschaft.* Dissertation, Univ. Hannover, 1987
- 24/1987 **Gärtner, S.** *Zur diskreten Approximation kontinuumsmechanischer Bilanzgleichungen.* Institutsbericht, davon 4 Abschnitte als Habilitationsschrift angenommen, Univ. Hannover, 1987
- 25/1988 **Rogalla, B.U.** *Zur statischen und dynamischen Berechnung geometrisch nichtlinearer Linientragwerke unter Strömungs- und Wellenlasten.* Dissertation, Univ. Hannover, 1988
- 26/1990 **Lang, G.** *Zur Schwebstoffdynamik von Trübungszonen in Ästuarien.* Dissertation, Univ. Hannover, 1990
- 27/1990 **Stittgen, M.** *Zur Fluid-Struktur-Wechselwirkung in flexiblen Offshore-Schlauchleitungen.* Dissertation, Univ. Hannover, 1990
- 28/1990 **Wollrath, J.** *Ein Strömungs- und Transportmodell für klüftiges Gestein und Untersuchungen zu homogenen Ersatzsystemen.* Dissertation, Univ. Hannover, 1990
- 29/1991 **Kröhn, K.-P.** *Simulation von Transportvorgängen im klüftigen Gestein mit der Methode der finiten Elemente.* Dissertation, Univ. Hannover, 1991
- 30/1991 **Lehfeldt, R.** *Ein algebraisches Turbulenzmodell für Ästuarare.* Dissertation, Univ. Hannover, 1991
- 31/1991 **Prüser, H.-H.** *Zur mathematischen Modellierung der Interaktion von Seegang und Strömung im flachen Wasser.* Dissertation, Univ. Hannover, 1991
- ditto **Schröter, A.** *Das numerische Seegangmodell BOWAM2 1990: Grundlagen und Verifikation.* Univ. Hannover, 1991
- 32/1992 **Leister, K.** *Anwendung numerischer Flachwassermodelle zur Bestimmung von Wasserlinien.* Dissertation, Univ. Hannover, 1992
- 33/1993 **Ramthun, B.** *Zur Druckstoßsicherung von Fernwärmenetzen und zur Dynamik von Abnehmeranlagen.* Dissertation, Univ. Hannover, 1993
- 34/1993 **Helmig, R.** *Theorie und Numerik der Mehrphasenströmungen in geklüftet-porösen Medien.* Dissertation, Univ. Hannover, 1993
- 35/1994 **Plüss, A.** *Netzbearbeitung und Verfahrensverbesserungen für Tidemodelle nach der Finiten Element Methode.* Dissertation, Univ. Hannover, 1994
- 36/1994 **Nöthel, H.** *Statistisch-numerische Beschreibung des Wellen- und Strömungsgeschehens in einem Bühnenfeld.* Dissertation, Univ. Hannover, 1994

- 37/1994 **Shao, H.** *Simulation von Strömungs- und Transportvorgängen in geklüfteten porösen Medien mit gekoppelten Finite-Element- und Rand-Element-Methoden.* Dissertation, Univ. Hannover, 1994
- 38/1994 **Stengel, T.** *Änderungen der Tidedynamik in der Deutschen Bucht und Auswirkungen eines Meeresspiegelanstiegs.* Dissertation, Univ. Hannover, 1994
- 39/1994 **Schubert, R.** *Ein Softwaresystem zur parallelen interaktiven Strömungssimulation und -visualisierung.* Dissertation, Univ. Hannover, 1994
- 40/1994 **Alm, W.** *Zur Gestaltung eines Informationssystems im Küsteningenieurwesen.* Dissertation, Univ. Hannover, 1994
- 41/1994 **Benali, H.** *Zur Kopplung von FEM- und CAD-Programmen im Bauwesen über neutrale Datenschnittstellen.* Dissertation, Univ. Hannover, 1994
- 42/1995 **Schröter, A.** *Nichtlineare zeitdiskrete Seegangssimulation im flachen und tieferen Wasser.* Dissertation, Univ. Hannover, 1995
- 43/1995 **Blase, T.** *Ein systemtechnischer Ansatz zur Modellierung von Hydraulik, Stofftransport und reaktionskinetischen Prozessen in Kläranlagen.* Dissertation, Univ. Hannover, 1995
- 44/1995 **Malcherek, A.** *Mathematische Modellierung von Strömungen und Stofftransportprozessen in Ästuaren.* Dissertation, Univ. Hannover, 1995
- 45/1995 **Lege, T.** *Modellierung des Kluftgesteins als geologische Barriere für Deponien.* Dissertation, Univ. Hannover, 1995
- 46/1996 **Arnold, H.** *Simulation dammbruchinduzierter Flutwellen.* Dissertation, Univ. Hannover, 1996
- 47/1996 **Kolditz, O.** *Strömung, Stoff- und Wärmetransport im Kluftgestein.* Habilitation, Univ. Hannover, 1996
- 48/1996 **Hunze, M.** *Numerische Modellierung reaktiver Strömungen in oberflächenbelüfteten Belebungsbecken.* Dissertation, Univ. Hannover, 1996
- 49/1996 **Wollschläger, A.** *Ein Random-Walk-Modell für Schwermetallpartikel in natürlichen Gewässern.* Dissertation, Univ. Hannover, 1996
- 50/1997 **Feist, M.** *Entwurf eines Modellierungssystems zur Simulation von Oberflächengewässern.* Dissertation, Univ. Hannover, 1997
- 51/1997 **Hinkelmann, R.** *Parallelisierung eines Lagrange-Euler-Verfahrens für Strömungs- und Stofftransportprozesse in Oberflächengewässern.* Dissertation, Univ. Hannover, 1997
- 52/1997 **Barlag, C.** *Adaptive Methoden zur Modellierung von Stofftransport im Kluftgestein.* Dissertation, Univ. Hannover, 1997
- 53/1997 **Saberi-Haghighi, K.** *Zur Ermittlung der verformungsabhängigen Windbelastung bei Hängedächern.* Dissertation, Univ. Hannover, 1997
- 54/1998 **Krüger, A.** *Physikalische Prozesse im Nachklärbecken: Modellbildung und Simulation.* Dissertation, Univ. Hannover, 1998
- 55/1998 **Wolters, A.H.** *Zur Modellierung des instationären thermohydraulischen Betriebsverhaltens von Fernwärmanlagen.* Dissertation, Univ. Hannover, 1998
- 56/1999 **Jankowski, J.A.** *A non-hydrostatic model for free surface flows.* Dissertation, Univ. Hannover, 1999
- 57/1999 **Kopmann, R.** *Mehrdimensionale Effekte in dimensionsreduzierten Gewässergütemodellen.* Dissertation, Univ. Hannover, 1999
- 58/1999 **Kahlfeld, A.** *Numerische Seegangmodellierung als Bestandteil einer funktionellen Hafenplanung.* Dissertation, Univ. Hannover, 1999

- 59/1999 *Festschrift zum 60. Geburtstag von Professor Werner Zielke*. Univ. Hannover, 1999
- 60/2000 **Kolditz, O., Zielke, W., Wriggers, P., Dürbaum H.-J., Wallner, M.** 3. *Workshop Kluft-Aquifere – Gekoppelte Prozesse in Geosystemen*. Univ. Hannover, 2000
- 61/2001 **Malcherek, A.** *Hydromechanik der Fließgewässer*. Habilitation, Univ. Hannover, 2001
- 62/2001 **Thorenz, C.** *Model adaptive simulation of multiphase and density driven flow in fractured and porous media*. Dissertation, Univ. Hannover, 2001
- 63/2001 **Kaiser, R.** *Gitteradaption für die Finite-Elemente-Modellierung gekoppelter Prozesse in geklüftet-porösen Medien*. Dissertation, Univ. Hannover, 2001
- 64/2001 **Rother, T.** *Geometric modelling of geo-systems*. Dissertation, Univ. Hannover, 2001
- 65/2001 **Habbar, A.** *Direkte und inverse Modellierung reaktiver Transportprozesse in klüftig-porösen Medien*. Dissertation, Univ. Hannover, 2001
- 66/2002 **Weilbeer, H.** *Numerische Simulation von Strömung und Kolkung an Wasserbauwerken*. Dissertation, Univ. Hannover, 2002
- 67/2002 **Hoyme, H.** *Mesoskalige morphodynamische Modellierungen am Beispiel der Meldorfer Bucht*. Dissertation, Univ. Hannover, 2002
- 68/2004 **Moenickes, S.** *Grid generation for simulation of flow and transport processes in fractured porous media*. Dissertation, Univ. Hannover, 2004
- 69/2004 **Strybny, J.** *Ein phasenauflösendes Seegangmodell zur Ermittlung von Bemessungsparametern für Küstenstrukturen*. Dissertation, Univ. Hannover, 2004
- 70/2004 **Weilbeer, J.** *Modellierung des Partikeltransports in Nachklärbecken als Mehrphasenströmung*. Dissertation, Univ. Hannover, 2004
- 71/2006 **Mittendorf, K.** *Hydromechanical design parameters and design loads for offshore wind energy converters*. Dissertation, Leibniz Universität Hannover, 2006
- 72/2006 **Kohlmeier, M.** *Coupling of thermal, hydraulic and mechanical processes for geotechnical simulations of partially saturated porous media*. Dissertation, Leibniz Universität Hannover, 2006
- 73/2006 **Schumacher, S.** *Leistungsbestimmende Prozesse in Nachklärbecken: Einflussgrößen, Modellbildung und Optimierung*. Dissertation, Leibniz Universität Hannover, 2006
- 74/2008 **Ziefle, G.** *Modeling aspects of coupled hydraulic-mechanical processes in clay material*. Dissertation, Leibniz Universität Hannover, 2008
- 75/2008 **Schimmels, S.** *Numerical simulation of the influence of circular cylinders on mixing and entrainment in natural density currents*. Dissertation, Leibniz Universität Hannover, 2007
- 76/2008 **Göthel, O.** *Numerical modelling of flow and wave induced scour around vertical circular piles*. Dissertation, Leibniz Universität Hannover, 2008
- 77/2009 **Maßmann, J.** *Modeling of excavation induced coupled hydraulic-mechanical processes in claystone*. Dissertation, Leibniz Universität Hannover, 2009
- 78/2014 **Erdal, E.D.** *Bias correction for compensating unresolved subsurface structure in unsaturated flow modelling*. Dissertation, Leibniz Universität Hannover, 2014
- 79/2015 **Hirthe, E.M.** *Optimizing simulations of variable-density flow and transport problems*. Dissertation, Leibniz Universität Hannover, 2015
- 80/2015 **Yang, J.** *Investigating processes and impacts of climate change on seawater intrusion in a coastal aquifer*. Dissertation, Leibniz Universität Hannover, 2015
- 81/2015 **Vujević, K.** *Free convection in fractured porous media*. Dissertation, Leibniz Universität Hannover, 2015

- 82/2016 **Stoeckl, L.** *Variable-Density Flow in the Subsurface of Oceanic Islands: Physical Experiments and Numerical Modeling.* Dissertation, Leibniz Universität Hannover, 2016
- 83/2016 **Guevara Morel, C.R.** *Numerical schemes for the simulation of plume fingering in variable-density flow and transport problems.* Dissertation, Leibniz Universität Hannover, 2016
- 84/2017 **Feng, D.** *Numerical Modeling of Oral Biofilm Growth Using Finite Element Method.* Dissertation, Leibniz Universität Hannover, 2017
- 85/2017 **Tecklenburg, J.-H.** *Upscaled modeling of flow and transport processes in fractured rock.* Dissertation, Leibniz Universität Hannover, 2017
- 86/2019 **Cremer, C.J.M.** *Numerical and laboratory studies on vadose zone flow and transport processes in the vicinity of the soil surface under cyclic boundary conditions.* Dissertation, Leibniz Universität Hannover, 2019
- 87/2019 **Peche, A.** *Numerical modeling of pipe leakage in variably saturated soil.* Dissertation, Leibniz Universität Hannover, 2019